Provenance of a boulder-bearing impact breccia from surface outcrops and a drill-core from the Wetumpka Impact Structure, Elmore County, Alabama

by

Neeraja Satish Chinchalkar

A thesis submitted to the Graduate Faculty of

Auburn University

in partial fulfillment of the

requirements for the Degree of

Master of Science

Auburn, Alabama

August 03, 2019

Approved by

Dr. David T. King, Jr., Chair, Professor of Geology

Dr. Willis E. Hames, Professor of Geology

Dr. Ashraf Uddin, Professor of Geology

Abstract

The Wetumpka crater is a shallow marine impact structure located in the Elmore County, Alabama. The impact event occurred at approximately 85 Ma, during Late Cretaceous. The target was a shallow marine environment with a water depth of about 30 m or less and the lithology consisted of soft sediments belonging to the Tuscaloosa Group and Eutaw Formation, and crystalline pre- Cretaceous Appalachian quarzitic schistose and gneissose basement rocks. The rim of the crater is made of the same crystalline Appalachian rocks as the local basement, whereas the crater floor consists of a mixed lithology of target sediments of the Tuscaloosa Group and Eutaw Formation, which form the trans-crater slide, are the provenance of the crater-filling impactite sands, and a boulder-bearing breccia deposit. The present study was aimed at understanding the mode of emplacement of this breccia unit, which occurs in the central crater floor area and resembles polymict proximal ejecta deposits as in other craters. In the present study, outcrop mapping, drill- core logging, and petrographic studies were completed to understand the nature and origin of this breccia unit.

Field mapping was done to characterize the breccia deposit and identify and map large oriented boulders in the deposit. Petrographic analyses indicated poorly sorted nature, which is characteristic of mass-movement deposition such as a debris flow. Possible shock features such as planar fractures in quartz, kink-banded micas, as well as potential impact-generated spherules were identified in thin sections and analyzed with electron microprobe. AU scientific drill core #09-02 was logged in order to characterize the subsurface nature of the

breccia. All results indicate that the breccia is very poorly sorted with clasts ranging in size from less than 0.5cm to more than 10m. Water did not play any significant role in the formation or emplacement of this breccia unit. Presence of large boulders in the breccia is best explained by a large mass movement of proximal ejecta from the crater rim to the crater floor during early modification. The oriented nature of the boulder sized clasts has been attributed to rotation during mass transport of the boulders in to the crater center. The emplacement of this breccia is interpreted as the last impact-related process to occur before the marine water resurge with accompanying deposition of chalk.

Acknowledgments

This research was supported by the Barringer Family Fund for Meteorite Impact Research, and grants from the Gulf Coast Association of Geological Societies and Geosciences Advisory Board (GAB) of Auburn University. The author also wishes to thank the National Aeronautics and Space Administration (NASA), the Geological Society of America (GSA), the Meteoritical Society, the Barringer Crater Company, and Auburn University College of Sciences and Mathematics (COSAM) for providing travel support. The author is grateful for the support and contribution by the thesis advisor, Dr. David T. King Jr. for the successful completion of the research for the MS program at Auburn. I also thank the thesis committee members, Dr. Willis Hames and Dr. Ashraf Uddin, for providing the necessary resources and lab facilities, and for their patience, advice and support for the past two years. I also acknowledge the support of local landowners in Wetumpka, Alabama, for allowing access to their properties, and the services and help provided by the City of Wetumpka, the Wetumpka Crater Commission, the Elmore County Highway Department, and National Petrographic Services. Lastly and most importantly, I thank my friends Shifat Monami, Mahfuj Rahman, Rahul Bhattacharya, Matthew Adams, Shanike Nawarathne, Kyle Parsons and Leticia De Marchi for helping me time and again.

Table of Contents

List of Tables

List of Figures

INTRODUCTION

Since its formation, the Earth has experienced innumerable bombardments by asteroids and comets, initially adding mass to the earliest Earth, contributing to the Earth's early melting phase, and then scarring its subsequent solid surface with large and small craters. Although meteors and meteorites have been regarded as omens or harbingers of destruction in ancient times, modern people have come to accept them as explicable, recurring natural phenomena. Geoscientists now regard the processes of impact cratering to be as significant in Earth history as a fundamental process such as volcanism or plate tectonics.

An impact crater forms when a cosmic object enters the atmosphere of the Earth (or other planetary bodies) with hypervelocity and a mass large enough to maintain that hypervelocity when it hits the surface. On Earth, approximately 190 impact craters have been identified presently (Earth Impact Database, 2019), and many more potential craters are being studied currently across the world. The amount of kinetic energy involved in the process of formation of an impact crater makes the geological process of impact cratering unique as compared to other normal geologic processes. Also, the entire process takes place in merely a few seconds. Such an instantaneous release of high amount of energy causes the target rocks to deform in unusual ways (as compared to other geological processes) and these impact-related deformations can be preserved in the impact-affected, or 'shocked,' rocks and minerals.

The size and nature of the resulting crater depends on the size and nature of the impactor as well as the geology of the target area, and these conditions also differ across the wide range of planetary bodies. Fragments of the impactor typically cannot be recovered, therefore shock features imbued in the target rocks and their constituent minerals can be used to establish that there has been an impact. Shock features, first identified in meteorites, are also used in understanding the pressure conditions of terrestrial impacts and the nature of the impactor. For

example, planar deformational features (PDFs) in framework silicate minerals like quartz or feldspar are diagnostic of an impact origin because these structures form under ultrahigh pressures, which exist only momentarily within hypervelocity impacts (and have been found as well in nuclear weapon test-detonation sites).

Depending on the size and morphology of the depression, craters can be broadly classified as simple craters or complex craters. Simple impact craters are smooth bowl-shaped depressions with a rim raised above the crater bowl and a concave-upward or flat crater floor, which is a crater morphology that directly reflects the original transient cavity. Complex craters are those which consist of a raised rim as well as an elevated portion in the crater floor known as a central uplift, which forms by rebound of materials during modification of the transient cavity of crater formation. Complex craters are typically larger in diameter than simple craters for any particular planetary body, and the transitional size from simple to complex varies depending on the gravity of the planet. Generally, on Earth, craters larger than 4 km in diameter tend to be complex, whereas smaller craters are simple. Some well-known examples of impact craters on Earth include the Barringer Crater (simple crater) in Arizona and the Chicxulub Crater (complex crater) in the Yucatan Peninsula of Mexico.

On Earth, craters can form on land as well as in water bodies. Marine impact craters are fairly common on Earth and, depending on the water depth at the time of impact and target lithology, form varied and complex morphologies. In marine craters, water depth plays an important role in the formation and modification of the transient cavity. At very large water depths, usually greater than the size of the bolide (Ormö et al., 2006), a crater may not form as a result of slowing down of the impactor owing to the depth of the water column. In shallower depths, however, where the impactor reaches the ocean or sea floor, a crater will form on in the crust below the water body. Marine craters are characterized by a bowl-shaped depression, presence or absence of a central uplift depending on the size of the crater, excavation and

ejection of basement rocks and sediments away from the crater center, and a resurge of the displaced water. Resurge in wet-target craters consists of graded deposits of shocked and unshocked ejecta material brought back into the crater floor due to return of the water during early modification stages. Other processes like faulting or slumping in unconsolidated sediments or in the rim of the crater, along with tsunamis and mass movements are also common in marine impacts (Ormö et al., 2006).

The Wetumpka structure in Elmore County, Alabama (Figure 1), is a well-known and established marine-target impact crater (King et al., 2002; 2006). The impact event at Wetumpka occurred during Late Cretaceous, about 84.4 +/- 1. 4 m.y. ago (Wartho et al., 2011), which is near in age to the Santonian-Campanian stage boundary.

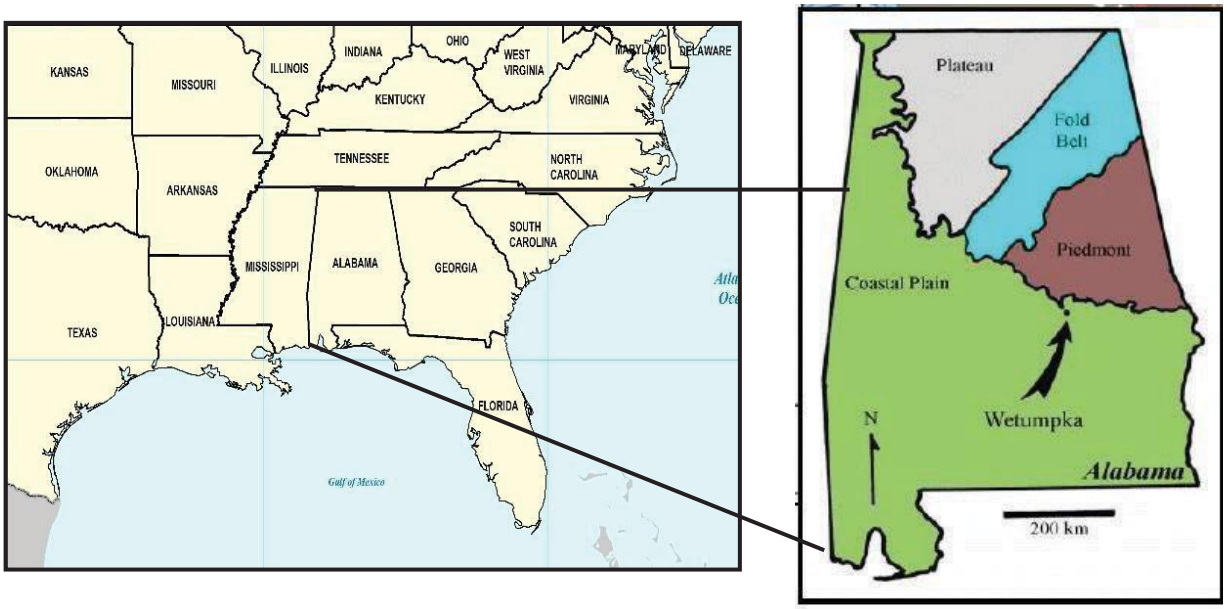

Figure 1: A map of the south-eastern United States showing the location of Alabama (left) and a map of Alabama showing the location of Wetumpka Crater (From King et al., 2002).

Although many older marine impact craters are buried or largely eroded, the Wetumpka impact structure is relatively well preserved, and thus allows for direct observations through outcrop studies.

Formation of an impact crater:

The process of formation of an impact crater can be understood by dividing it into 3 distinct stages. These stages are classified based on the mechanisms that the initial depression undergoes beginning with the contact of the impactor with the target. The stages of impact crater formation have been discussed in detail by French (1998), and are diagrammatically presented in Figure 2.

Formation of a crater begins with the contact and compression stage, which is followed by the excavation stage. The first contact of the bolide with the target marks the beginning of the contact and compression stage. Shock waves travel from the projectile into the ground as well as inside the impactor itself. The impactor and the target undergo compression due to the high-velocity shock waves and depending on the amount of energy, the impactor may shatter into pieces or become molten or vaporized. Stresses exceeding the compressive strengths of the target rocks are generated in the compression stage, which causes deformation of target rocks, and a rise in temperature is responsible for melting of the target rocks.

The opening of the crater depression is the beginning of the excavation stage. A bowl-shaped cavity forms from an outward ejection of target rocks. This initial depression is known as a transient crater. The target rocks are uplifted and overturned (at the rim) giving rise to a raised, nearly circular rim (French, 1998). When the crater bowl reaches its maximum size and the displacement of ejecta material is complete, the excavation stage ends, and the modification stage begins.

The modification stage is characterized by slumping of the crater walls. Processes in this stage are merely the result of the force of gravity and rocks collapsing under their own weight. Faulting and slumping of the crater walls takes place along with debris flows. The crater moat gets filled with breccias during the modification stage. In complex craters, a central

uplift develops as the ground tries to revert to its original condition. In marine craters, this stage also consists of a resurge of the displaced water column (Figure 3). The end of this stage completes the formation of the final crater.

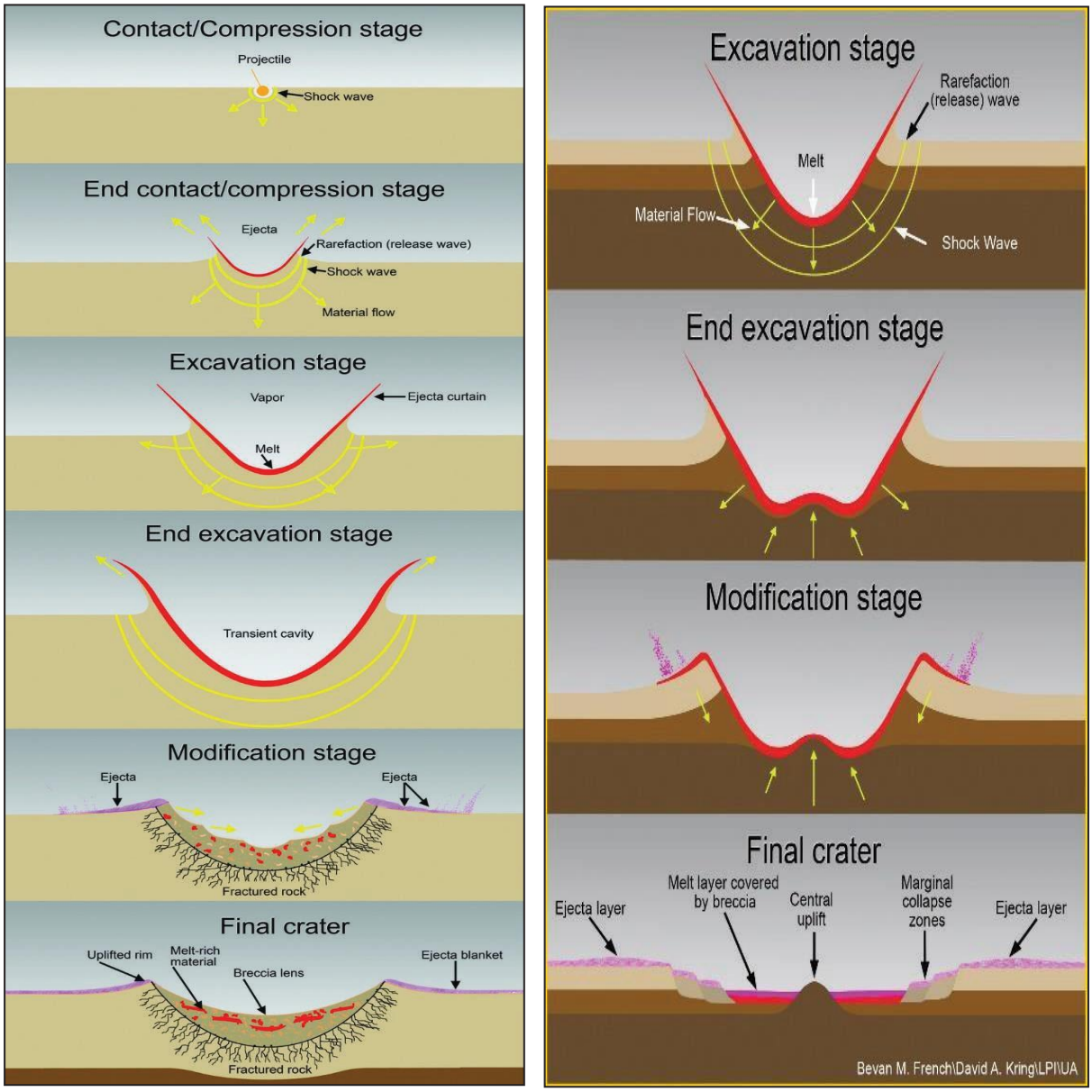

Figure 2: Schematic diagrams showing the formation of: A: a simple impact crater, B: a complex impact crater (From lpi.usra.edu, 2019)

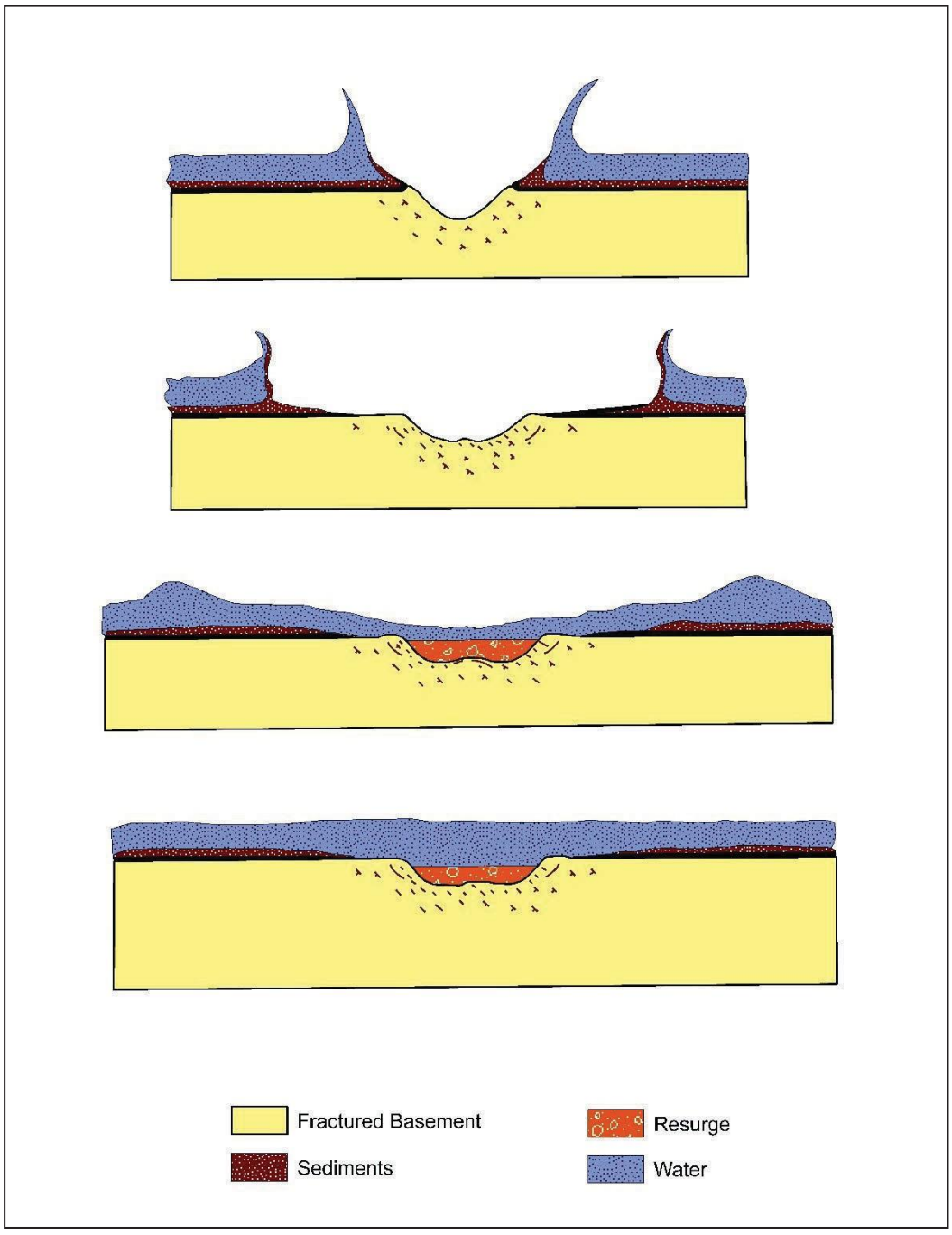

Figure 3: Schematic diagram showing formation of a marine impact crater (Modified from Ormö and Lindström, 2000).

Shock metamorphism in impact craters:

A hypervelocity impact event involves transmission of a large proportion of the high kinetic energy contained in the cosmic object to the target rocks at the site of impact. Such an instantaneous release of energy at impact brings about formation of very high-pressure shock waves in the target lithology. Almost immediately, these shock waves are distributed radially into the target rocks (Melosh, 1989). This unusual process causes the target rocks to deform in a way unlike normal deformation generally seen in slower geologic processes. The target rocks undergo shock metamorphism in response to the sudden conditions of high temperature and pressure created by the shock waves. Shock metamorphism can give rise to the formation of brecciated rocks, melt rocks, pseudotachylites, as well as high pressure/temperature polymorphs of the original minerals present in the rocks. Such shock metamorphosed rocks and minerals can be studied to deduce the conditions prevalent at the time of impact as well as other parameters of the impact event itself, like the nature of the bolide, the direction of impact, the amount of energy released, etc.

To understand the processes occurring in an impact more accurately, it is important to distinguish between the diagnostic shock metamorphic features from those which may be found in other geologic settings. French and Koeberl (2010) have divided impact related deformational processes broadly in to two categories: the first being high pressure shock features produced at pressures greater than 10 GPa typically diagnostic of an impact event; and the second being features produced at lower pressures, i.e., pressures less than 10 GPa, in impact events but which can also occur in other geologic processes. Table 1 summarizes these two categories of impact related deformational features.

Diagnostic indicators for shock metamorphism and meteorite impact	**Non-diagnostic features produced by meteorite impact and by other geological processes.**
Preserved meteorite fragments	Circular morphology
Chemical and isotopic projectile signatures	Circular structural deformation
Shatter cones	Circular geophysical anomalies
High-pressure (diaplectic) mineral glasses	Fracturing and brecciation
High-pressure mineral phases	Kink banding in micas
High-temperature glasses and melts	Mosaicism in crystals
Planar fractures (PFs) in quartz	Pseudotachylite and pseudotachylite breccias
Planar deformation features (PDFs) in quartz	Igneous rocks and glasses
	Spherules and microspherules
	Other problematic criteria

Table 1: Diagnostic and non-diagnostic impact related deformation (Modified from French and Koeberl, 2010). Note that the columns are not comparative.

The rocks carrying the diagnostic signatures of impact are known to be spatially distributed within certain regions of the impact crater (Dence, 1965; 1968; 1971; 1972). For example, melt rocks and high-pressure mineral phases can be expected in the suevitic or polymictic breccia units of the crater moat area, whereas highly fractured and shock metamorphosed rocks and shocked minerals can be found in the central portion of the crater floor of simple craters (or central uplifts of complex craters), the subsurface of the crater center and proximal or distal ejecta deposits depending on the target lithology and size of the crater. With increasing distance from the crater center, the shock waves begin to dissipate, and deformation features begin to define regions of lower and lower pressure-temperature conditions.

Quartz and feldspars are the most commonly studied minerals in impact-affected rocks, and these minerals clearly preserve diagnostic impact signatures. The crystal structures of these minerals are affected by shock compression, and they develop multiple sets of parallel lamella known as planar deformational features (PDFs). At Wetumpka, shocked quartz grains with PDFs have been found within the breccia units, both exposed in the crater center and in drill cores from near the crater center (King et al., 2002; Morrow and King, 2007). Other minerals like zircons, garnets, Ti-oxides, amphiboles, etc. can also undergo shock deformation and phase transformation. Examples of shocked zircon are known from the Ries crater in Germany, Popigai in Siberia, Chicxulub in Mexico, Woodleigh crater in Australia, etc. (e.g., see Wittmann et al., 2006; Cox et al., 2019).

The current study focuses on understanding the mode of emplacement of the central breccia unit of Wetumpka, which closely resembles proximal ejecta deposits, with the help of examination of field studies, outcrop studies, and petrographic and other laboratory analyses.

GEOLOGIC SETTING AND BACKGROUND

At the time of impact, the geological setting of the cosmic event at Wetumpka was a shallow marine area just offshore from the Gulf coastal alluvial plain region of what is now central Alabama. The impact penetrated shallow marine water, the underlying Upper Cretaceous sedimentary layers (the younger Eutaw Formation and the underlying Tuscaloosa Group), and the upper part of the Appalachian metamorphic basement rock, specifically the Upper Paleozoic Emuckfaw Schist (King et al., 2002). The soft sedimentary target and underlying weathered but still intact crystalline basement may have caused Wetumpka to have an unusual morphology for its size (De Marchi et al., 2019).

The rim of the crater has a horse-shoe shape (Figure 4), which consists of crystalline rocks of the Appalachian basement that is open on the southern side. The southern part of the crater is composed of a wide, structurally deformed region, which is located adjacent to the part of the southern segment of the rim, which is missing. The lithology of the rim consists of steeply dipping schists and gneisses, whereas the southern deformed region (called the extra-crater terrain; King et al., 2002) is composed of faulted, poorly consolidated target sediments of the Upper Cretaceous Eutaw Formation and Tuscaloosa Group. The absence of a portion of rim in the southern part has been attributed to post impact rim collapse, which is thought to have been caused by weakness and heterogeneity in the target stratigraphy. King et al. (2006) have interpreted the southern deformed region as a gigantic *in situ* series of slump blocks that are related to the lower levels of the collapsed southern rim of the crater due to mass movement processes associated with rim collapse following soon after the impact.

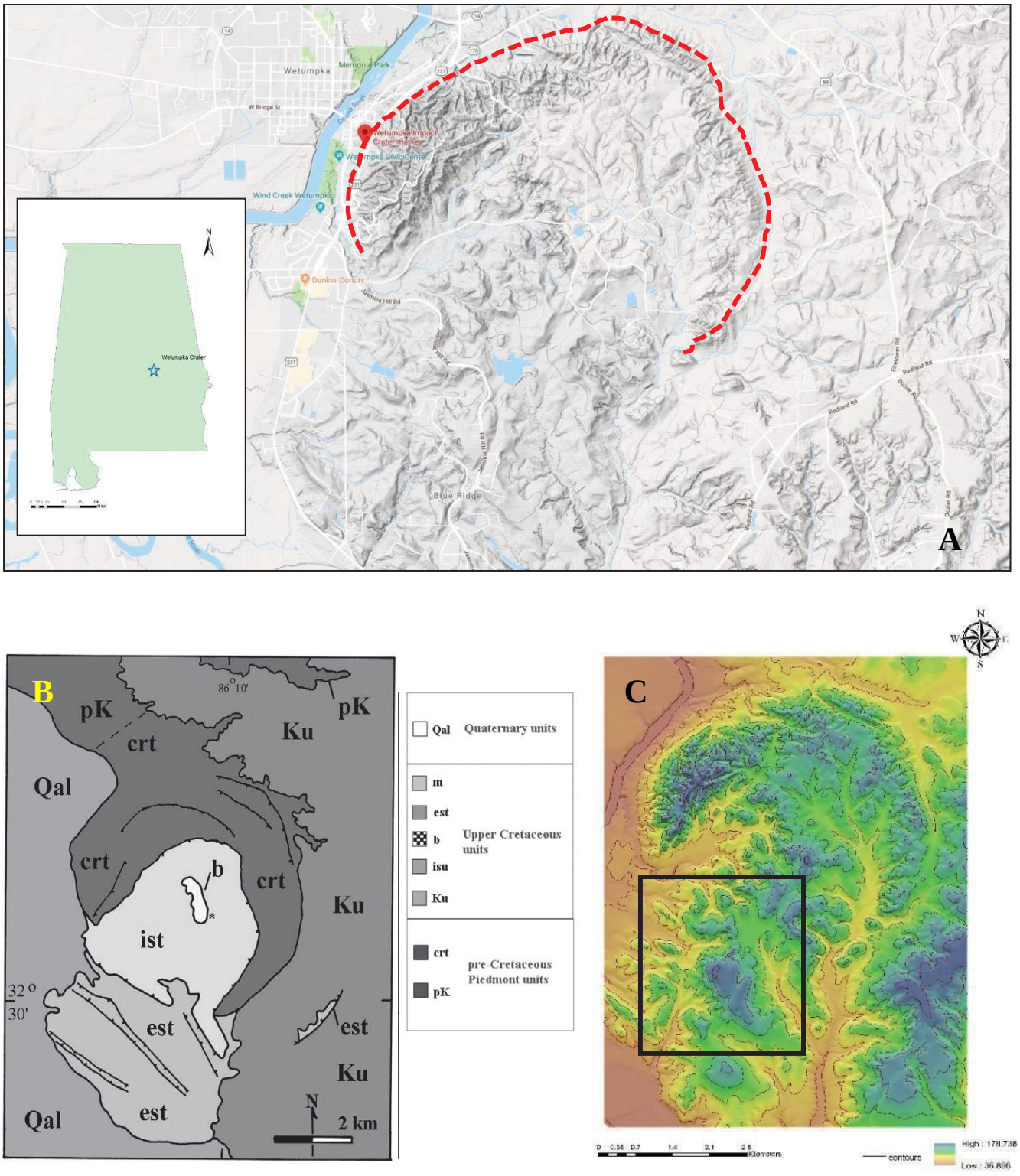

Figure 4: A: Red dashed line shows the extent of the horseshoe-shaped rim of Wetumpka impact structure (modified Google Map image). B: Geologic map of Wetumpka (From King et al., 2002). C: Shaded relief map of Wetumpka compiled from a 10m resolution DEM (from www.alabamaview.org) and a hillshade map. Black square shows the structurally disturbed extra-crater terrain.

Whereas the rim is mainly Appalachian basement metamorphic rocks, the intra-crater region and the crater floor consist of mixed sedimentary units that characterized the upper stratigraphy of the target area. These sedimentary units are Upper Cretaceous formations, consisting of Tuscaloosa Group and Eutaw Formation. Mooreville Chalk, which lies above the Eutaw Formation outside the target area, is also present in some places. The Tuscaloosa and Eutaw show evidence of original bedding, even though that bedding may be deformed or upside down in some places (Heider and King, 2016), but the Mooreville Chalk in the crater area shows evidence of being re-deposited (probably by return of tsunami flow or resurge; King and Ormö, 2011). Re-deposited layers of the uppermost target unit, the Mooreville Chalk, occur as thin, intermittent beds at and near the ground surface, both within and near the crater. This chalk, which is more like marl in composition, contains shelfal fauna and a small component of fine Wetumpka ejecta including melt particles, shocked grains, and impact-formed aggregates (Petruny and King, 2018). CT-scan studies by Markin and King (2012) and Markin (2015) show that there are graded beds within the crater-floor Mooreville Chalk, which supports the resurge hypothesis for its origin.

Previous Work

The earliest research suggesting an impact origin for the crater is summarized in the work done by Neathery et al. (1976). However, confirmation of an impact origin was first provided by King et al. (2002) through investigation of drill-core samples of crater-filling breccias. King et al. (2002) reported presence of multiple sets of planar deformational features (PDFs) in numerous quartz grains from the sandy matrix of impact breccias recovered from depths of over 100 m. PDFs are micro-scale sets of closely spaced planar fractures that form in framework silicate minerals like quartz and feldspar, and are one of the most important evidences of shock metamorphism. PDFs within framework silicate minerals are not known to form in any way other than by hypervelocity shock wave damage to crystal structures. As corroborating evidence of impact, King et al. (2002) also found elevated concentrations of Ir,

Co, Ni and Cr in the matrix of these impact breccias, which is a typical meteorite-imbued chemical signature. They interpreted the impactor to have most likely been a carbonaceous chondrite asteroid.

Because it is a marine impact crater, the Wetumpka crater's morphology and early modification was probably strongly by the presence of water. For example, the heterolithic, unconsolidated and water-saturated southern rim would have been weaker as compared to the indurated, crystalline northern rim and likely would have slumped inwards almost immediately after the collapse of the transient crater, thus leaving the northern rim intact (King and Ormö, 2011). Heider and King (2016) suggested a sequence of events in the inward slumping, including (from first to last) mixed provenance impactite sands, the trans-crater slide unit of bedded Upper Cretaceous target strata, and a boulder-bearing polymict breccia. Subsequently, these field interpretations were supported by digital model simulations of Wetumpka's marine impact (De Marchi et al., 2019), which indicate a sequence of events in Wetumpka's rim failure consistent with the observed crater-filling stratigraphy. The digital model of De Marchi et al. (2019) indicates that return of shallow sea water was a relatively late event, which is consistent with the relatively thin, discontinuous blanket of Mooreville Chalk as a marine resurge deposit formed in a very shallow marine target setting.

Geophysical data from across the crater are restricted to one trans-crater gravity survey and its initial interpretations by Wolf et al. (1997), plus some further work by Robbins et al. (2011). The results of the gravity survey were characteristic of a typical complex impact crater and showed a negative gravity anomaly in the center of the crater, which might be interpreted as evidence of impact-related broken rock below the crater center, plus a small high area that may be evidence of a possible central peak. However, no discernible surficial expression of a central uplift is seen in the present topography of the crater.

Two drilling projects inside the crater, one during 1998 (King et al., 2002), and the other during 2009 (King and Ormö, 2011), resulted in the acquisition of drill-core samples from near the center of the impact structure, as well as from the crater rim and crater moat area (Figure 5). These drill cores have been studied and analyzed by several graduate students in the Department of Geosciences, Auburn University. Specifically, the two 1998 drill cores from the crater center were analyzed and logged by Reuben C. Johnson (Johnson, 2007), whereas some of the latter ones from the crater floor have been analyzed by James K. Markin (Markin, 2015) and Steven N. Rodesney (Rodesney, 2015). A drill core on the western rim was described and interpreted by Pascual Tabares (Rodenas, 2012).

The current work focuses on Wetumpka's central breccia deposit, which is located near the geographic center of the crater floor. This breccia unit was first described by King (1997) as a polymict impact breccia unit. This breccia unit is very poorly sorted and consists of a small but noteworthy population of very large clasts of quartzitic schists and gneisses that are situated within a pebbly and clayey-sand matrix. This breccia crops out in a small area (approximately 0.5 km^2) along a local residential road (Buck Ridge Road), which forms a small loop that encircles most of the central breccia outcrop upon the crater floor (Figure 6). As this breccia unit lies approximately where a central uplift would normally be expected, it was originally thought to be part of a central uplift (Johnson, 2007). However, after drill cores were obtained that penetrated this breccia unit and thus its subsurface extent was known, it was determined that this unit is not related to deeper breccias at Wetumpka (King and Ormö, 2011).

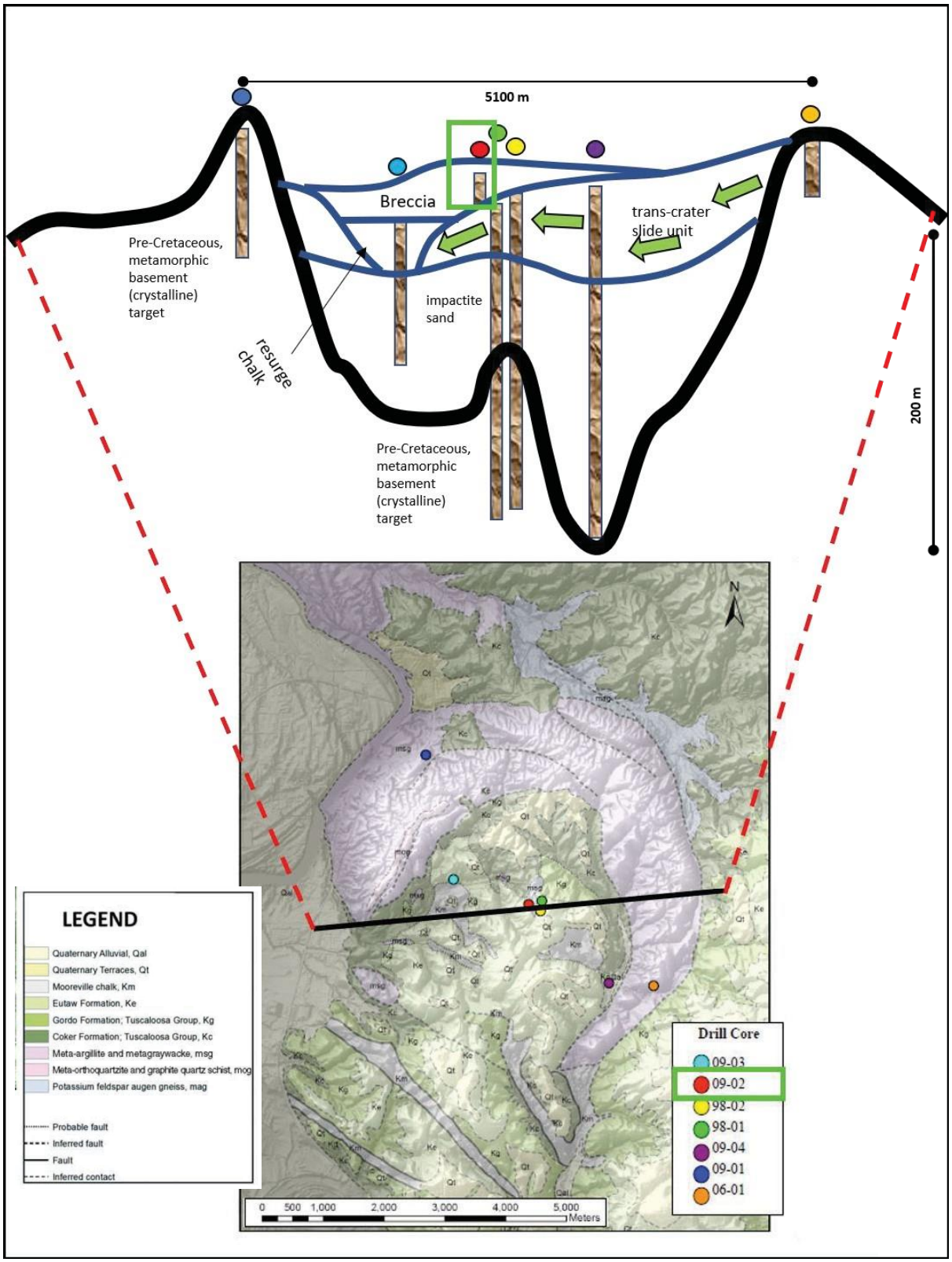

Figure 5: (Top) A profile of Wetumpka (heavy black line) derived from the gravity data of Wolf et al. (1997), which also showslocation of drill cores in the crater. (Bottom) Map of Wetumpka showing the drill core locations (From Rodenas, 2012).

Discovery of shocked quartz within this central breccia unit, specifically quartz grains with shock features that were demonstrably different from those found within quartz grains from the deeper Wetumpka breccias, was the first indication that the central breccias might be of ejecta origin (Morrow and King, 2007). This led to the preliminary interpretation of the central breccia as being part of the proximal ejecta of Wetumpka impact crater that may have been deposited on a failed part of the crater rim (King and Ormö, 2011; King et al., 2015). Slumping or a related type of mass-movement processes during early modification of the crater was suggested as a mechanism for placement of proximal ejecta upon the crater floor (King et al., 2015).

Core drilling and field observations have shown that the subject of the present study, the polymict boulder-bearing breccia, has a stratigraphic position within the Wetumpka crater fill that is atop the trans-crater slide unit (King et al., 2019). Recent observations suggest that the central breccia unit is a matrix-supported diamicton (Chinchalkar and King, 2018), which is composed of clasts ranging in size from pebbles to boulders. Grain sizes in the matrix of the Wetumpka diamicton are clay-dominated, but also contain a significant proportion of non-clast supported pebbles, cobbles, and boulders. The grain-size distribution is strongly bi-modal. In three sequential outcrops on the western side of Buck Ridge Road, several exposed boulders range in size from 15-20 m in apparent long dimension. Lithologically these are mica schists, quartzitic schists and gneisses, which means that all these boulders came from the deeper target metamorphic basement rock that underlies the Upper Cretaceous soft sediment of the upper target layer (King et al., 2015; Chinchalkar and King, 2018). The foliation in these boulders is consistently vertical, which indicates the role of a specific physical process or sequence of processes in the origin and emplacement of the unit.

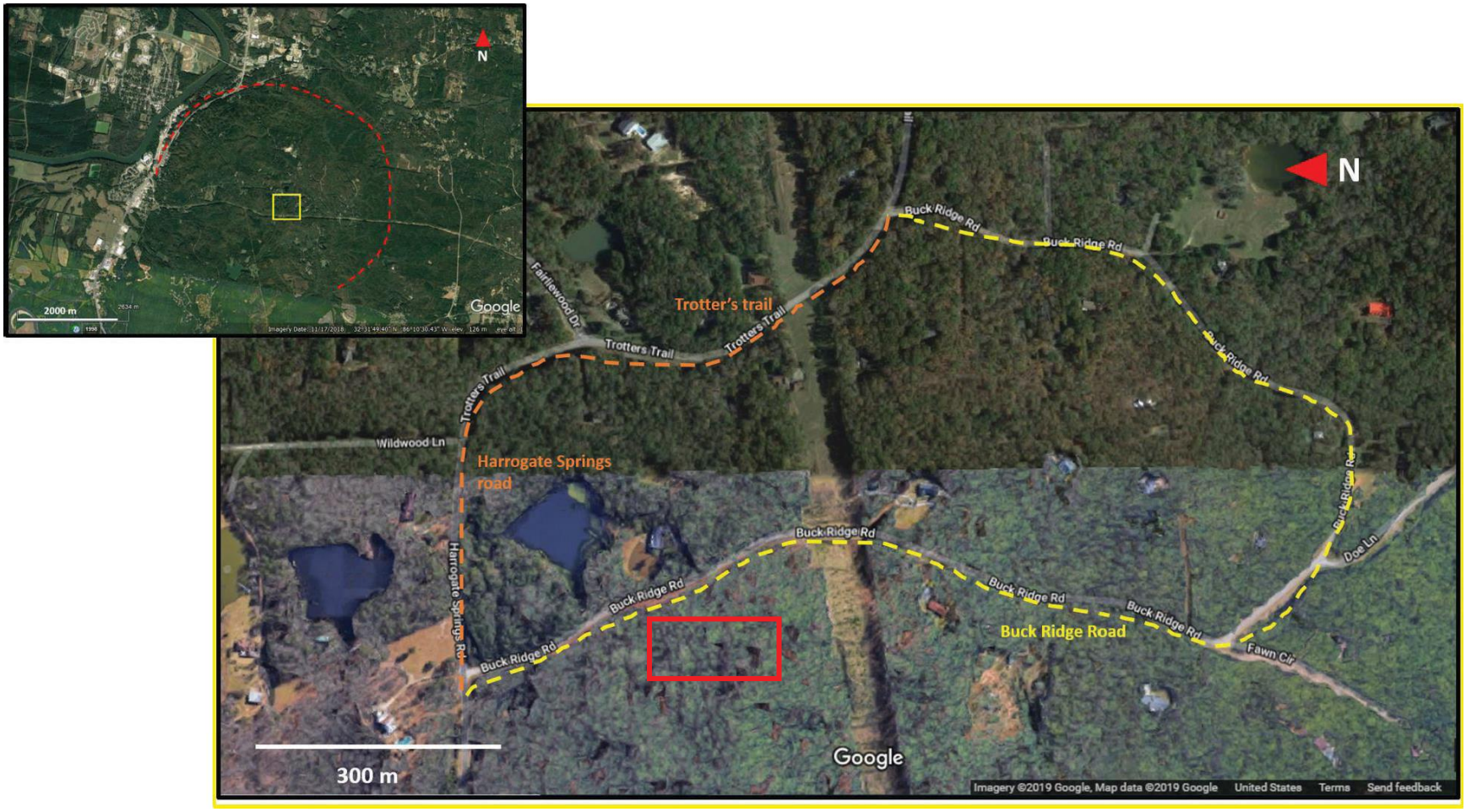

Figure 6: Google Earth © image showing the Buck Ridge Road loop marked by dashed lines and approximate location of studied outcrops marked with red square. Inset is a Google Earth © image of Wetumpka (scale: 2000 m) showing the extent of crater with red dashed line and the location of buck ridge road with a yellow square.

METHODOLOGY

The current project was undertaken with the aim of understanding the characteristics and origin of the impact breccia that crops out within small areas near the central portion of Wetumpka Crater's floor. This breccia unit's shocked quartz grains have been previously studied by Morrow and King (2007) and King et al. (2015), and its stratigraphic relations examined by King and Ormö (2011) and King et al. (2015). These previous studies suggested that the shocked quartz grains were likely evidence of proximal ejecta, and their observations provided a starting point for the present work.

Proximal ejecta of impact craters is known to contain a combination of shocked target material, which contains a mixture of shock level indicators and a mixture of shocked and unshocked target rocks and minerals. Hence, the adjective polymict is commonly used for such impact deposits. The shocked portion of proximal ejecta has been identified with distinctly diagnostic features that develop in the minerals at high shock pressures (King et al., 2015). One purpose of this study was to look for other indicators of impact ejecta and evidence of emplacement mechanisms for this central breccia unit. This was undertaken in order to lead to a better understanding of the origin and mode of emplacement of this diamicton within Wetumpka impact structure. The disparate field and laboratory methods adopted for a comprehensive investigation of the breccia unit are listed sequentially within this methodology section.

Selection of outcrops

A major portion of land in Wetumpka is privately owned by individuals who have residences on their property, therefore any field work in the area requires permission from the land owners. The vast majority of the crater floor area is also densely covered with

thick vegetation. Mainly on account of these two realities, it is best to work on outcrops that are located along paved roads where there is a standard right-of-way for public access and where the road margins are maintained clear of dense vegetation. Specifically, the right-of-way outcrops occurring along Buck Ridge Road (Figure 7), a road that forms a loop around a large part of the central breccia's main exposure, are the ones most easily accessible and therefore used for the study. These outcrops also allow for a direct observation of a small cross-sectional profile of the breccia unit and are well-situated for taking samples, photographs, and direct measurements of the breccia's lithic components.

Outcrop excavation

During early November 2017, reconnaissance field work was conducted to identify potential outcrops for potential excavation. One outcrop (named herein as BRR-O; Figure 8), which is close to the Schroeder home on Buck Ridge Road was the subject of previous studies regarding the breccia (Morrow and King, 2007; King et al., 2015). Newly selected outcrops (named herein as BRR-N1 and BRR-N2; Figure 9), which are located a few 10s of meters uphill (going south on Buck Ridge Road), were also chosen to be part of this study because they constitute good outcrops of the central breccia unit. These new outcrops are stratigraphically higher than BRR-O.

The new outcrops were overgrown with tree roots and other vegetation and were covered in slumped lateritic soil. Presence of excessive vegetation on the outcrop is an obstruction to observing and photographing the breccia, and the soil can cause difficulties in proper investigation of the lithology (because much of the matrix of the breccia is composed of red-colored ferruginous clayey sand). Hence, it was necessary to clean the outcrops to rid the breccia of the vegetation and soil.

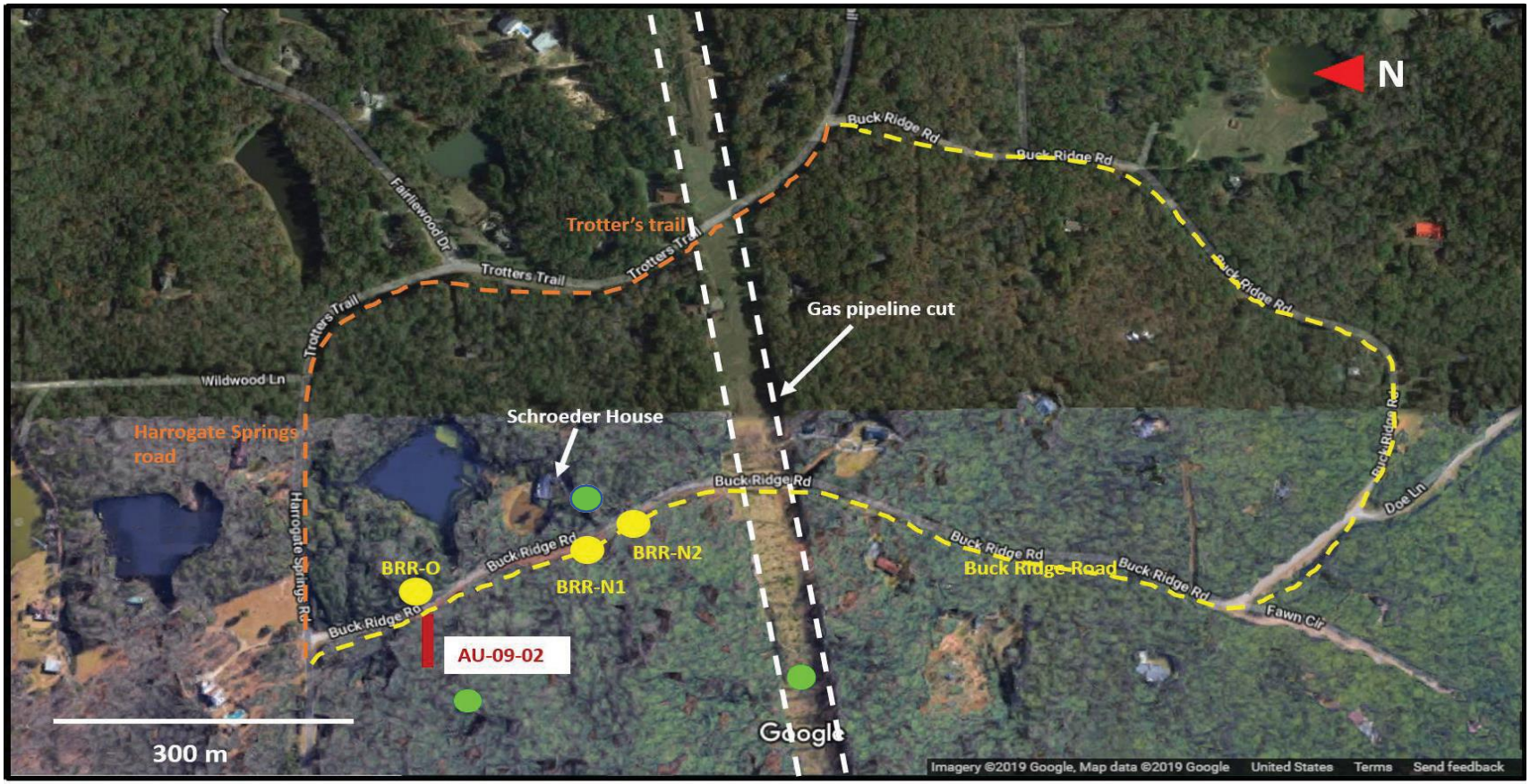

Figure 7: Google Earth ©image showing the Buck Ridge Road, some important landmarks, and locations of outcrops studied for this project. The yellow circles represent the boulder-breccia units investigated in this study and the green circles denote locations of other known boulders that were not included in the current project. The location of the drill core from AU scientific borehole 09-02 is marked with a red bar.

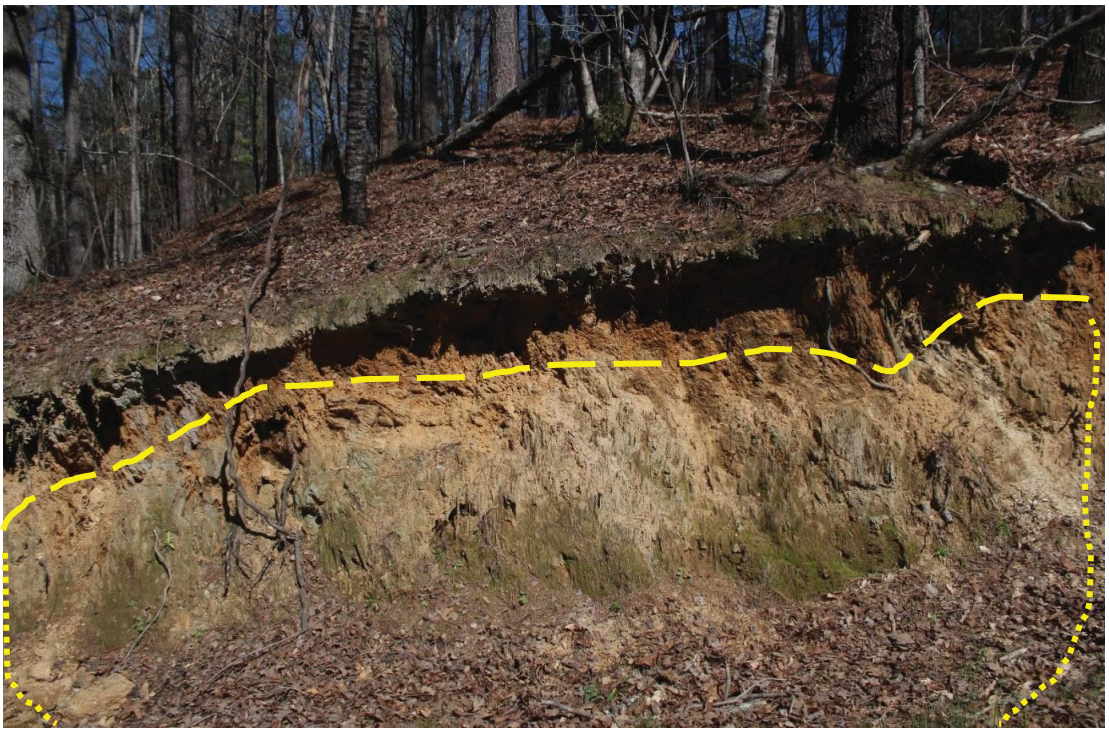

Figure 8: Outcrop BRR-O on Buck Ridge Road close to the Schroeder House. Figure BB1: Close up of outcrop BRR-O showing part of a schist boulder (demarcated with yellow line).

Figure 9: Outcrops BRR-N1 (top) and BRR-N2 (bottom) on Buck Ridge Road before excavation (Width of outcrops is about 10 m and height about 3 m).

The excavation was accomplished during the month of June 2018 by a work crew from the Public Works Department of Elmore County who used large mechanical excavators (Figure 11). Because these outcrops lie close to the road and the road-side ditch draining the area lies adjacent to a small creek, adequate erosion control measures such as rip-rap and straw-netting were deployed at the site by the workers. The outcrops were scraped clean and the top soil was loaded in trucks and removed from the area (Figure 10).

After this outcrop scraping process, the newly formed outcrops were allowed to sit undisturbed for a few weeks while they were naturally washed by rain and thus more easily observed in a fresh but slightly eroded state.

Figure 10: Outcrops BRR-N1 (top) and BRR-N2 (bottom) after excavation (Height of outcrop is about 3m).

Figure 11: Excavation of outcrops by Public Works Department crew (top) and an example of erosion control measures implemented at the site (bottom).

Field mapping

Once the outcrops were free of unwanted organic rich top layer and soil and had been slightly washed by rain, field mapping techniques were used to produce a detailed description of the characteristics of the matrix and clasts, including photography, mapping, and sampling.

Photographing outcrops

All the outcrops were photographed in high resolution with the help of a DSLR camera and photo-editing software was used to compose panoramic photo mosaics (Figure 12).

Mapping of boulders and cross section

In order to accomplish detailed mapping, the global positioning satellite (GPS) locations of each outcrop were obtained by instrument and plotted on a geologic map. The breccia unit consists of boulders as large as 20 m in apparent diameter, and the locations of the apparent centers of these boulders were also obtained, along with measurements of their dimensions and structural features like strike, dip and orientation of internal foliation. Although the primary outcrops for the study were the ones along the Buck Ridge Road, the locations and dimensions of boulders in the other outcrops of the breccia within the area were also noted for providing geologic context and for understanding the extent of the unit. These other adjacent areas included the El Paso natural gas pipeline cut at Buck Ridge Road, the driveway of the Schroeder home on Buck Ridge Road, and the valley of an unnamed stream draining from the main lake on the Schroeder home property on Buck Ridge Road and along Harrogate Springs Road (to an eventual junction with the Coosa River at a point near the present Wind Creek Casino.

Figure 12: Panoramic photographs of outcrop BRR-N1

Meter grids

To understand the size distribution of clasts and relative amount of clasts tomatrix in the breccia, one-meter-square grids were posted using string and nails upon selected, representative sections of the intra-boulder matrix of the three outcrops. The meter-square area was used to measure clast dimensions (i.e., longest and shortest axes) and to assess clast size, shape, and density in a standard area for each outcrop. These data were used to help describe the breccia matrix and to present frequency distribution of clast size, as discussed in the results section.

Sample collection

Samples of clasts and matrix were collected from each of the outcrops for further analyses. The matrix of the breccia consists of mixture of target sands composed of shocked and unshocked material, whereas the clasts are mainly unshocked crystalline schistose or gneissose pieces of target rocks. As shock effects were known to exist in the minerals of the breccia the matrix, all of the petrographic analyses were done on the matrix itself rather than the constituent clasts. Matrix samples collected from the newly excavated outcrops (BRR-N1 and BRR-N2) consist of bright red-colored, iron-rich clayey sand, whereas the matrix from the previously known outcrop (BRR-O) consists of two distinct sands, one similar to the aforementioned red clayey sand, and another more siliceous, grey- colored sand.

Petrographic analysis

Samples collected from the three outcrops were sent to National Petrographic Services, Houston, for preparation of uncovered, polished thin sections. A total of 12 thin sections of the matrix, which came from all three BRR outcrops, were made for petrographic analysis. Petrographic descriptions were made for each thin section by

documenting the dominant mineralogy, relative percentage of the abundant minerals as well as any features that may be related to shock metamorphism. The petrographic analysis also served as a preliminary step for electron microprobe analysis.

Electron Microprobe analysis: Sample preparation, probe parameters, techniques and tools, image processing.

Based on an initial petrographic study under a standard petrographic light microscope, 2 thin sections, one from BRR-O and the other from BRR-N2, were selected for electron microprobe analysis. Electron Microprobe analysis was done on the JEOL – JXA 8600 Superprobe and accompanying Geller System automation in the Department of Geosciences, Auburn University. The thin sections were carbon-coated in the microprobe lab and inserted in the probe with the specimen holder. The AU microprobe is equipped with BSE and SEM imaging along with EDS and WDS detectors, which were instrumental in understanding the composition of mineral phases in the matrix. BSE and SEM images were obtained at a current of ~ 40 mA and an accelerating voltage of 15KeV. EDS detector was used to evaluate the qualitative composition of mineral phases in the matrix and quantitative spot and line analyses by WDS were performed on some minerals to determine major oxide weight percentages. The standards used for peak calibration and standardization are listed in the appendix at the end. Elements like Fe, Al, Si, Na, Mg, K, and Ti were mapped within certain areas of the thin section. The following software programs were used for each of the analyses:

(i.) Geller System dPict: BSE and SEM Imaging and Elemental Mapping

(ii.) Geller System dQuant and dSpec: Spot and line analyses for major oxide weight percentages

(iii.) Princeton Gamma Technologies Excalibur: EDS analysis

(iv.) National Institute of Health Image J: Image processing

Drill core analysis

Drill core from AU scientific borehole #09-02 was used for the current study to understand the subsurface lithology and characteristics of the impact breccia. During 2009, this core was obtained by Department of Geosciences, Auburn University, using funding from a NASA PGG grant. The core hole was drilled adjacent to the outcrop BRR-O (near the Schroeder house on Buck Ridge Road; for exact location). This drill core was obtained in order to better understand the vertical extent of the central breccia unit and its underlying stratigraphic relationships. The total length of the central breccia drill core is 23.3 m.
The #09-02 drill core was photographed and logged with respect to the relative proportions of clasts and matrix, clast lithology, matrix mineralogy and sedimentological/structural features. The results from core logging were compared to the results from the outcrop mapping (and meter square grids) to compare the subsurface extent of the central breccia to the exposed central breccia in outcrop. An example photograph of a drill core box is in Figure 13 and other core box photographs are located in the Appendix.

Figure 13: Example of a drill core box of borehole #09-02. Top of core is upper right of box and bottom is bottom left.

RESULTS

Field study and outcrop mapping

For the current study, three outcrops on Buck Ridge Road were selected and investigated for detailed description of lithology and sedimentological characteristics. The outcrops are designated as BRR-O, BRR- N1, and BRR-N2 for the previously known (old) outcrop and the two recently excavated outcrops, respectively. The location of each outcrop is depicted in Figure 14.

The old outcrop is located adjacent to the Schroeder family house on Buck Ridge Road. It is 63 meters in length and the exposed height varies from 2 to 4 meters. The outcrop consists of matrix, small boulders, and a boulder of schist with an exposed length of 19 meters (Figures 15 and 16). The boulder's foliation strikes NNE-SSW with an almost vertical (~90^{o}) dip. The schist consists mainly of muscovite mica and quartz and is generally similar to the Emuckfaw Schist observed in the western rim of the crater. Therefore, these schistose rocks are interpreted to be basement rocks of the Appalachian orogenic belt. This large schistose boulder only makes up part of the outcrop. The remaining outcrop is mainly polymict breccia consisting of a fine-grained matrix, which consists of clay, silt, sand, and a wide range of crystalline clast sizes.

The matrix of the breccia is composed of ferruginous to silicic sand with a wide range of sizes and fine clay. Within the outcrop, the matrix shows two distinct compositions. Some of the matrix is red due to a high amount of iron, and some matrix is light grey to buff-colored due to low iron content and more silica. There is no sharp boundary between the two types of matrix, and it appears to be mixed together.

The clasts of the breccia range in size from pebble to boulder sizes and are randomly oriented. For a more quantitative analysis of the clast sizes, a one meter-square grid was prepared and laid on the outcrop and clasts were counted along with measurements of their observable dimensions (with a cut off size of 5mm). The results of this counting are presented below in Table 2 and Figures 17 and 18, and the complete data can be found in Appendix.

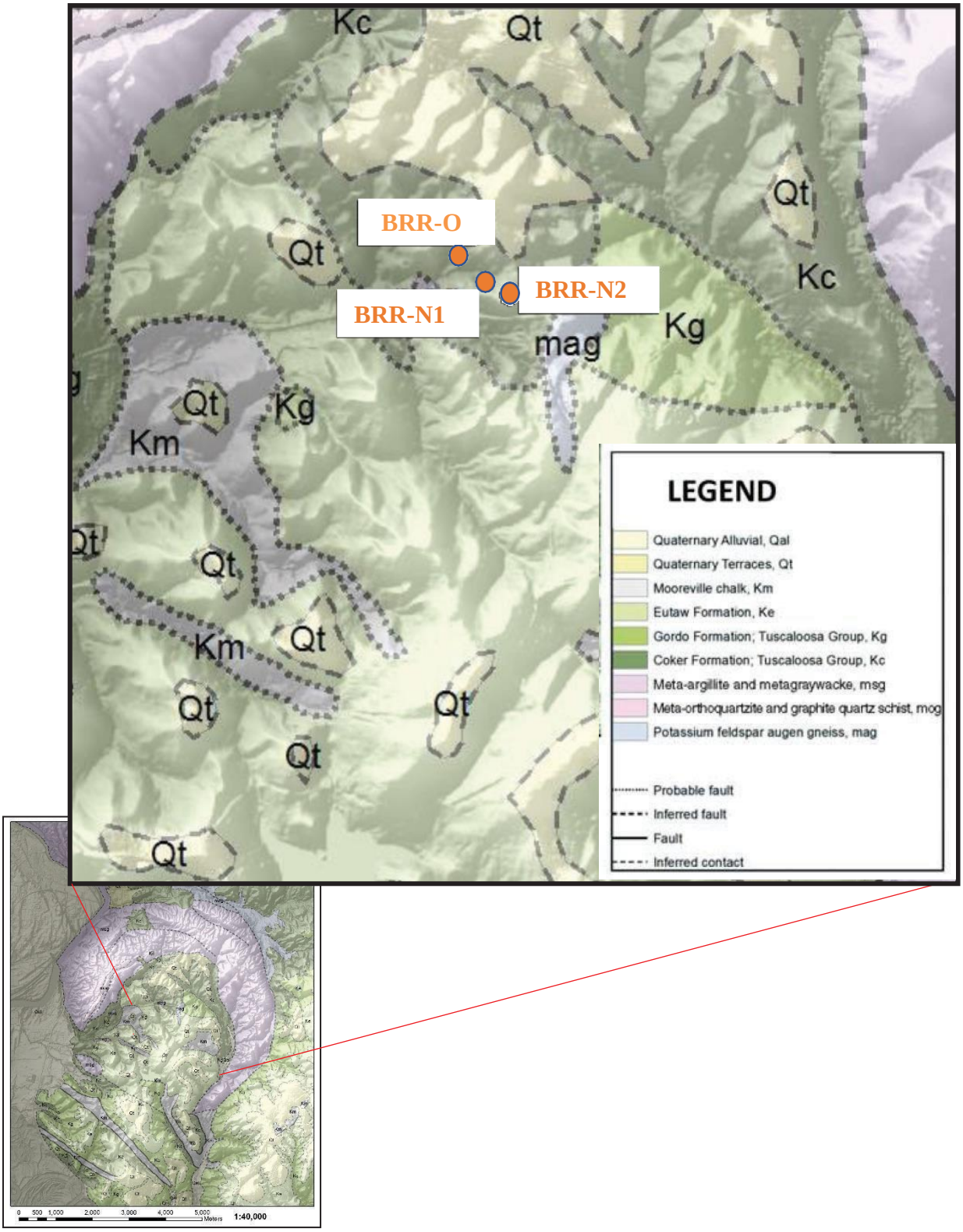

Figure 14: Locations of the outcrops of central breccia on a geologic map of Wetumpka (Base map from Rodenas, 2012).

Figure 15: Breccia outcrop at Buck Ridge Road with a boulder of schist embedded in a clayey-sandy matrix (Width of outcrop is about 25 m and height is about 4 m). Close up of area in red box is shown below.

Figure 16: Close up of the schist boulder showing a nearly vertical foliation.

Class limit	Frequency
<10	5
11 - 20	10
21 - 30	12
31 - 40	7
41 - 50	5
51 - 60	3
61 - 70	0
71 - 80	0
81 - 90	1
91 - 100	0
101 - 110	1
111 - 120	0
121 - 130	0
131 - 140	1
141 - 150	0
151 - 160	0
161 - 170	0
171 - 180	0
181 - 190	0
191 - 200	1
>200	0

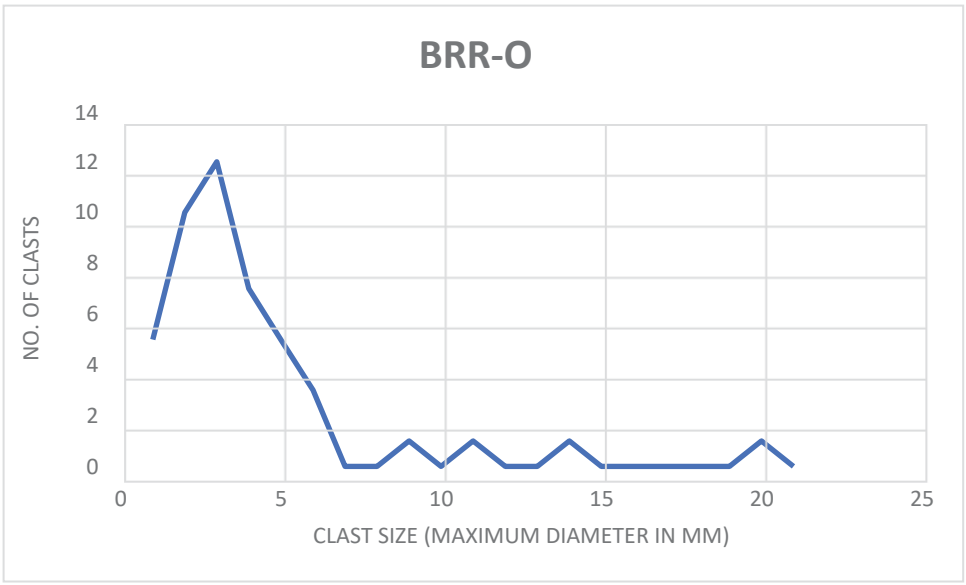

Figure 17: Scatter plot based on Table 2.

Table 2: Frequency distribution of data from meter grid analysis.

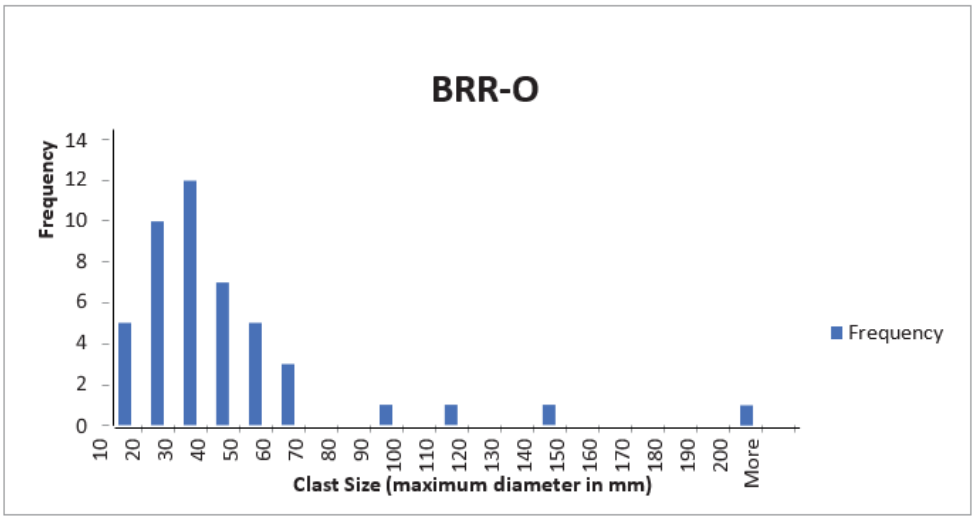

Figure 18: Histogram for the frequency distribution based on Table 2.

The two newly excavated outcrops (BRR-N1 and BRR-N2) are located about 200 meters uphill, i.e. towards south, from the first outcrop. They were created by excavation equipment during 2018. The length of the outcrop BRR-N1 is about 39 m and that of BRR-N2 is about 70 m. These outcrops also contain large boulders of schist (Figures 19-22). A total of 3 boulders are exposed within the two outcrops. BRR-N1 consists of one boulder of fragmented quartzitic schist with an approximate exposed length of 15 m while outcrop BRR-N2 consists of two boulders of mica schists with exposed lengths of 15.8 m and 22 m. The general trend of these boulders is similar to the boulder in the outcrop BRR-O, with a strike of NNW-SSE and an average dip of 85º. Although minor folding and fractures can be seen in the schists, these boulders lack any significant structural deformation other than their nearly vertical orientation.

Similar methods as those used for the older outcrop were used for counting and measuring clasts within the outcrops. The results are presented below in Table 3 and Figures 23 and 24, and complete data is given in the appendix. The clasts of the breccia range in size from pebble to boulder sizes. Lithology of the clasts is mainly mica schist with occasional quartzite. These clasts, unlike the large boulders, are randomly oriented. The matrix in both these outcrops is rich in iron and is stained red with particles ranging from coarse sand to fine clay. The grey matrix which was seen in BRR-O is absent from these outcrops. The nature of these outcrops as seen from the presence of large, oriented schistose boulders along with smaller clasts in a clayey-sandy matrix indicate that these outcrops represent the same breccia unit as the older outcrop.

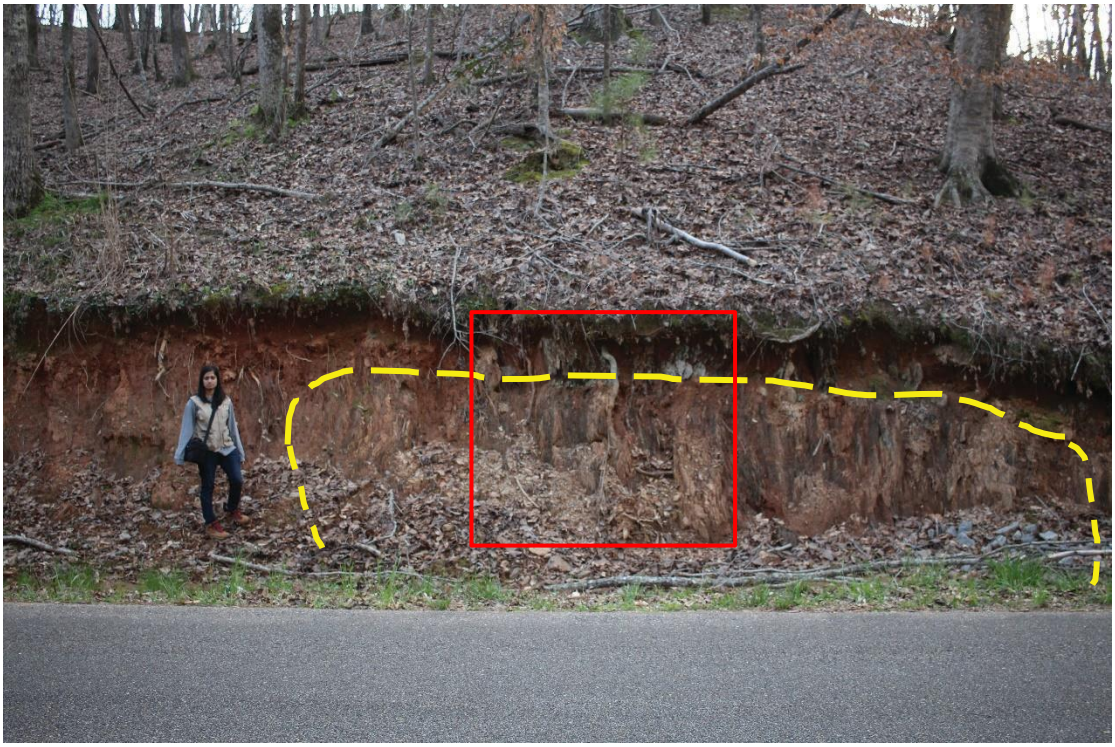

Figure 19: Photograph of outcrop BRR-N1 showing part of a schist boulder. Close up of area in red box is shown below.

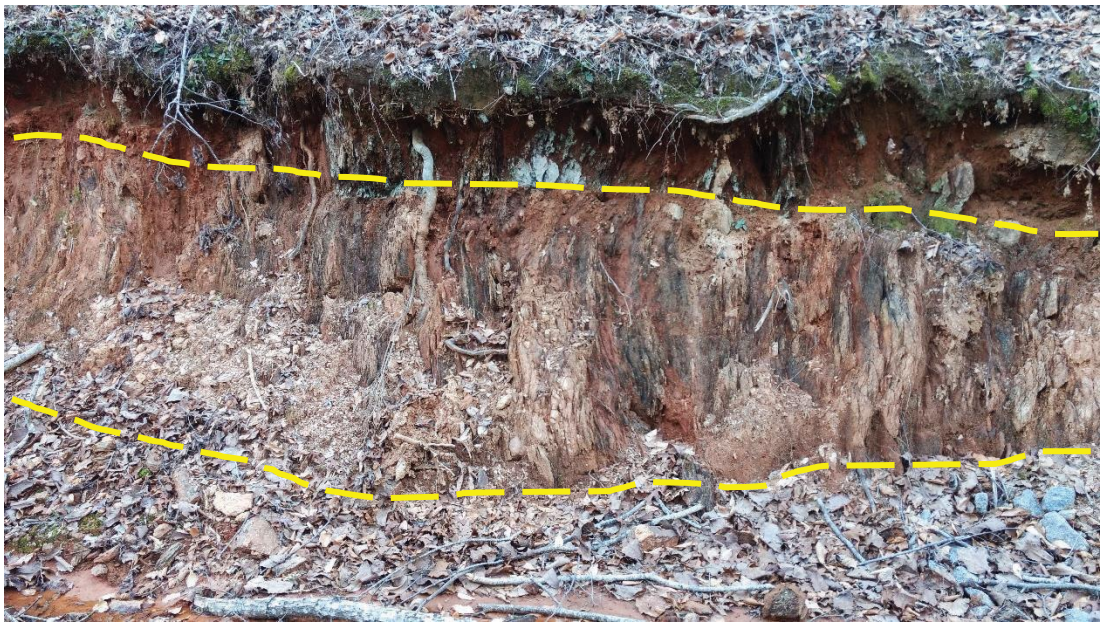

Figure 20: Close up of the schist boulder in the BRR-N1 outcrop. Note the nearly vertical foliation (length of boulder seen in photograph is about 10 m and height of outcrop is 4 m).

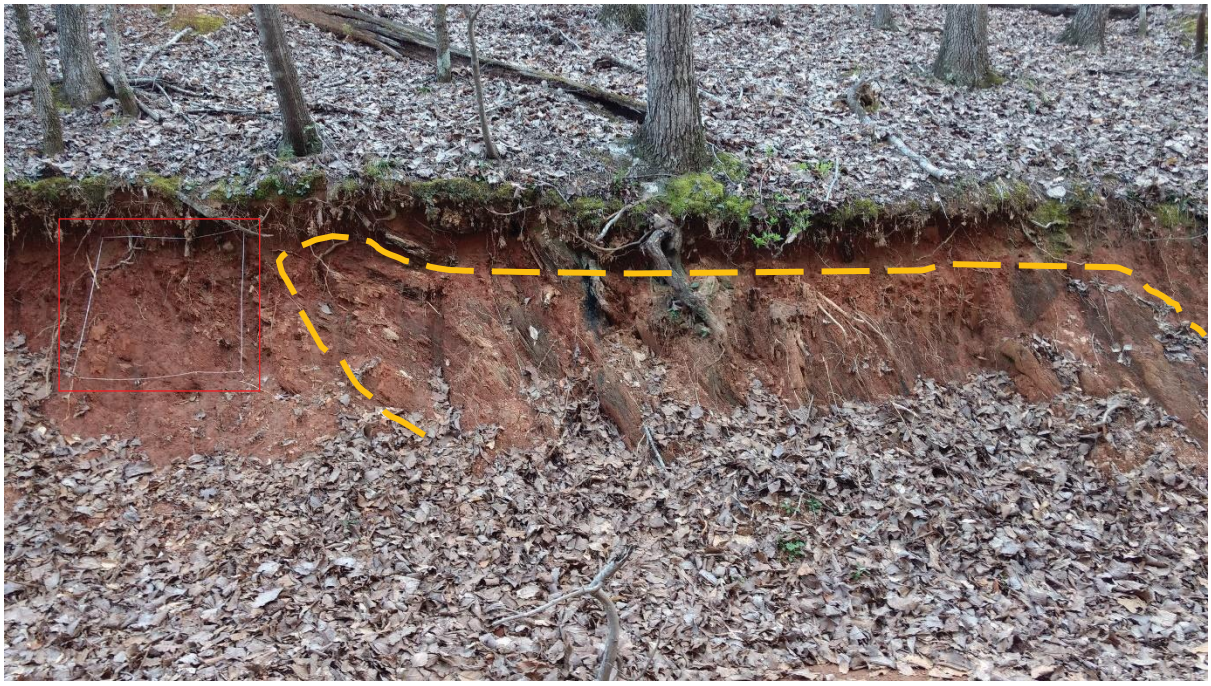

Figure 21: Outcrop BRR-N2 with a boulder of schist (demarcated with dashed yellow line) and a meter-square (red box) grid used for clast counting.

Figure 22: Close-up image of outcrop BRR-N2 showing the nature of clasts and matrix of the breccia.

Class limit	*Frequency*
<10	8
11 - 20	15
21 - 30	8
31 - 40	6
41 - 50	11
51 - 60	4
61 - 70	3
71 - 80	7
81 - 90	4
91 - 100	0
101 - 110	3
111 - 120	2
121 - 130	2
131 - 140	1
141 - 150	1
151 - 160	2
161 - 170	1
171 - 180	0
181 - 190	0
191 - 200	1
201-300	3

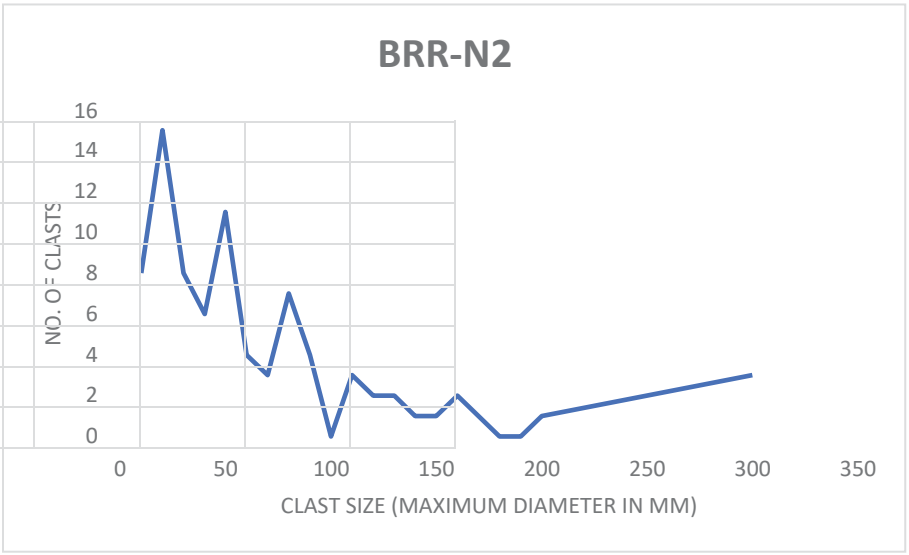

Figure 23: Scatter plot based on table 3.

Table 3: Frequency distribution of data from meter grid analysis.

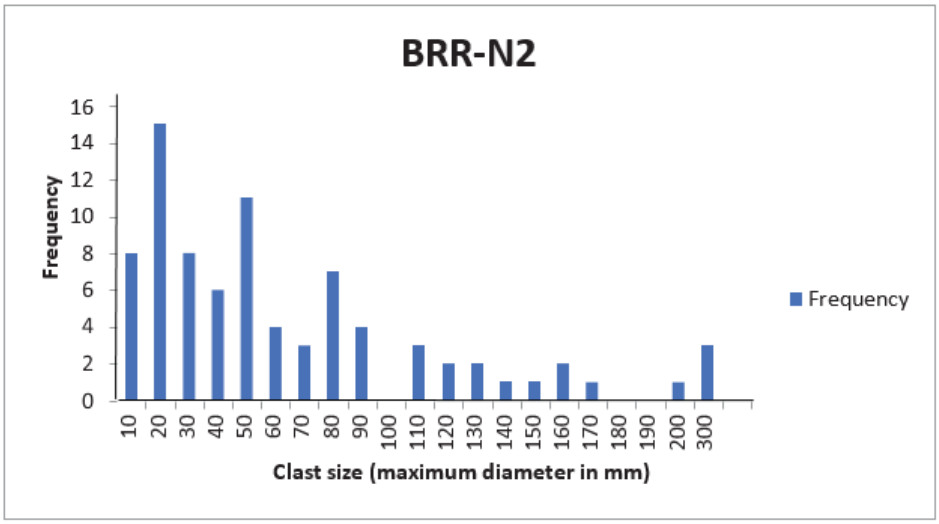

Figure 24: Histogram for the frequency distribution based on clast counts.

Even though clasts finer than 0.5 cm were not considered in these measurements, it can be seen from the counting and clast size measurements that the breccia is very poorly sorted. There is a huge gap in size distribution of clasts in all outcrops. The boulders are ranging in size from 15-20 meters and smaller clasts are ranging in size from 0.5 cm to about 30 cm.

All boulders that are exposed and easily accessible were measured and their locations and altitudes with respect to the sea level were measured. A schematic cross section of the breccia was developed based on the locations of these boulders and is presented in Figure 25.

More boulders than those studied for this project are known to exist (or have existed previously but removed due to recent anthropogenic reasons) in the Buck Ridge Road area. One such boulder, a gneiss, is seen along a creek bed across the BRR-O outcrop. This boulder is located downhill from the Buck Ridge Road outcrops, at approximately 40 m below the BRR-O outcrop. Another schistose boulder was previously seen at the top of the hill where the El Paso natural gas pipeline crosses Buck Ridge Road, which just a few meters uphill from the BRR-N2 outcrop. Thus, in an area of about 500 meters, and a vertical distance of about 50 m, 6 boulders have been located within the breccia. Exact GPS co-ordinates of these boulders can be found in the appendix. A combined result of all outcrops for the qualitative/relative volume percentages of the clasts is presented in Figure 26.

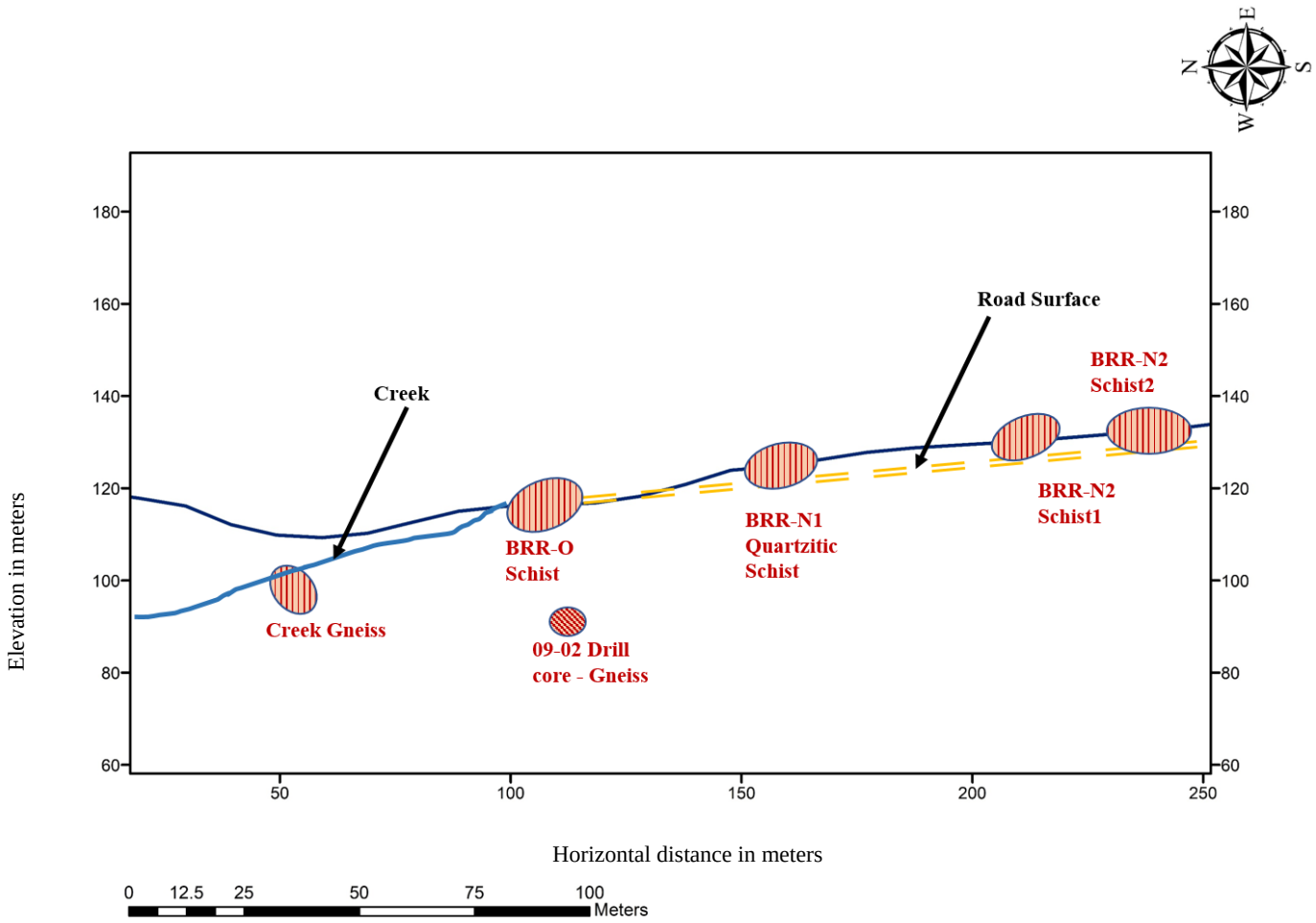

Figure 25: Cross section of the breccia unit at Buck Ridge Road showing the locations of boulders within the unit. Plane of cross section is roughly north-south and the view to toward the east. Note that boulders shown are not to scale.

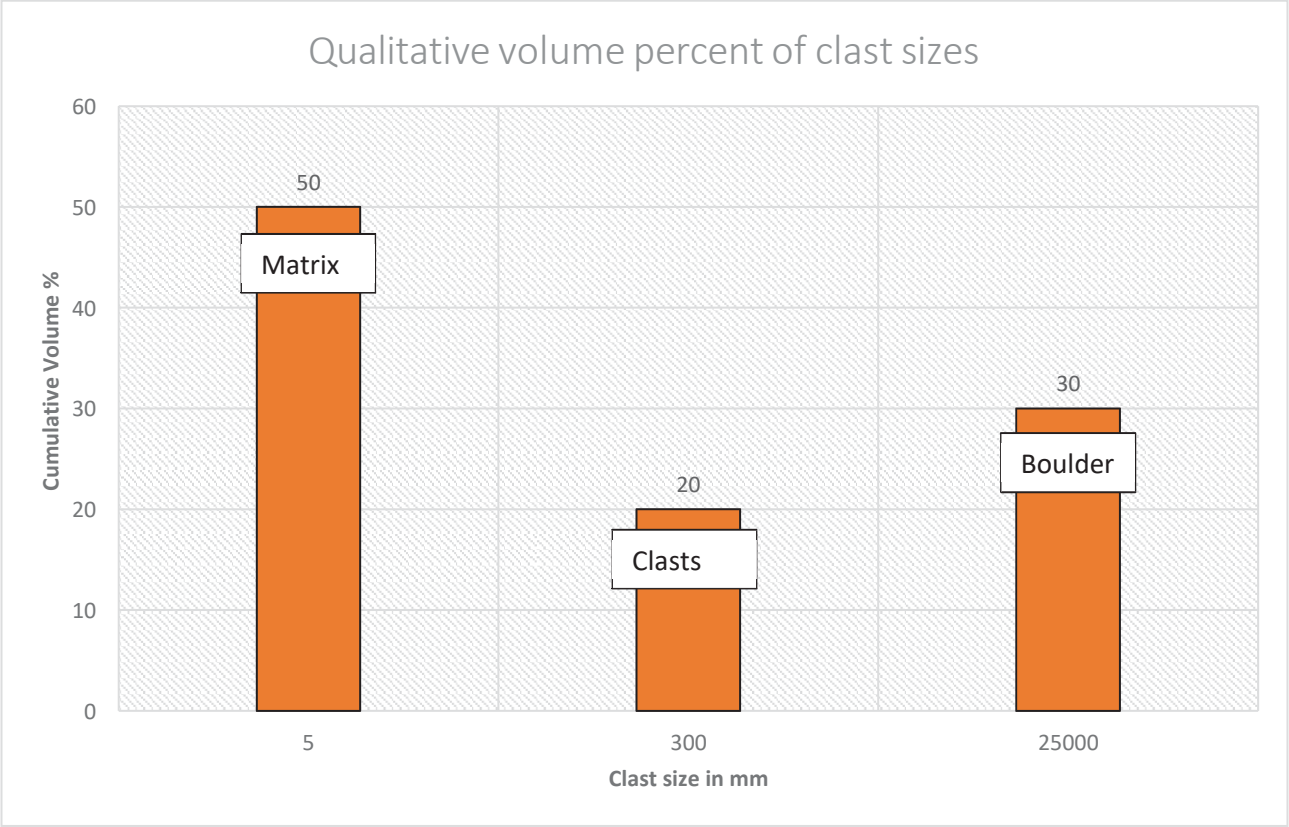

Figure 26: A schematic (approximate) plot showing a qualitative volume percent of the clast sizes and matrix for the areas studied.

Drill Core Logging

The Auburn University scientific drill core #09-02 (Figure 27), which was drilled in front of outcrop BRR-O, was studied in detail for its lithological and sedimentological characteristics. Its close proximity to the outcrop makes it an important resource for the understanding the vertical sequence of the central breccia unit. This core, which has a diameter of 5 cm, was previously studied in lesser detail by Heider (2015). Total length of the drill core is 23.3 m and a vertical description in the form of a core log is presented in the Appendix.

Figure 27: Photograph showing all eight boxes of the AU Drill Core #09-02, which was acquired from in front of the Buck Ridge Road breccia outcrop BRR-O. Core is organized in each box with the top being at the top right of each box and bottom is at the bottom left of each box. Depth markers are in feet.

The top of the core, which starts at 0.3 m depth from surface, consists of buff sand that contains very coarse and angular quartz grains. This sand is similar to the matrix of the breccia seen in the Buck Ridge Road outcrop. It consists of poorly sorted sand with clasts of muscovite schist ranging in size up to 3-4 cm. Mineralogically, this sand is dominated by quartz and muscovite, subordinate amount of biotite and rarely clay.

At about a depth of 2.5 m, the matrix begins to transition into darker colored sand with first a mixture of the buff and red sand and then transitioning to deeper red, more iron-rich sand at 3.5 m. This ferruginous sand continues up to 4.8 m and consists of very poorly sorted angular grains of sand ranging in size up to a cm along with muscovite mica.

A gneiss boulder is encountered at a depth of 4.9 m (Figure 28). This boulder is about 5 m in apparent diameter and is similar to a larger block of gneiss found in the outcrop in the unnamed creek that flows west from Buck Ridge Road. It is strongly foliated with the foliations being more convoluted at the top and becoming more planar towards the deeper end of the block. Compositionally, the gneiss consists mainly of muscovite, quartz, and some biotite. Below the boulder, there is a mixture of poorly sorted buff to grey sand and red sand. These mixed color sands are similar to the sandy matrix of the breccia found in the BRR outcrops, and consists of significant amounts of clay. The sands also contain small sand injections or dike-like cross-cutting structures, which are common in the outcrops. Combined with iron-staining and bleaching in some places, these features give the sand a red to yellow color at greater depths. These red and grey sands appear in alternating sequences and continue to the end of the core.

Figure 28: One of the drill core boxes of borehole #09-02 containing a gneissose boulder. The top of core is upper right and bottom is lower left. Depth markers are in feet.

Petrography and electron probe microanalysis

A total of 12 standard, polished and uncovered thin sections were made by the National Petrographic Services, Houston, Texas, and used in the present study to assess the petrographic characteristics and to conduct electron probe microanalysis of selected samples from the boulder bearing diamictite. All thin sections were prepared from samples of the matrix of the breccia unit. Due to the poorly consolidated nature of the sand, the thin sections were prepared with vacuum impregnation of blue epoxy. The thin sections were investigated using a Nikon standard petrographic microscope. The thin sections were described with respect to the dominant silicate minerals present in the matrix and the accessory heavy minerals. They were also studied with an aim to identify any shock-metamorphic features within the framework silicate minerals. Out of the 12 thin sections, 3 (BRR-B, BRR-OG1 and BRR-N22) were selected for investigation with an electron microprobe. Two of these thin sections (BRR-B and BRR-OG1) were of the matrix from the old outcrop (BRR-O), where shocked quartz had previously been reported (Morrow and King, 2007), and one thin section (BRR-N22) is from the new outcrop and was selected to study in detail some of the opaque phases from the matrix. The instrument used for microprobe analysis was a JEOL- JXA8600 Superprobe in the Department of Geosciences, Auburn University. Petrographic description of the sands in each of the three outcrops is presented in detail below.

The old outcrop on Buck Ridge Road lies near the Schroeder House, about 200 m downhill from the two new outcrops. The new outcrops, which are located uphill from the old outcrop, are relatively very close to each other, separated by about 20 m.

Buck Ridge Road – Old Outcrop (BRR-O)

The sandy matrix of the breccia unit in Buck Ridge Road's old outcrop is very poorly sorted (Figure 29) and consists of a dominant clay portion. The sand occurs as two distinct portions, one being iron-rich with a red-colored appearance in the outcrop and the other being a buff to grey-colored being, apparently, less rich in iron. Both the sands, however, are petrographically very similar. Quartz is present as the most abundant mineral with sizes ranging from less than 0.5mm to more than 5mm. About 60% of the sand is quartz, 25% potash feldspar and about 10% mica (dominantly biotite with lesser amount of muscovite) and minor amount (about 5%) of accessory heavy minerals or opaque oxides. Most of the grains in the sand, about 90%, are angular with roughly 8-9% being sub-angular and less than 1% are sub rounded.

Possible shock features were also documented in the thin sections. Quartz grains are intensely fractured and some also show presence of planar fractures (Figure 30-33). Planar deformational features (PDFs) in the quartz grains in the grey matrix of this outcrop, which were described in earlier studies and had provided unequivocal evidence of the shock origin of Wetumpka (Morrow and King 2007, King et al., 2015), were not found in the samples taken for the present study. Along with fractured quartz, many constituent micas also appear to show intense deformation. Kink-banded micas were found in two of the thin sections from this outcrop (Figure 34). Although kink bands are not diagnostic shock features, their close association with intensely fractured quartz, and previously documented shocked quartz grains, may be of significance.

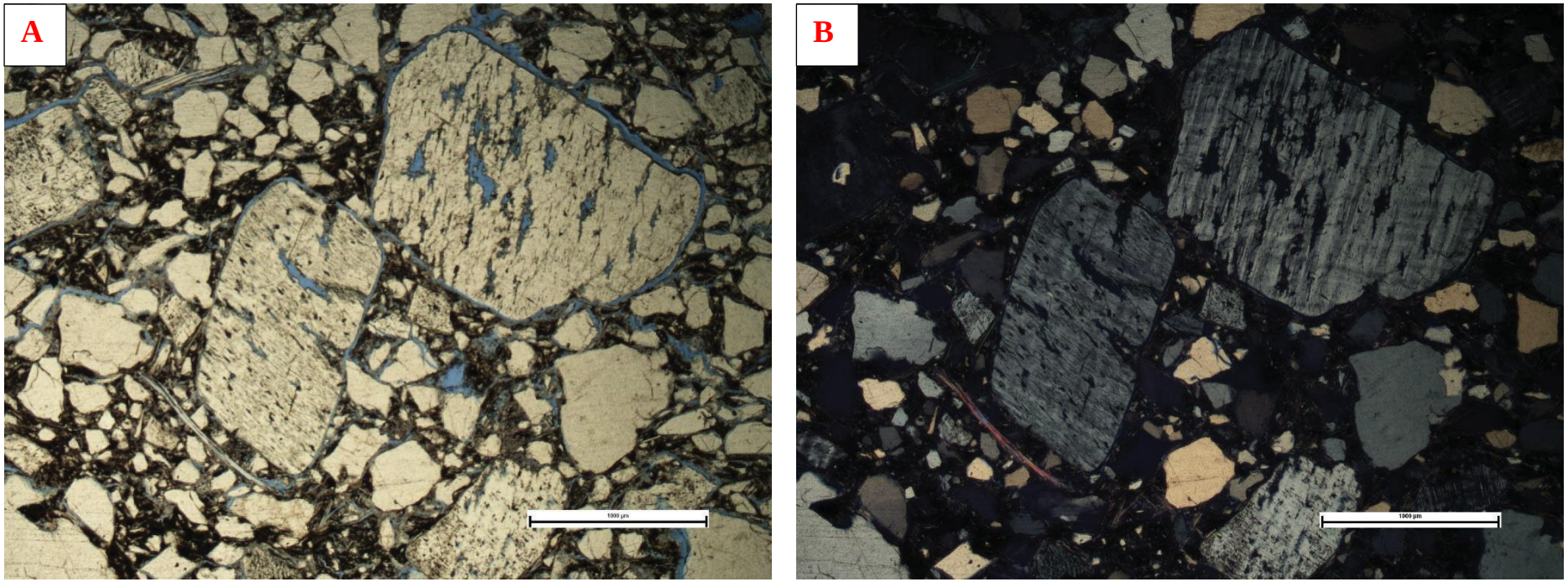

Figure 29: Photomicrograph of matrix of the boulder-bearing breccia in the old outcrop (A: plane polarized light; B: Under crossed polars) showing very poorly sorted nature of the sand. Quartz is present as the dominant mineral with moderate amount of potash feldspar. The minerals are embedded in a matrix of Fe-rich clay. [Thin section BR-OG1, scale of photographs: 1000 um].

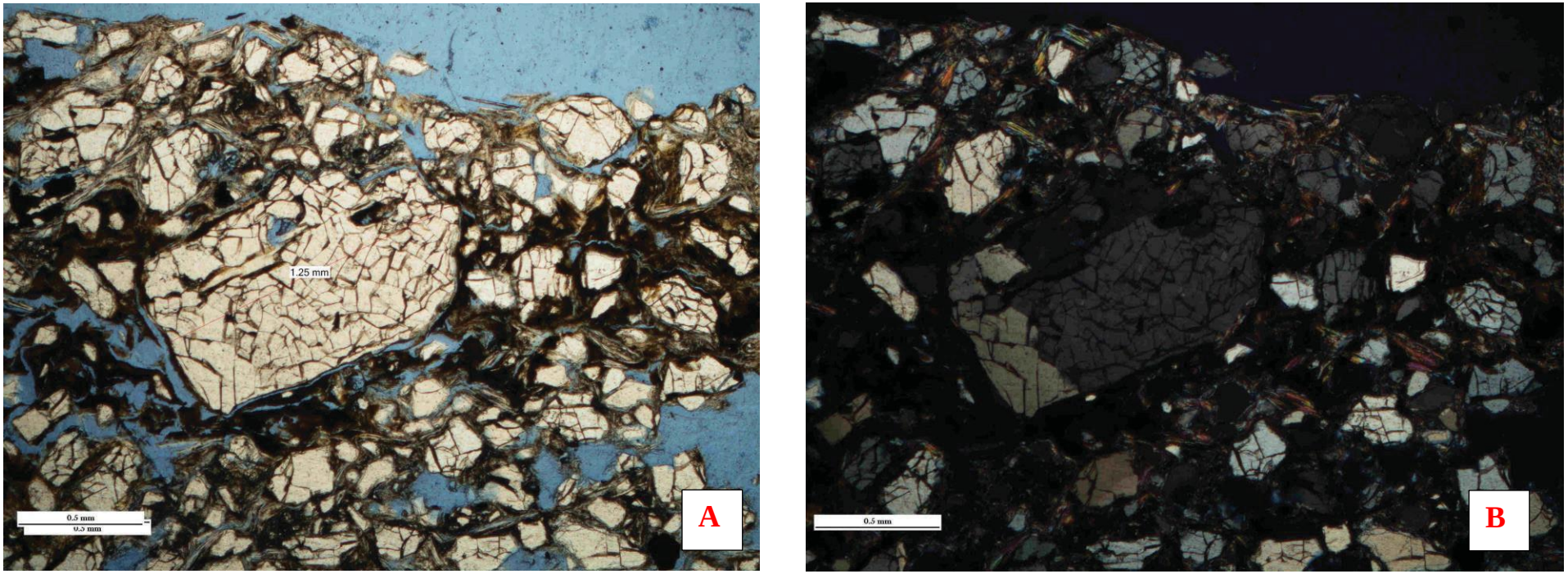

Figure 30: Photomicrographs of intensely fractured quartz grains in the matrix in thin section BRR-OG1. (A: plane polarized light; B: Under crossed polars; Scale: 0.5mm)

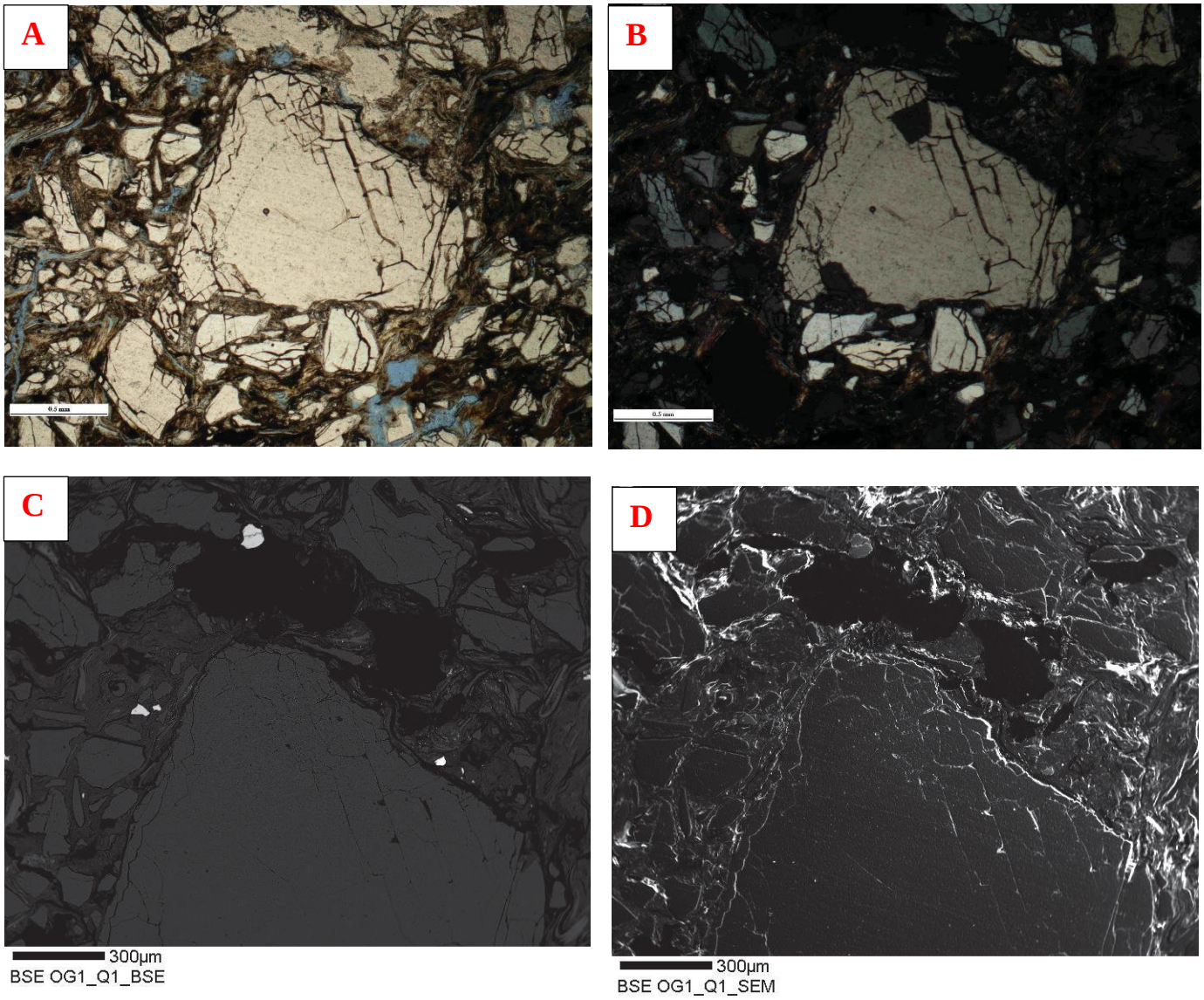

Figure 31: Photomicrographs of planar fractures in quartz seen in this section BRR-OG1: A: under plane polarized light (scale: 0.5 mm); B: under crossed polars (scale: 0.5mm); C: BSE image (scale: 300 um); D: SEM image (scale: 300 um).

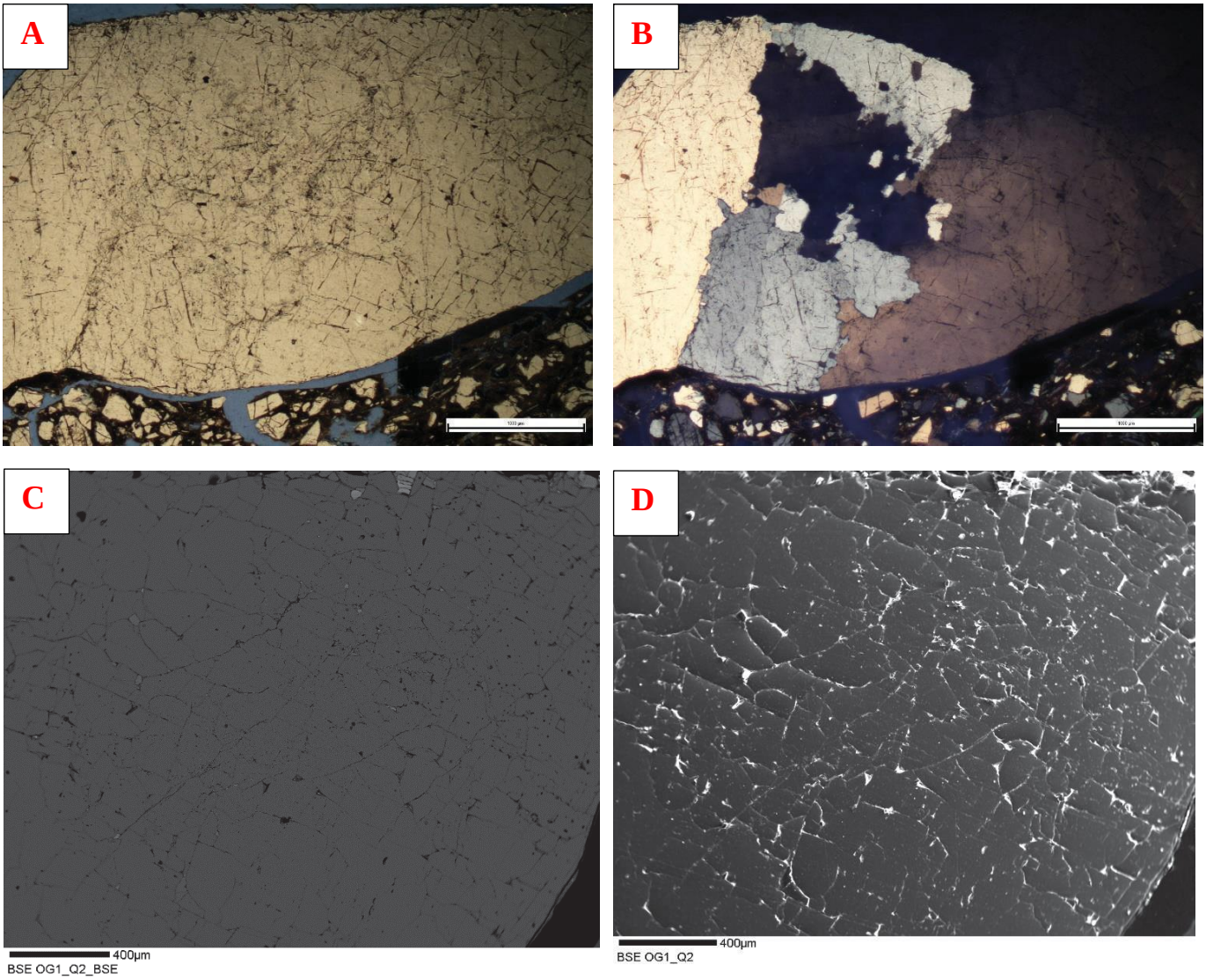

Figure 32: Photomicrographs of planar fractures in quartz in thin section BR-OG1 (scale: 100 um) : A: under plane polarized light; B: under crossed polars; C: BSE image (scale: 400 um); D: SEM image (scale: 400 um).

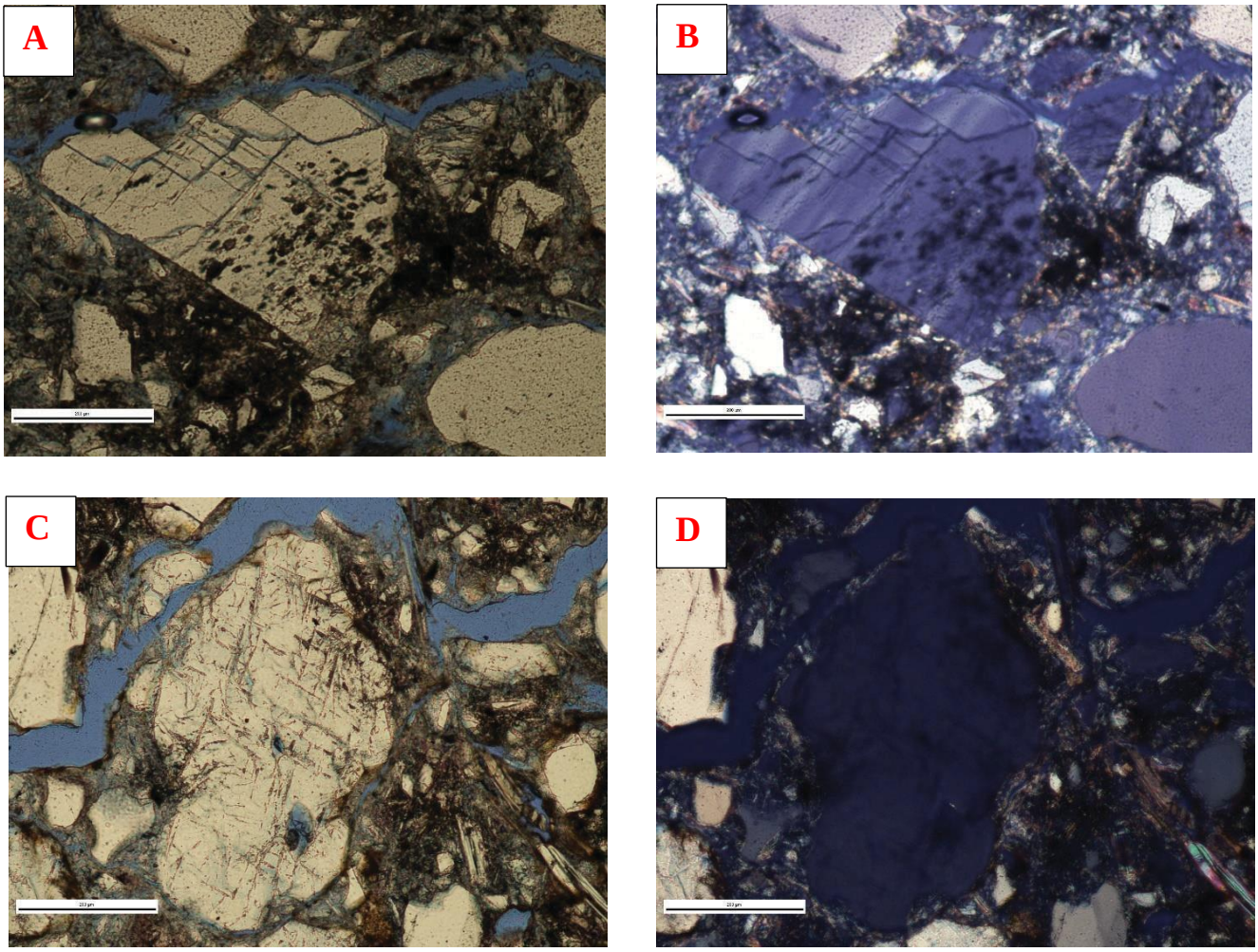

Figure 33: Photomicrographs of planar fractures in quartz in thin section BRR-B; (A and C: in plane polarized light and B and D: under crossed polars (scale: 200 um).

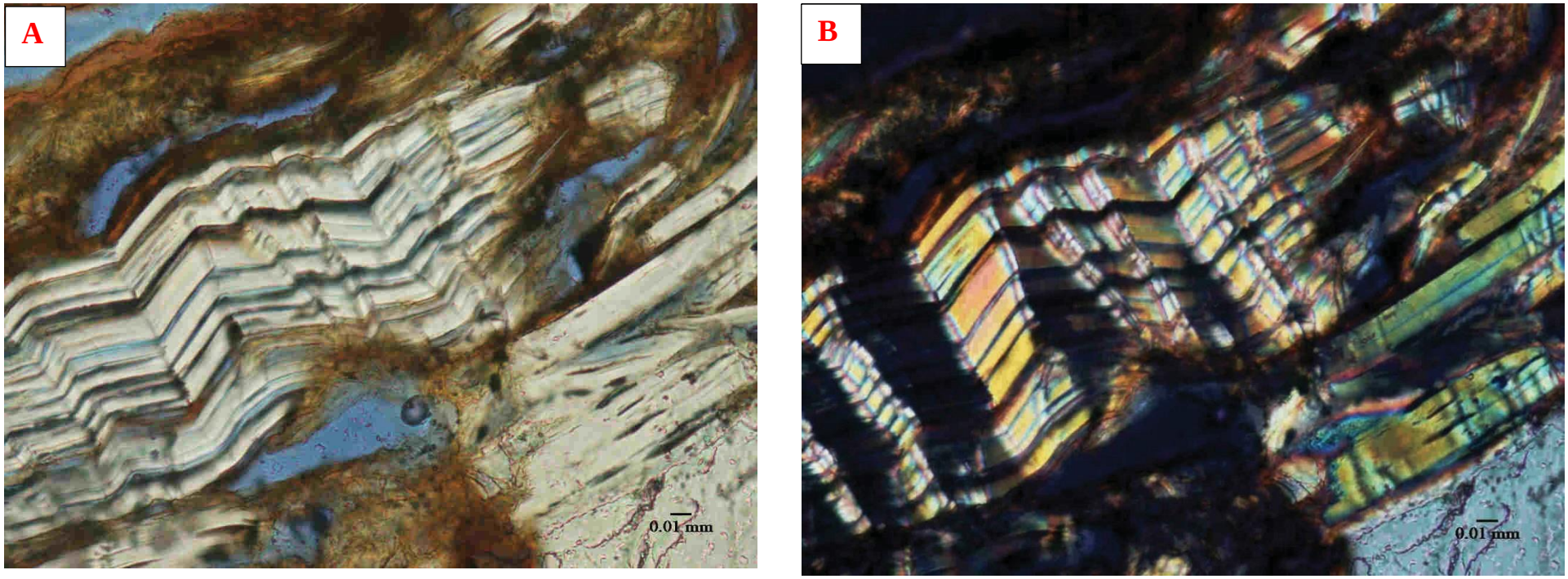

Figure 34:Photomicrographs of kink-banded mica in thin section BRR-B (scale: 0.01 mm) ; A:under plane polarized light and B: under crossed polars.

Two thin sections (BRR-B and BRR-OG1) from these were selected for microprobe analysis. A stage scan was done on the thin section BRR-B to obtain Back Scattered Electron (BSE) image and elemental maps of Fe, K and Mg (Figure 35). A smaller region of interest was selected from the stage raster and was mapped for BSE and Fe and K (Figure 36). From the BSE image of this scan, bright phases were studied further to look for presence of potential shock effects in heavy minerals. One grain of rutile with possible impact effects was found (Figure 37). This grain shows lamellae that may contain high pressure polymorphs of TiO_2. Fe and Ti maps were obtained for this rutile but no compositional variation was noted in either of the two maps.

The other thin section (BRR-OG1) was used for similar analysis by obtaining BSE images and elemental maps. Multiple heavy minerals, such as ilmenite and rutile, (Figure 38) were identified but no distinct shock features were visible. Composition of these phases was determined with the help of Energy Dispersive Spectroscopy (EDS), along with spot analyses by Wavelength Dispersive Spectroscopy (WDS). Detailed results of these analyses can be found in the Appendix.

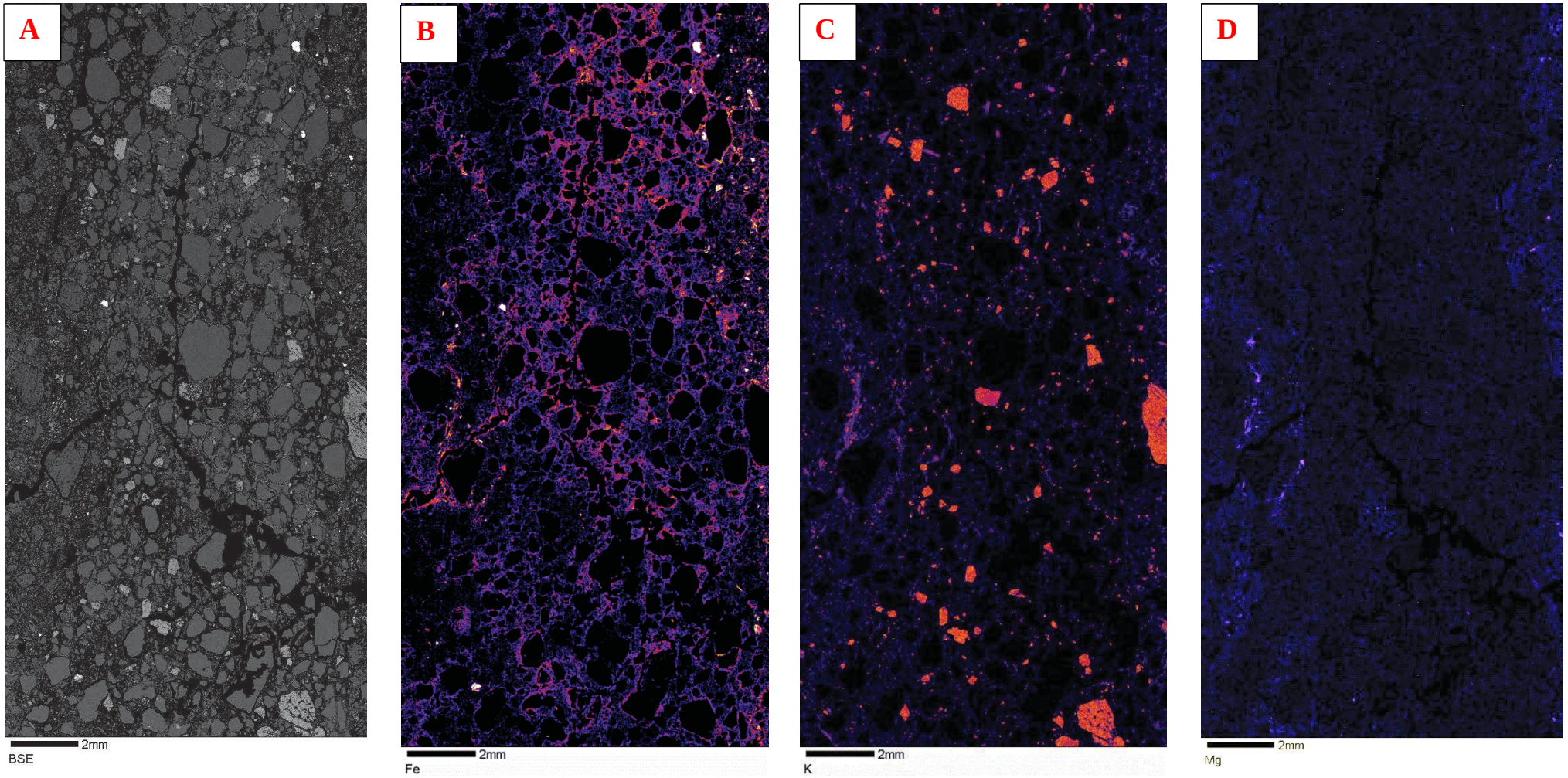

Figure 35: Stage -raster photomicrographs of thin section BRR-B of sandy matrix of breccia in thin section BRR-B: A: BSE image; B: Fe map; C: K map and D: Mg map. The matrix is very Fe rich and K is seen mostly in feldspars. Mg content of the matrix is low. (scale: 2mm)

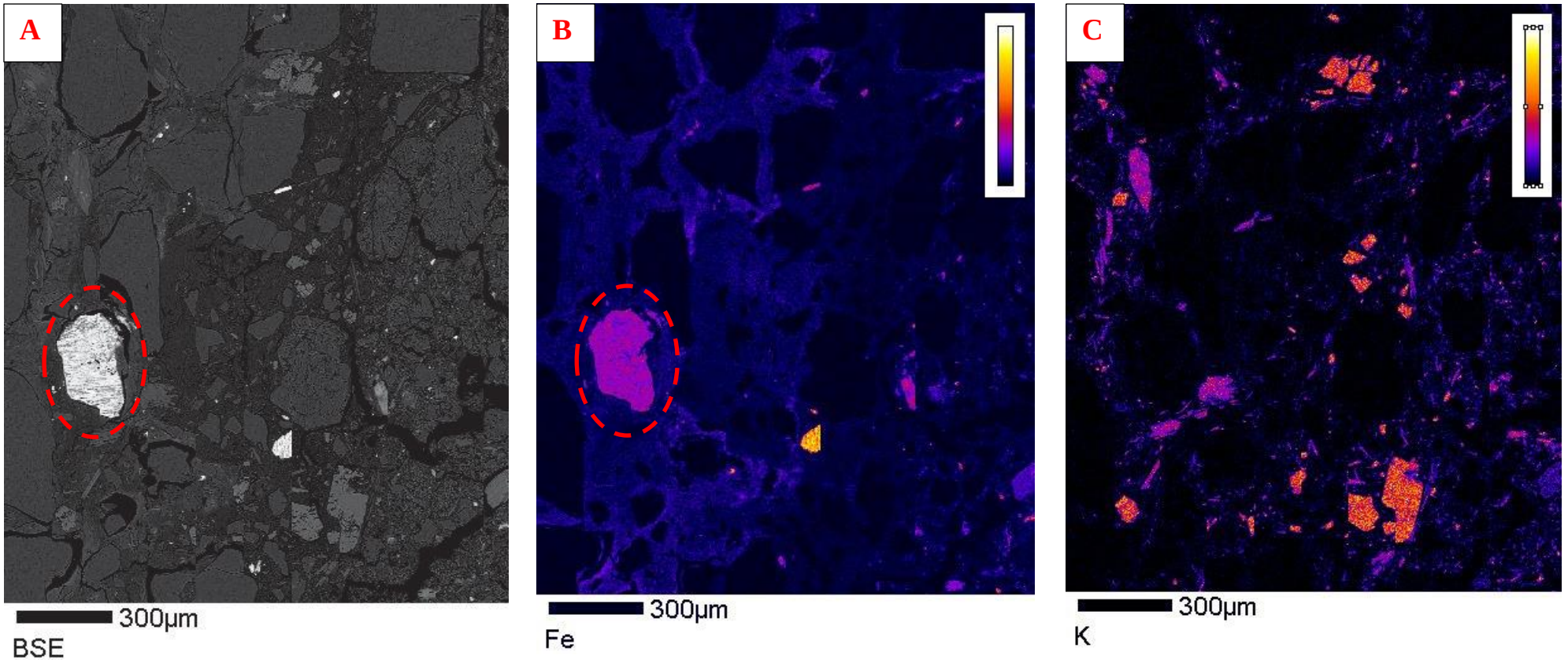

Figure 36: Beam raster photomicrographs of smaller portion of the thin section BRR-B (scale: 300 um). A: BSE image; B: Fe map and C: K map. Red circle shows the rutile grain mapped for Fe and Ti (see figure 37). Rutile can be easily identified on the Fe-map. K is seen to be present in feldspars.

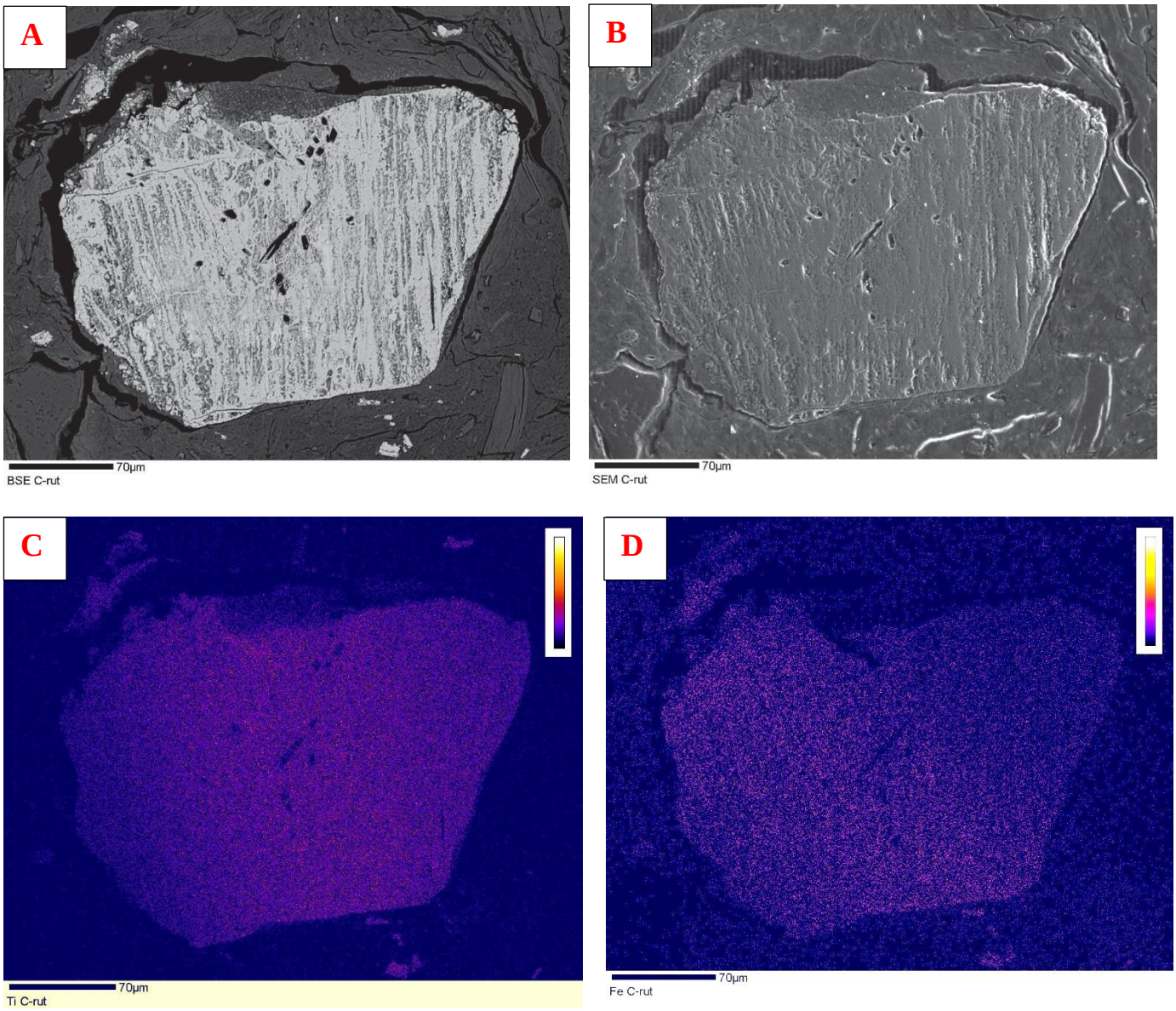

Figure 37: Beam raster photomicrographs of rutile grain in thin section BRR-B (scale: 70 um): A: BSE image; B: SEM image; C: Ti map and D: Fe map. Note that the lamellae seen in BSE image are not compositional variations as seen from the Fe/Ti maps.

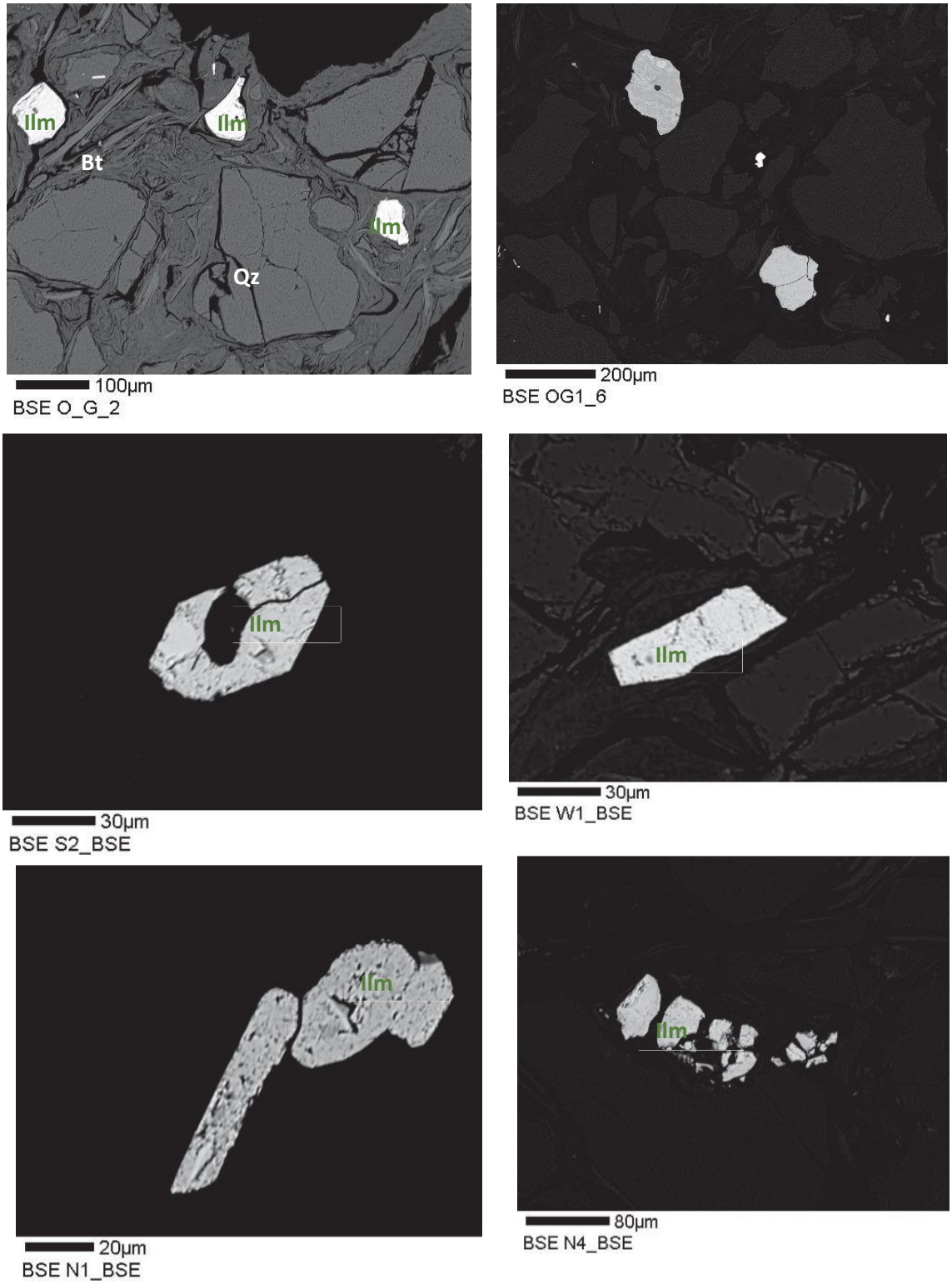

Figure 38: BSE photomicrographs of accessory minerals in the matrix in thin section BRR-N22. All the bright phases seen here are ilmenites. Ilmenite is seen to occur as subhedral to anhedral grains and any impact related features were not identified in these grains.(Ilm: ilmenite, Qz: Quartz, Bt: Biotite). Detailed EDS analyses are given in the Appendix.

Buck Ridge Road – New Outcrops (BRR-N1 and N2)

The matrix of the central breccia in the new outcrops BRR-N1 and BRR-N2 exhibits slight differences in petrographic characteristics as compared to the old outcrop. The sand is poorly sorted (Figure 39) with minerals ranging from clay size to about 5 mm. Quartz is the dominant mineral, about 60%, and occurs as angular to subrounded grains. The quartz grains in these sands are more intact, i.e., less fractured and planar fractures are rare. Micas (mostly biotite with rare muscovite) make up about 20% of the sand and some of the micas show presence of kink bands (Figure 40). Amount of feldspar is very low, only about 5% as opposed to the higher feldspar content of the BRR-O sands. All minerals are embedded in fine-grained clayey matrix, which is rich in iron.

Other than these major mineral phases, the matrix is composed of anomalous iron-rich spherules (Figure 41). These spherules appear pale brown in plane polarized light and are mostly isotropic under crossed polars. These unknown spherules were studied with the microprobe for backscattered electron image analyses (Figures 42 and 44), detailed mapping of selected elements such as Fe, Al, Si and Cr (Figures 43 and 45) and spot analyses. The data (major oxide compositions) from EDS analysis are presented in the Appendix.

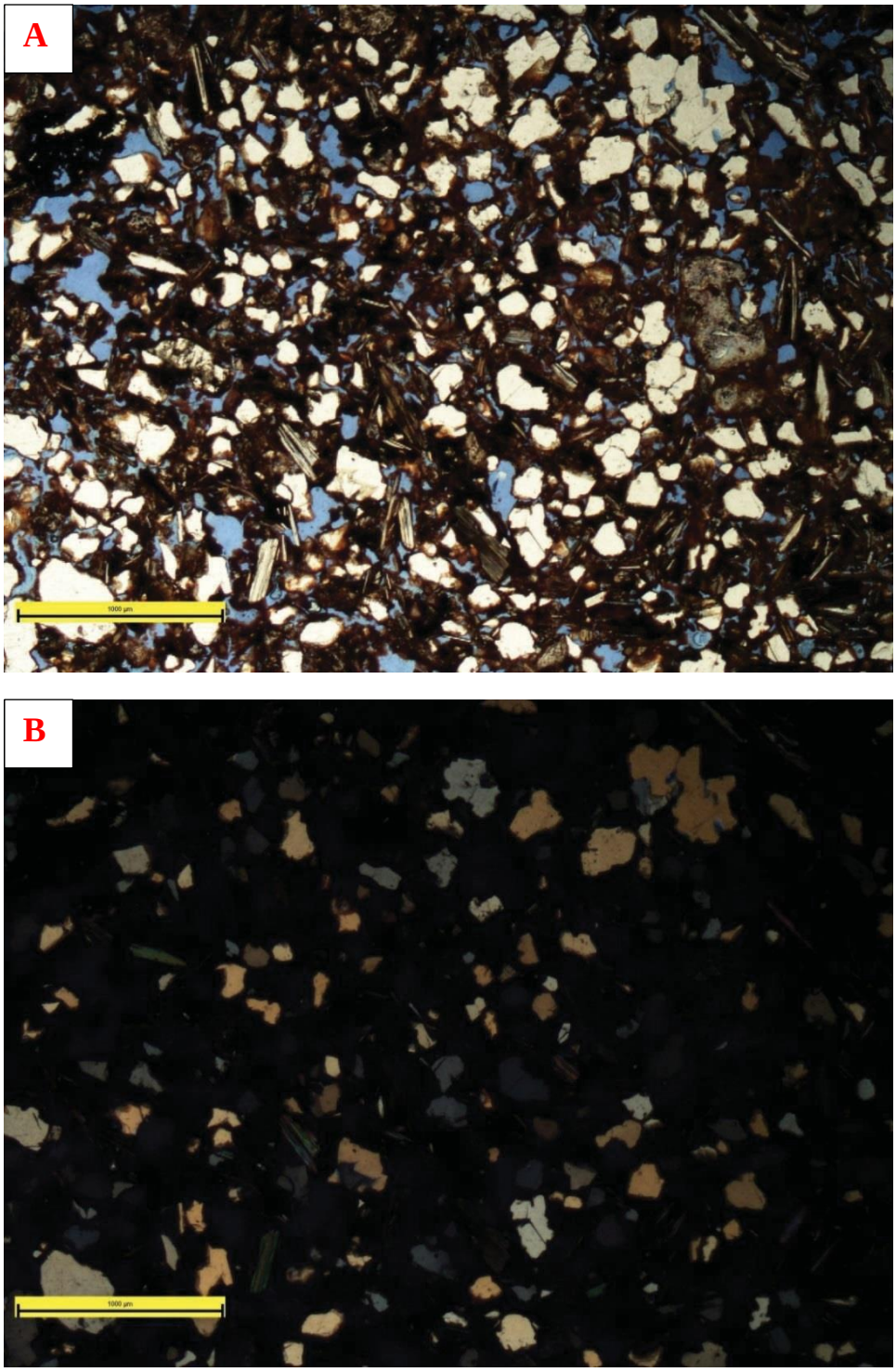

Figure 39: Photomicrographs of poorly sorted sandy matrix of the breccia in thin section BRR-N11. A: Plane polarized light, B: under crossed polars (Scale in photo: 100um).

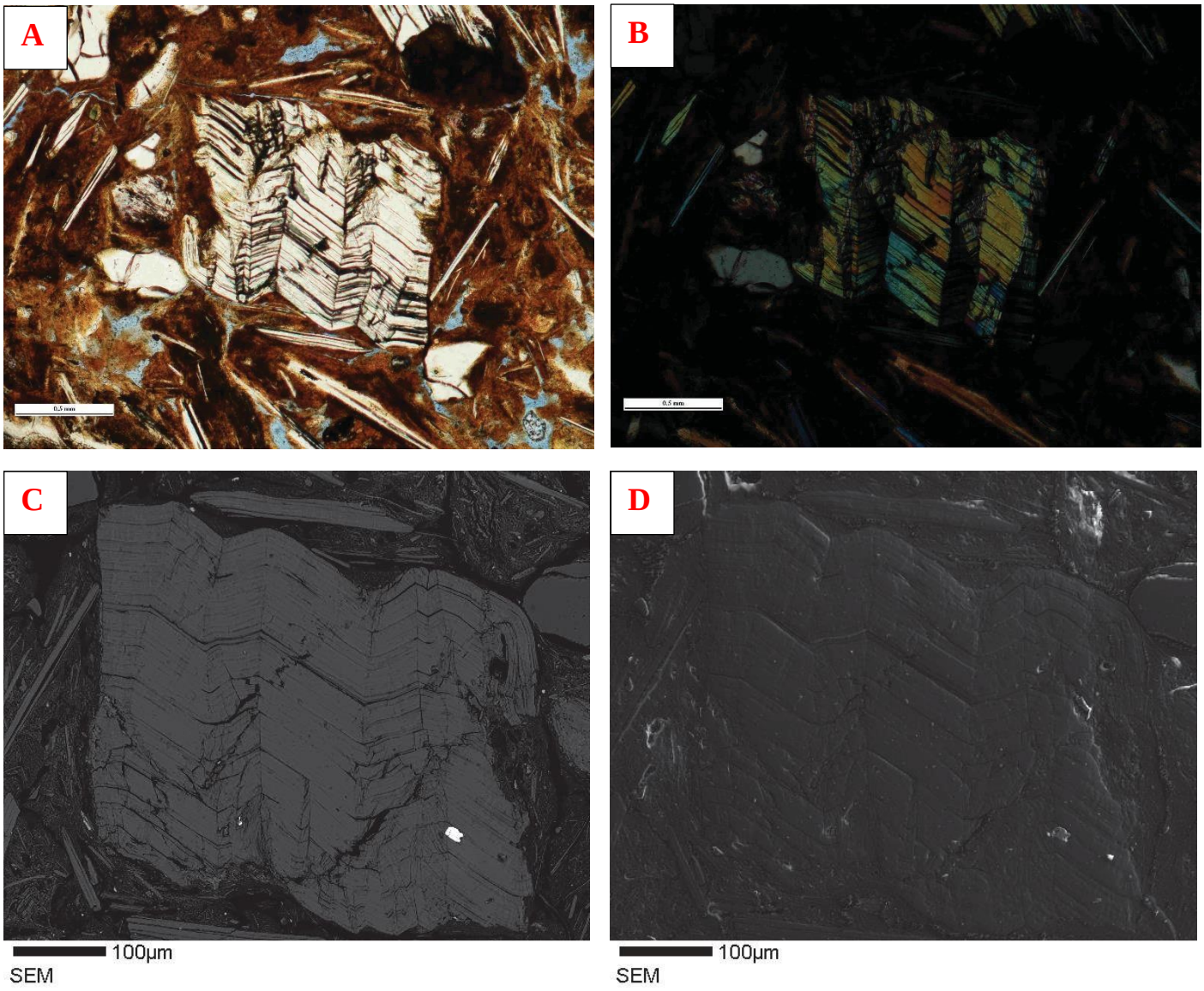

Figure 40: Photomicrographs of kink -banded mica in thin section BRR-N22. A : under plane polarized light (scale: 0.5 mm); B: under crossed polars (scale: 0.5 mm); C: BSE image (scale: 100 um); D: SEM image (scale: 100 um).

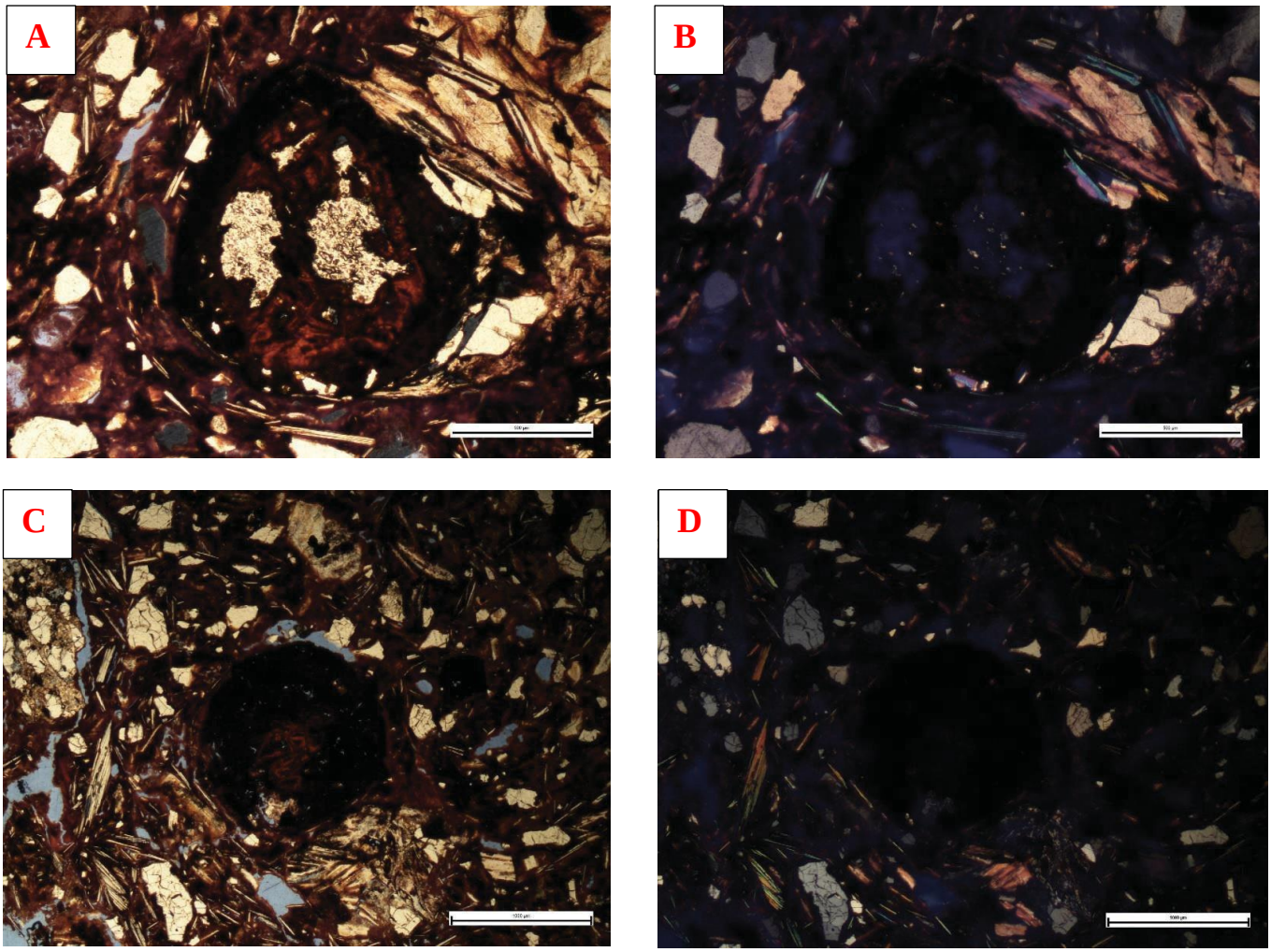

Figure 41: Photomicrographs of spherules in the breccia matrix in thin section BRR-N22. A and C: photomicrographs in plane polarized light, B and D: photomicrographs under crossed polars. Note that the micas appear to be tangential to the globular structure of the objects, and thus appear to be wrapping around these iron-rich objects. Scale in photo: 1000um. See Figures 42- 45 for backscattered electron images and X-ray elemental maps.

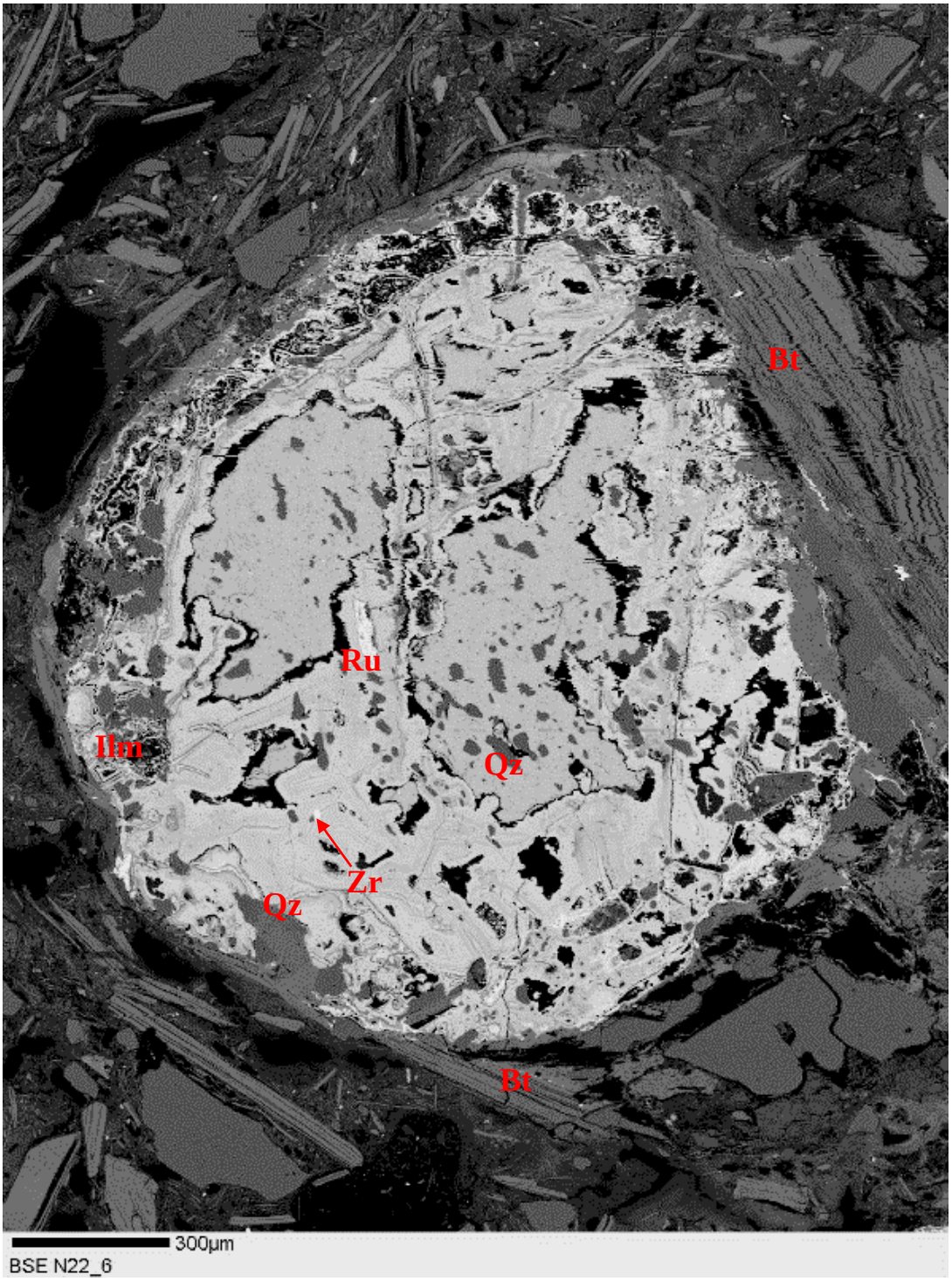

Figure 42: Beam raster photomicrograph (BSE image) of a spherule in thin section BRR-N2. Individual mineral phases in the spherule were identified with EDS and the EDS spectra are presented in appendix (Ru: Rutile, Ilm: ilmenite, Qz: quartz, Bt: Biotite, Zr: zircon).

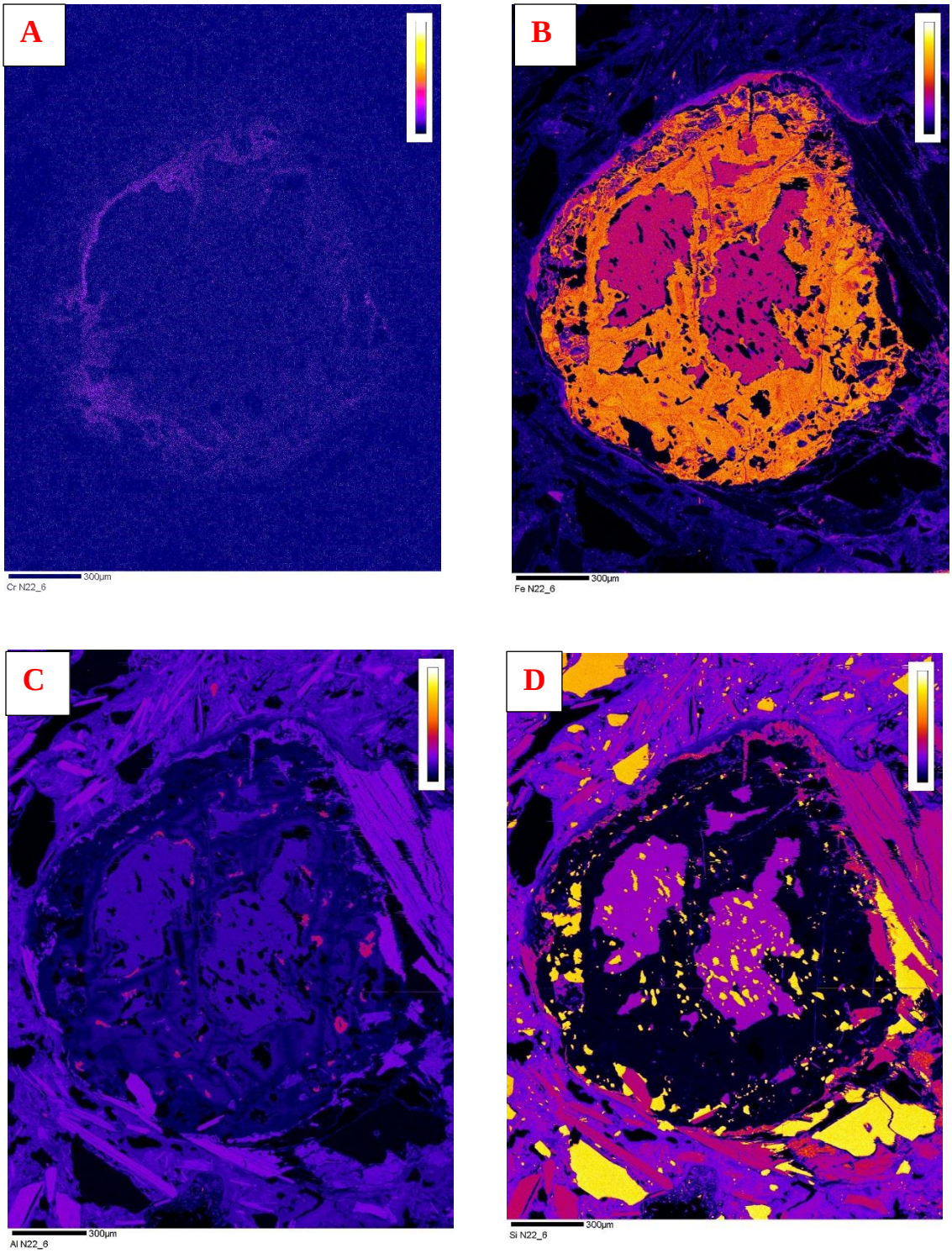

Figure 43: Beam raster photomicrographs of a spherule in thin section BRR-N22. A: Cr map, B: Fe map, C: Al map and D: Si map. It can be seen that the distribution of iron is not consistent within the phase, but overall iron content is high. Silica is scarce and distributed unevenly (scale: 400 um).

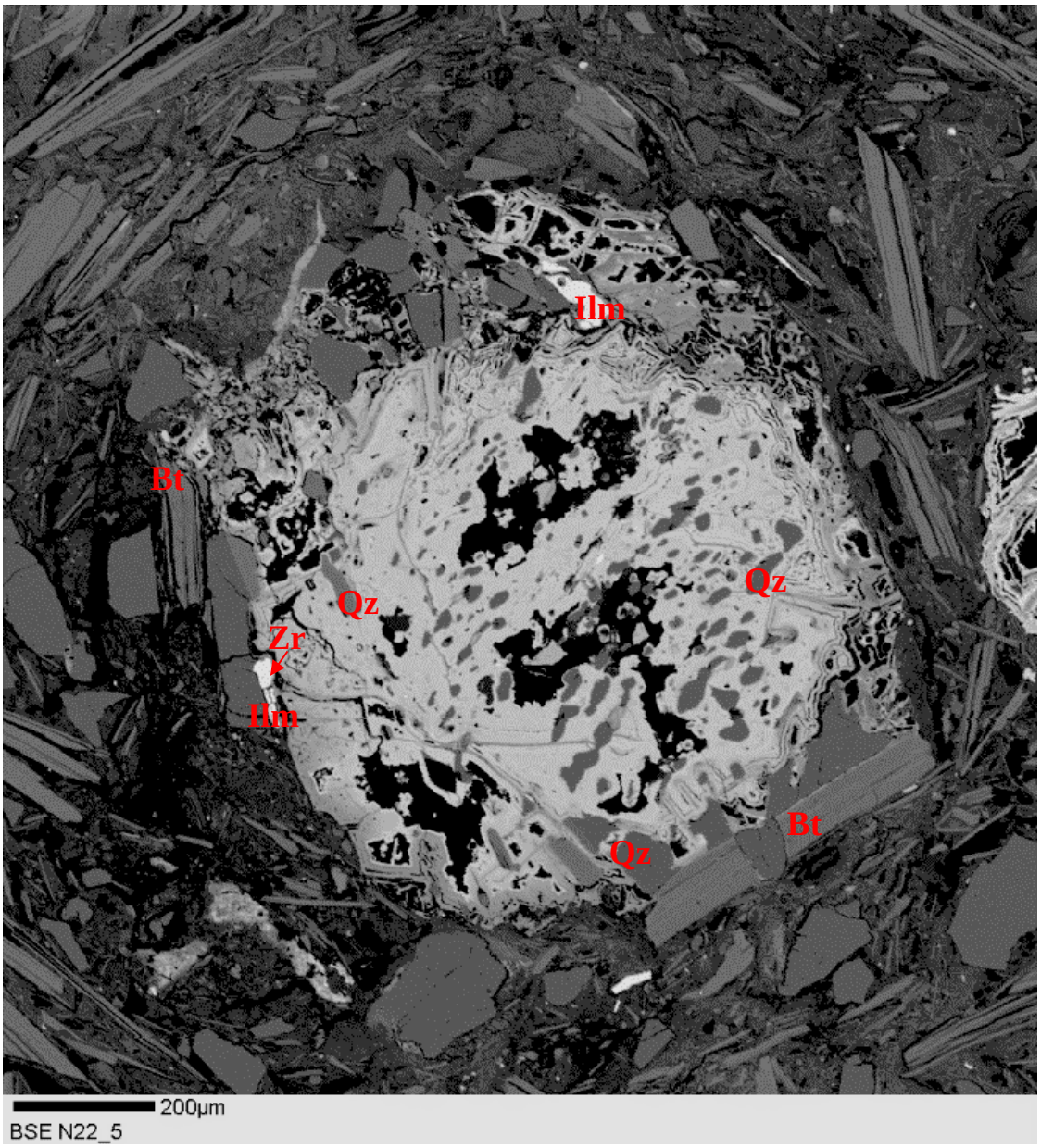

Figure 44: Beam raster photomicrograph (BSE image) of a spherule in thin section BRR-N22 (as shown in Figure 41 C and D). Individual mineral phases in the spherule were identified with EDS and the EDS spectra are presented in appendix. (Ru: Rutile, Ilm: ilmenite, Qz: quartz, Bt: Biotite, Zr: zircon).

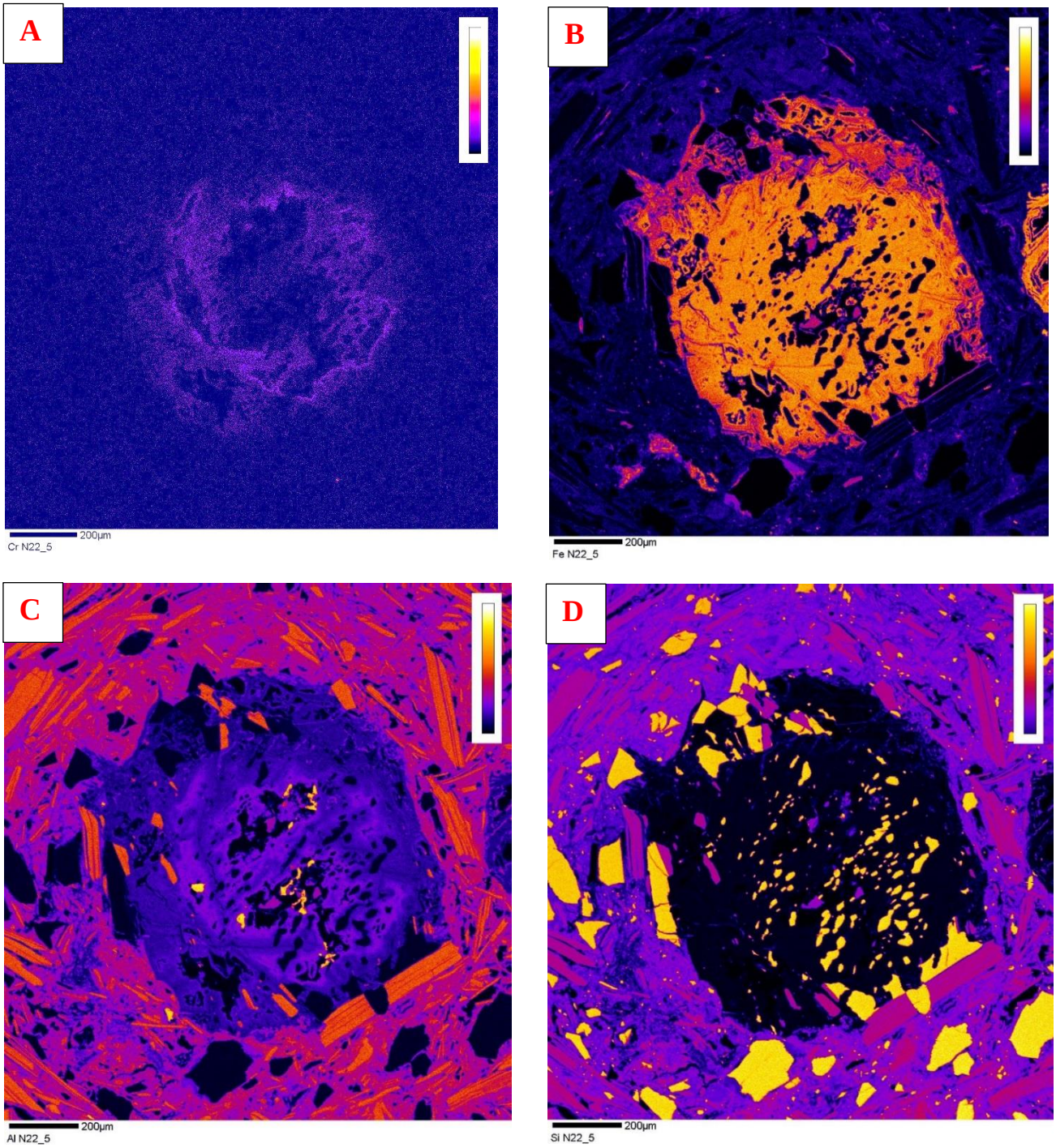

Figure 45: Beam raster photomicrographs of a spherule in thin section BRR-N22 (as shown in figure 41 C and D): A: Cr map, B: Fe map, C: Al map and D: Si map. Micas are enveloping the phase. The distribution of iron is not consistent within the phase, but overall iron content is high. Silica is relatively scarce and is distributed unevenly.

A backscattered electron (BSE) image's contrast depends upon the average atomic number, i.e., the atomic radius of the element that is being imaged. Elements with higher atomic number appear brighter than those with lower atomic radius. The brightest phases in the iron-rich spherules were analyzed with EDS to determine their compositions and the matrix was analyzed using WDS spot analyses to yield oxide weight percentages.

From the BSE images of the spherules (Figures 42 and 44), it is seen that the spherules have a bright core compared to its surroundings. Along with a bright central core, the spherules show a thin layering towards the outer edges. Micas in the sand are seen to tangentially wrap around these spherules. The Fe and Al maps (Figures 43 and 45) show the distribution of iron and aluminium in the core of the spherules. A silica map was also obtained for each spherule and figures 43 D and 45 D show the distribution of Si in the spherules. Silica appears to be mostly in the form of quartz (or amorphous silica) as seen from EDS analyses (found in the appendix). From figures 43 and 45, it can be seen that chromium is present in minor concentration in the core of the spherules. Trace amounts of chromium (along with other siderophile elements such as Ni, Co, Ir) can be indicators of extraterrestrial components (e.g. Mista et al., 2009).

The spot analyses of the core of the spherules (presented in tables 4 and 5 below) reveal that it is mostly composed of iron and aluminium hydroxides and some silica. Na2O, K2O and CaO are present in very minor amounts. Aluminum hydroxide phases may include gibbsite, boehmite or diaspore while Fe-oxide phases may be hematite and goethite. Silica can be occurring as an impurity or a secondary deposit within fractures in the spherules.

SiO2	37.26	37.23	37.36	37.39	34.87	37.45	36.25	35.57	36.25	35.98
Al2O3	21.27	20.89	20.96	21.39	19.63	21.43	20.64	20.63	21.22	20.61
FeO	30.17	30.09	30.69	30.04	29.91	29.22	29.07	28.92	31.24	30.37
MgO	2.5617	2.5167	2.4749	2.3033	1.9296	2.3534	2.1451	2.285	2.5099	2.5981
CaO	3.2	3.4	3.57	3.5	3.77	3.61	3.58	3.2	3.55	3.5
Na2O	0.1055	0.2438	0	0.0527	0	0.0159	0.0635	0.0422	0	0
K2O	0.0062	0.0098	0.0009	0	0	0	0.0071	0.0053	0.0124	0.0133
BaO	0.0706	0.0109	0	0	0.0217	0.033	0	0	0.0976	0.0217
Total	**94.64**	**94.39**	**95.05**	**94.68**	**90.13**	**94.11**	**91.75**	**90.65**	**94.87**	**93.09**

Table 4: Spot analyses of core of the spherule in Figure 42.

SiO2	2.0523	2.0514	1.8055	3.41	4.13	1.9068	1.6163	0.8738	2.3552	1.7563
Al2O3	13.42	20.26	17.68	15.05	25.93	19.14	20.38	6.46	14.66	15.3
FeO	56.08	49.58	50.35	52.5	42.44	47.62	50.84	23.76	54.04	55.38
MgO	0.0305	0.0253	0	0.032	0.0386	0	0.0487	0	0.0201	0
CaO	0	0.0116	0.0128	0.0249	0.0189	0.0181	0.023	0.0076	0.0095	0.0242
Na2O	0	0	0.0889	0.1378	0.0249	0.0337	0	0	0	0
K2O	0.015	0.011	0.011	0.0093	0	0.0128	0	0	0.0226	0.0076
BaO	0.0048	0	0.0588	0	0.0754	0	0	0.0048	0	0.0485
Total	**71.6**	**71.93**	**70**	**71.17**	**72.65**	**68.73**	**72.92**	**31.11**	**71.11**	**72.52**

Table 5: Spot analyses of core of the spherule in Figure 44.

The accessory phases observed in the spherules are mostly titanium oxides or iron-titanium oxides (rutile and ilmenite). A few smaller grains of zircon were also identified with the help of EDS. The microtexture and composition of the spherules and the presence of phases such as rutile and ilmenite are comparable to pisolitic texture that is characteristic of bauxite deposits and aluminium hydroxide deposits found in karstic terraines (Ling et al., 2015, Vind et al., 2018).

DISCUSSION

The present work focuses on better understanding the origin and mode of emplacement of the polymict breccia facies seen in the central portion of the Wetumpka impact structure. Fieldwork was conducted with the aim of locating large, oriented boulder sized clasts within the sandy matrix of the breccia unit as well as understanding clast size distribution in the breccia with the help of outcrop investigations, petrographic studies and drill core logging. Matrix of the breccia was analyzed for petrographic and microprobe studies. Field mapping was integrated with logging of a shallow drill core obtained from near the outcrop to better understand the nature of the breccia unit in the subsurface.

Combined results from fieldwork and laboratory analyses help in deducing the processes that occurred during crater formation and modification and in developing an understanding of the sequence of events that led to formation of the central breccia unit.

Here I present interpretations of the evidences seen from the different analytical results mentioned above, combined with a discussion on natural analogues of these sedimentary process in other craters as well as different geologic settings.

The polymict breccia studied in this research occurs mainly near the center of the crater, as noted by Heider and King (2016). Heider (2015), in his research on early modification stages of the crater based on studies of the transcrater slide and other crater filling units, proposed a conceptual model for the sequence of events active during crater modification that included proximal ejecta. In his model, the ejecta is seen to have been emplaced on to the overturned rim flaps of the crater on all sides and transported in to the interior of the crater by riding on top of the trans-crater slide.

Evidence supporting this model and the hypothesis that the boulder-breccia landed on the rim shortly after impact can be seen in the recent computer simulation modelling by De Marchi et al. (2019). These simulations show 200 seconds of the crater forming processes encompassing the formation of the crater rim, subsequent emplacement of the crystalline boulders on to the rim, rim collapse, tsunami resulting from excavation of the shallow water column and the water resurge (De Marchi et al., 2019). The model predicts the displacement of the crystalline material from the excavated basement on to the rim on top of sediments to occur early in the process of crater formation. It is followed by emplacement of ejecta and subsequent slumping of the rim prior to the trans-crater slide event (Figures 46 and47).

The boulder-sized blocks observed in the breccia would have formed as detached fragments of the overturned rim flap while the rim was forming. At that time, the blocks may be expected to land horizontally up to a distance of a few crater radii from the crater center. This process was immediately followed by emplacement of the ejecta which would interact with these crystalline rocks. A mixture of the crystalline boulders intermingled with the underlying sediments and overlying ejecta is interpreted to be a precursor to the polymict breccia seen in the outcrops at Buck Ridge Road.

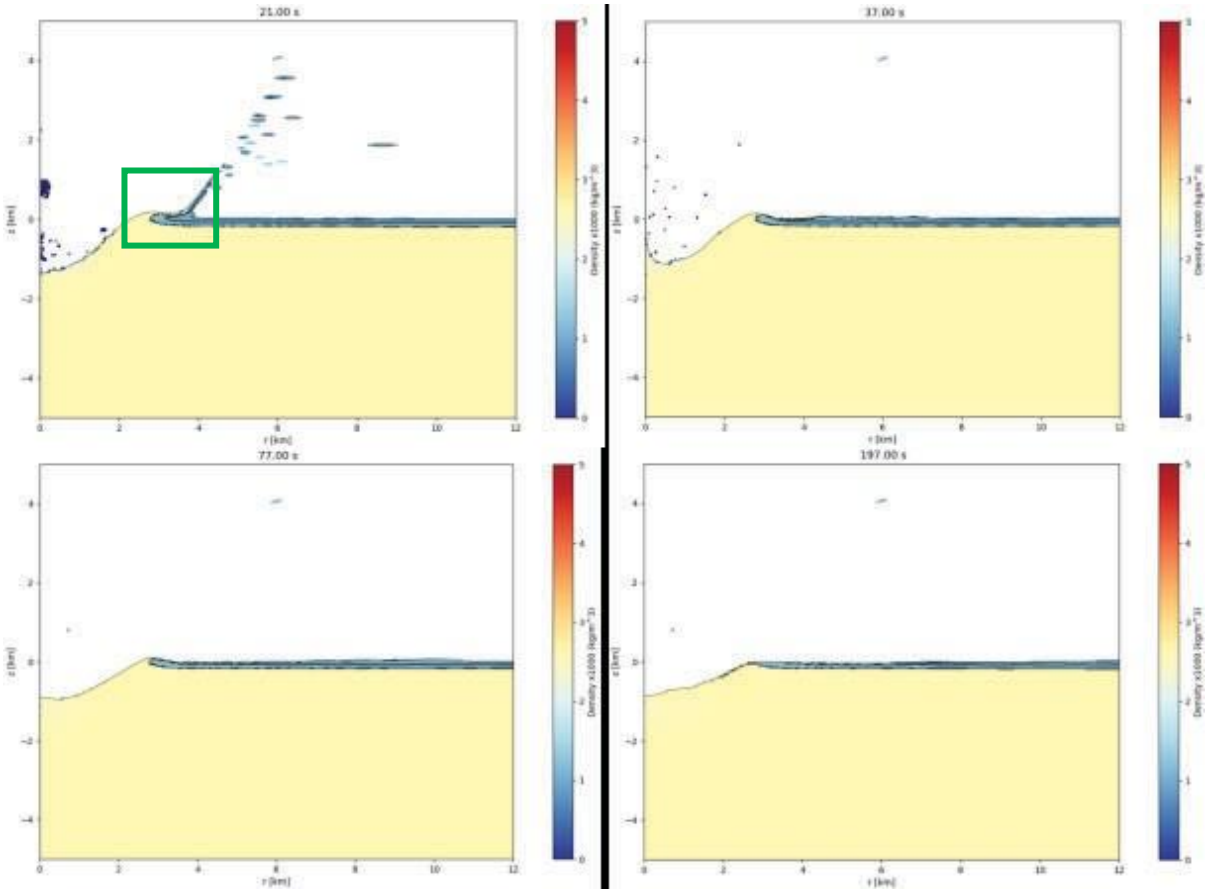

Figure 46: Simulation model of Wetumpka from De Marchi et al. (2019) showing the formation of the crater. The square shows the crystalline material ejected on the rim. Note that later in the sequence, this material slides in to the crater along with the sediments from the rim.

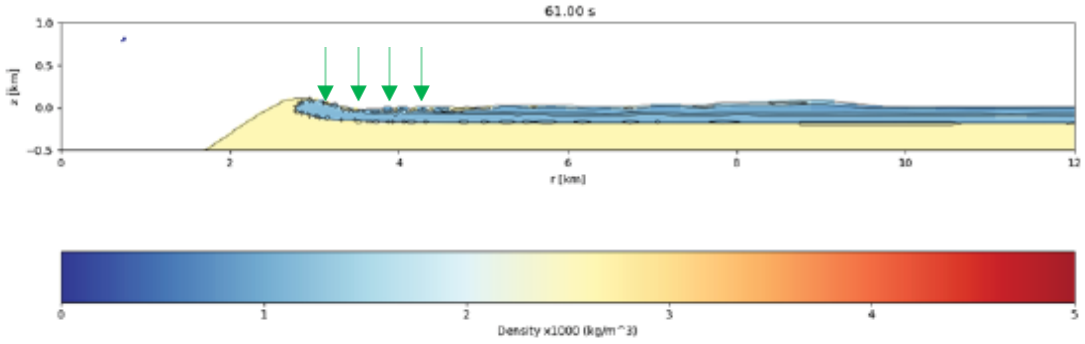

Figure 47: Zoomed profile of the crater showing the crystalline material lying on top of the rim (Modified from De Marchi et al., 2019). Crystalline material denoted with arrows.

With the detachment of the rim flap during rim collapse, the material lying on top of it began to be transported towards the crater center. The trans-crater slide moved over the impactite sand before coming to rest against the western rim as seen in the model by Heider (2015). We predict that this process was followed by a turbulent mass movement which brought the boulder bearing breccia in to the crater center. This is in conformity with field observations where the breccia is clearly seen to overlie the trans-crater slide unit.

The mechanism causing the transport of the large boulders maybe explained from the results of outcrop mapping. The outcrops consisted of very poorly sorted breccia with a wide range of clast sizes from boulders as large as 20 m and sand sized clasts up to 1 cm embedded in sandy-clayey matrix. The drill core analyzed showed a similar poorly sorted nature of clasts. Such a distribution of clast sizes implies deposition in a turbulent environment such as a debris flow. No grading or sorting was seen in any of the outcrops and hence any role of water or marine resurge can be ruled out in the emplacement of this breccia.

Schistose rocks tend to break parallel to their schistosity, making their longer dimension oriented along the schistosity. Thus, the boulders landing on the rim would have had an original horizontal trend with respect to their schistosity and larger dimension. However, as seen from the outcrops at Buck Ridge Road, all boulders except one have vertically oriented foliation, and it is assumed that the original foliated block was longer in the dimension parallel to foliation than other dimensions. This preferential orientation may be attributed to liquefaction in the sediments that were carrying the boulders. Liquefaction, perhaps due to turbulence in the sediment flow transporting the boulders, would cause them to reorient vertically possibly due to uneven mass distribution within the boulders themselves (Figure 48). Arrival of this breccia in the center of the crater would be the last process to occur before the marine resurge.

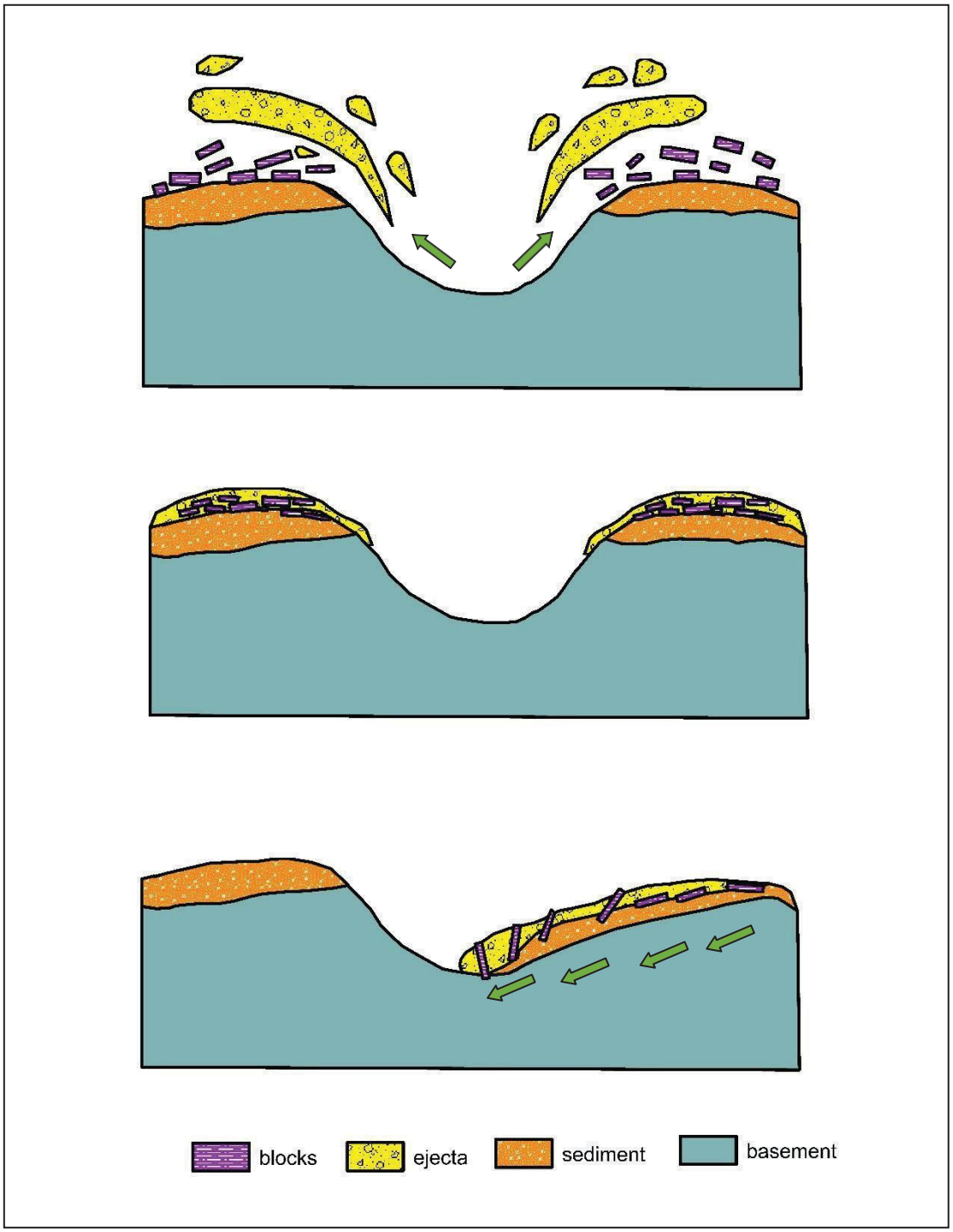

Figure 48: Conceptual model (not to scale) showing the interpreted mechanism for the emplacement of the polymict breccia. Note that the resurge is not shown as it is interpreted to have had no role in the breccia's mode of transport and occurred later in the sequence of events.

Petrographic investigations coupled with geochemical data support the hypothesis that the boulder-bearing polymict breccia was mixing with part of the proximal ejecta. Proximal ejecta deposits consist of highly shocked matter mixed with unshocked material. In the Buck Ridge Road breccia, several potential impact related features have been observed in the matrix. Shocked quartz has been previously reported by Morrow and King (2007). The present study also found other indications in minerals such as kink banded micas, rutile showing unusual planes in BSE images along with abundant fractured and toasted quartz grains. Although kinked micas are not diagnostic of impact, their close association with other impact affected minerals is significant. Rutile with lamellae (as that seen in Figure 37) may contain high pressure phases of TiO_2 such as anatase or TiO_2-II . Shocked rutile is uncommon and very few terrestrial craters are known to have produced high pressure polymorphs, one example being the TiO_2-II recently discovered from Chicxulub crater's peak ring (Schmieder et al., 2019). These mineralogical features imply a strong correlation with proximal ejecta deposit.

The spherules found in the matrix of the boulder bearing diamictite in the new outcrops contain titanium oxide phases such as rutile and ilmenite surrounded by iron and aluminium oxides/hydroxides. Presence of trace amounts of Cr in the core of the spherules points towards evidence of extraterrestrial component in the spherules (e.g. Misra et al., 2009). In order to better understand the significance of Cr in the spherules, it is important to identify the presence and distribution of other siderophile elements as well as platinum group elements (PGEs) in the spherules as those are more indicative of a meteoritic origin. It is also significant to understand the concentrations of these elements in the original target stratigraphy.

The morphology of the spherules indicates possible aggregation due to aerodynamic accretionary effects from being ejected as part of the excavated material in the vapor plume. Distal ejecta of impact craters is known to contain spheroidal particles that are characterized by glassy interior (microtektites) or crystallites (microkrystites) (Simonson and Glass, 2004). As glass or glassy phases were not reported from the Wetumpka spherules, their origin is more likely close to accretionary particles such as lapilli commonly formed in explosive volcanic environments or vapor clouds of impact craters. Accretionary lapilli are mechanical aggregates, rather than melt particles, that form due to turbulence in the vapor plume of phreatomagmatic explosions or impacts (e.g. Simonson, 2003).

Spheroidal particles can also form under conditions other than those in impact craters. Possible non-impact related explanations for the formation of these spherules may come from the mineralogy of the phases in their core. Accessory minerals such as rutile, ilmenite and zircons within Fe-Al hydroxides are commonly seen in pisolites or ooids that form in bauxites or lateritic weathering horizons. To better constrain the origin for these spherical particles, more geochemical analyses such as trace element concentrations and isotopic abundances are needed.

Overall, the mineralogical evidences combined with previously known shock features, the model from Heider (2015) and simulations from De Marchi et al. (2019) support the hypothesis that the polymict breccia consists material from the proximal ejecta deposit that landed on the crater rim during formation of the crater.

Analogues to the Buck Ridge Road breccia:

Wetumpka crater is a transitional crater between simple and complex type morphology. Although the processes occurring at Wetumpka might be unique, similarities with the polymict breccia from Wetumpka exist in breccia deposits of other impact craters around the world.

One such example is the Bunte breccia deposits of the Nördlinger Ries crater. The Nördlinger Ries, or simply the Ries crater, is a complex, terrestrial middle Miocene impact crater in Germany having a diameter of 24 km (Schmieder et al., 2018). The target lithology of the crater was mostly Mesozoic and Cenozoic sediments overlying a crystalline Paleozoic basement (Graup, 1978). The continuous ejecta of the crater is characterized by the Ries suevite and the Bunte Breccia. The Ries suevite consists of shocked material with impact melt derived from a crystalline basement (e.g., von Engelhardt., 1972; Hörz, 1983; von Engelhardt, 1997; Stöffler et al., 2002; 2013; Osinski et al., 2011; Kring, 2005, Pietrek and Kenkmann, 2016; Schmieder, 2018). The Ries suevite is overlain by the Bunte Breccia which is a polymict breccia consisting of large boulder-sized clasts (e.g. Hörz et al., 1983; Pietrek et al., 2015; Schmieder et al., 2018).

The Bunte Breccia consists of a highly chaotic, poorly sorted deposit of weakly shocked material composed of sandy matrix with boulder sized crystalline clasts (Hörz et al., 1983). It is the largest unit of the continuous ejecta of the crater and is mostly derived from the sedimentary cover of the crater's target lithology with the crystalline clasts being

insignificant volumetrically (Hörz et al., 1983; Pietrek and Kenkmann, 2016). Although texturally similar to Wetumpka's polymict breccia, the clasts in the Bunte Breccia are randomly oriented (Hörz et al., 1983). Another difference between the two breccias is that the Bunte Breccia lies outside the rim of the Ries crater. Several models have been suggested for the emplacement mechanism of the Bunte Breccia. These models usually involve ballistic sedimentation during crater excavation, secondary cratering and associated debris flow as well as a ground-hugging turbulent surge (Oberbeck, 1975; Chao et al., 1978; Hörz et al., 1983; Pietrek and Kenkmann, 2016). Pietrek and Kenkmann (2016) also proposed a model involving a translational gliding motion in the emplacement of Bunte breccia based on presence of volatiles in basal clay units in some parts of the deposits.

Thus, Bunte breccia compares well to Wetumpka's central breccia unit with respect to lithological characteristics and meso-scale textures but exhibits some differences in the mode of emplacement.

A second analogue to Wetumpka's breccia can be found at the Manson Crater in Iowa. The Manson Crater, with a diameter of 35 km, is one of the largest known impact structures in the United States. The crater formed in a shallow marine environment has been dated at 74 Ma (Izett et al., 1998) and lies buried underneath recent Pleistocene deposits. Drill-core investigations over the past century have yielded information on the geology and stratigraphy within the crater (e.g., Hoppin and Dryden, 1958; Bell et al., 1993; Anderson et al., 1994)

The target rocks are mainly Precambrian and Paleozoic (Hartung and Anderson, 1988). The main geologic units that have been affected by the impact are structurally undisturbed ring graben, fall-back deposits in the crater moat, and a central uplift underlying

a polymict crystalline-clast breccia (Hartung and Anderson, 1988). The breccia deposit overlying the central peak has been described as polymict impact breccia that consists of mostly sedimentary clasts along with rare crystalline clasts of schist and gneiss (Hartung and Anderson, 1988; Izett et al., 1998). This breccia has been further classified into different categories and these categories have a variety of names in literature such as igneous clast breccia with sand matrix, igneous clast breccia with glass matrix, and sedimentary clast breccia (Anderson et al., 1994), or suevite breccia, impact melt breccia, Keweenawan shale-clast breccia, and Phanerozoic clast breccia (Anderson et al., 1996), whereas Koeberl et al. (1996) classified these rocks as impact melt breccia, suevite, and fragmental breccia.

Anderson et al. (1994) have compared the Phanerozoic clast breccia of Manson crater to the Bunte breccia of Ries. The polymict clasts of this breccia range in size from millimetres to more than 100 meters. These clasts differ in lithology over distance from the crater center but are dominated by sedimentary clasts. Unlike Bunte Breccia, the Manson breccia occurs in the center of the crater. Anderson et al. (1994) have suggested that this deposit was originally emplaced outside the crater but got transported to the center by high energy debris flow that carried the large clasts at least 17 km, over the crater moat, to rest on top of the central peak. This process appears to compare at least in part with the emplacement mechanism interpreted at Wetumpka.

Wetumpka's breccia resembles more closely debris flow deposits where the clasts and matrix are poorly sorted as they are derived mostly from the crystalline basement and the sediment cover along with ejecta material. Debris flows are characterized by such poorly sorted nature deposited in high energy environments.

CONCLUSIONS

Outcrop mapping in the field, laboratory analysis involving petrography and microprobe analysis, and drill core logging were conducted in order to characterize the boulder bearing polymict breccia unit occurring in the centre of Wetumpka crater along with understanding its mode of emplacement.

- Wetumpka's interior boulder breccia has characteristics that strongly suggest it was a proximal ejecta deposit that has moved back into the central bowl of the crater by gravity-driven processes. In the absence of evidence for involvement of water in the deposition of these breccias, a process of mass movement such as a debris flow is more consistent with the observations.

- Large crystalline boulders that characterize this deposit were likely part of the crystalline flap of Wetumpka impact crater, which moved back into the crater along with the proximal ejecta deposit of the crater rim.

- The orientation of these blocks is best explained by rotation during emplacement movement through a newly proposed mechanism of liquification in the fine clayey matrix.

- Impact-affected materials such as kink-banded micas and toasted quartz, and potential impact generated spherules in the clastic matrix of the boulder breccia strongly signals a relationship to proximal ejecta emplacement.

- Further study of these boulder breccia deposits as well as the spheroidal particles in the matrix of the breccia is indicated in order to better understand their shock levels and provenance during the excavation stage of impact crater formation.

APPENDIX

Contents of Appendix

1. Outcrop clast count data

2. GPS locations of boulders

3. Other microprobe results and images

4. Core-box Photographs

5. Drill core logs

Outcrop Clast Count Data

#	Longest Axis cm	mm	Lithology	#	Longest Axis cm	mm	Lithology
1	2	20	Schist	**24**	2	20	Schist
2	2	20	Schist	**25**	3.2	32	Schist
3	2	20	Schist	**26**	4.2	42	Schist
4	1	10	Schist	**27**	1.1	11	Schist
5	4	40	Schist	**28**	0.8	8	Quartzite
6	2	20	Schist	**29**	1.1	11	Schist
7	3.5	35	Schist	**30**	2.5	25	Schist
8	3	30	Schist	**31**	3	30	Schist
9	2.3	23	Schist	**32**	3	30	Schist
10	1	10	Quartzite	**33**	3	30	Schist
11	4	40	Schist	**34**	3.5	35	Schist
12	6	60	Schist	**35**	4.5	45	Schist
13	20	200	Schist	**36**	2	20	Schist
14	11	110	Schist	**37**	3.8	38	Schist
15	3.5	35	Schist	**38**	9	90	Schist
16	2.5	25	Schist	**39**	5	50	Schist
17	6	60	Schist	**40**	2.5	25	Schist

18	5	50	Schist	**41**	2	20	Schist
19	2	20	Schist	**42**	5	50	Schist
20	14	140	Schist	**43**	5.1	51	Schist
21	1	10	Schist	**44**	3	30	Schist
22	1	10	Schist	**45**	3	30	Schist
23	2.5	25	Schist	**46**	2.5	25	Schist

Table A1: Results of counting clasts and sizes in a one meter-square grid from BRR-O.

#	Longest Axis in cm	mm	Lithology	#	Longest Axis in cm	mm	Lithology
1	5	50	Schist	**42**	4.6	46	Schist
2	2	20	Schist	**43**	1.6	16	Schist
3	2	20	Schist	**44**	1	10	Schist
4	2.6	26	Schist	**45**	1	10	Quartzite
5	5	50	Schist	**46**	12	120	Schist
6	2.7	27	Schist	**47**	11	110	Schist
7	1.7	17	Schist	**48**	3	30	Schist
8	2.2	22	Schist	**49**	8	80	Schist
9	4.5	45	Schist	**50**	4.5	45	Schist
10	5	50	Schist	**51**	13	130	Schist
11	3.7	37	Schist	**52**	8	80	Schist
12	17	170	Schist	**53**	3.9	39	Schist
13	6	60	Schist	**54**	4.5	45	Schist
14	7	70	Schist	**55**	5	50	Schist
15	19.5	195	Schist	**56**	2	20	Schist
16	8	80	Schist	**57**	16	160	Schist
17	3.5	35	Schist	**58**	2.9	29	Schist
18	5	50	Schist	**59**	5.5	55	Schist
19	6.5	65	Schist	**60**	2	20	Schist
20	4	40	Schist	**61**	3	30	Schist
21	23	230	Schist	**62**	4.5	45	Schist
22	16	160	Schist	**63**	8	80	Schist
23	12	120	Schist	**64**	8	80	Schist
24	7	70	Schist	**65**	1.5	15	Schist
25	8	80	Schist	**66**	2.3	23	Schist
26	11	110	Schist	**67**	11	110	Schist
27	4	40	Schist	**68**	5	50	Schist
28	1.5	15	Schist	**69**	14	140	Schist
29	2.5	25	Schist	**70**	21	210	Schist
30	2	20	Schist	**71**	9	90	Schist
31	13	130	Schist	**72**	1	10	Quartzite
32	1	10	Schist	**73**	1.4	14	Schist
33	1	10	Schist	**74**	2	20	Schist
34	6	60	Schist	**75**	1.5	15	Schist

35	6	60	Schist	**76**	28	280	Schist
36	1	10	Schist	**77**	15	150	Schist
37	9	90	Schist	**78**	2	20	Schist
38	8	80	Schist	**79**	2	20	Schist
39	9	90	Schist	**80**	1.8	18	Schist
40	9	90	Schist	**81**	0.7	7	Quartzite
41	4	40	Schist	**82**	1	10	Schist

TableA2: Results of counting clasts and sizes in a one meter-square grid from BRR-N2.

Gps Locations of Boulders

Boulder no.	Lat	Long	Alt(above msl)
1 (BRR-O)	32.52391	-86.17461	114m
2 (BRR-N1)	32.52413	-86.17479	121m
3(BRR-N2)	32.52247	-86.17405	138m
4(BRR-N2	32.52213	-86.17375	153m
5 (Schroder House)	32.52283	-86.17358	143m
6 (Creek)	32.52411	-86.17572	123m

Table A3: GPS locations of boulders.

Microprobe EDS And Quantitative Analyses Data

THIN SECTION BRR-OG1

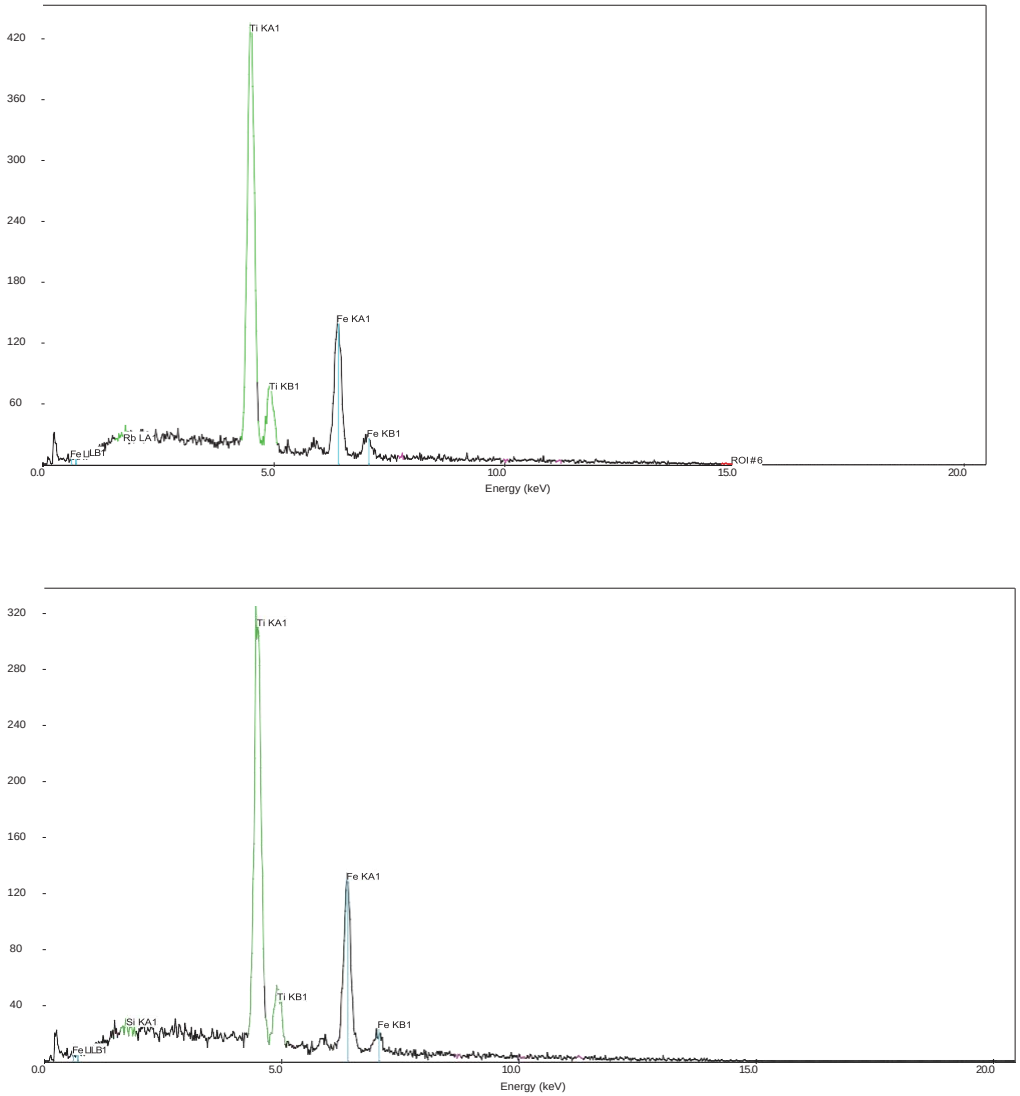

Figure A1 (Top and Bottom): EDS of ilmenite from thin section BRR-OG1

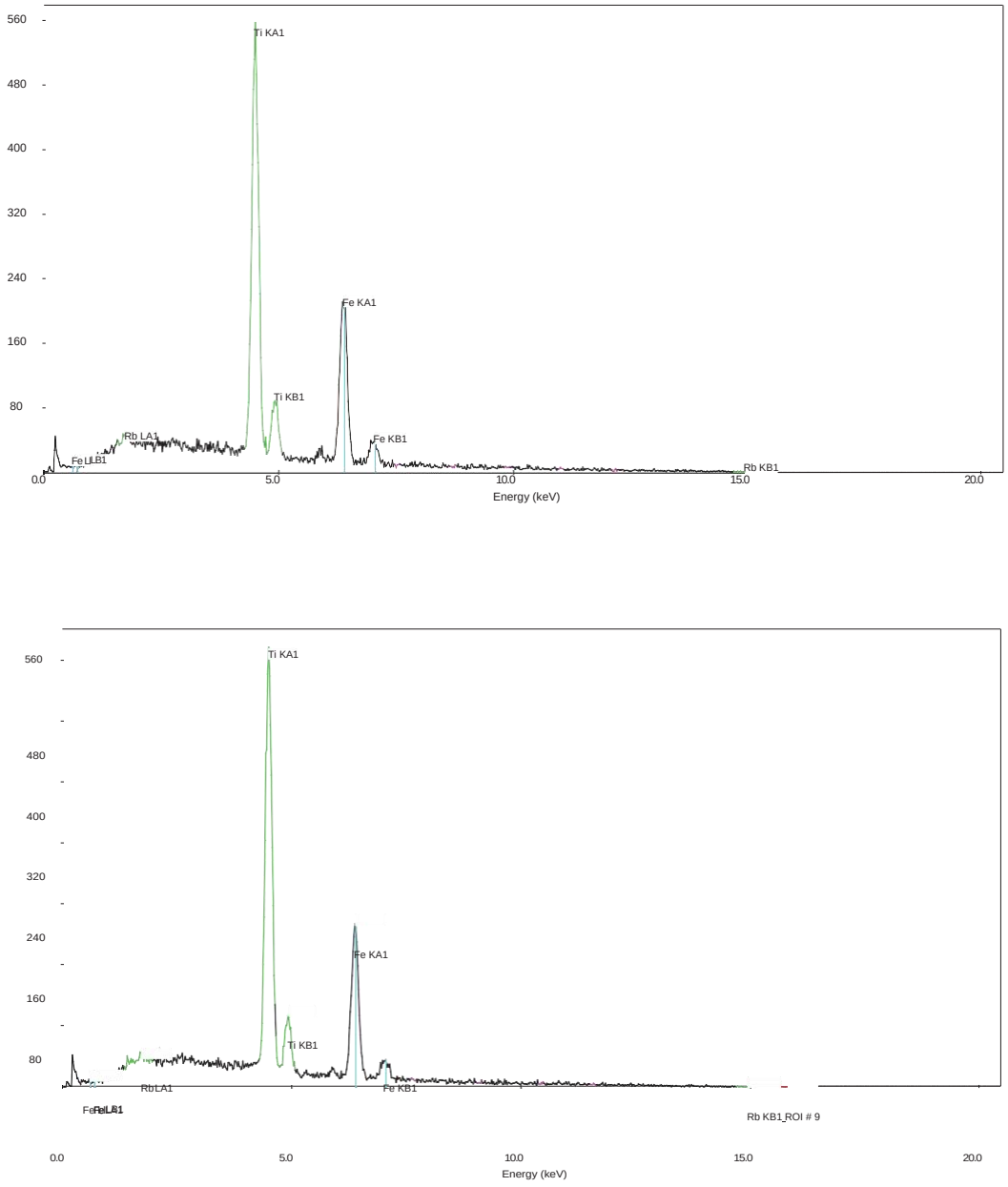

Figure A2 (Top and Bottom): EDS of ilmenite from thin section BRR-OG1

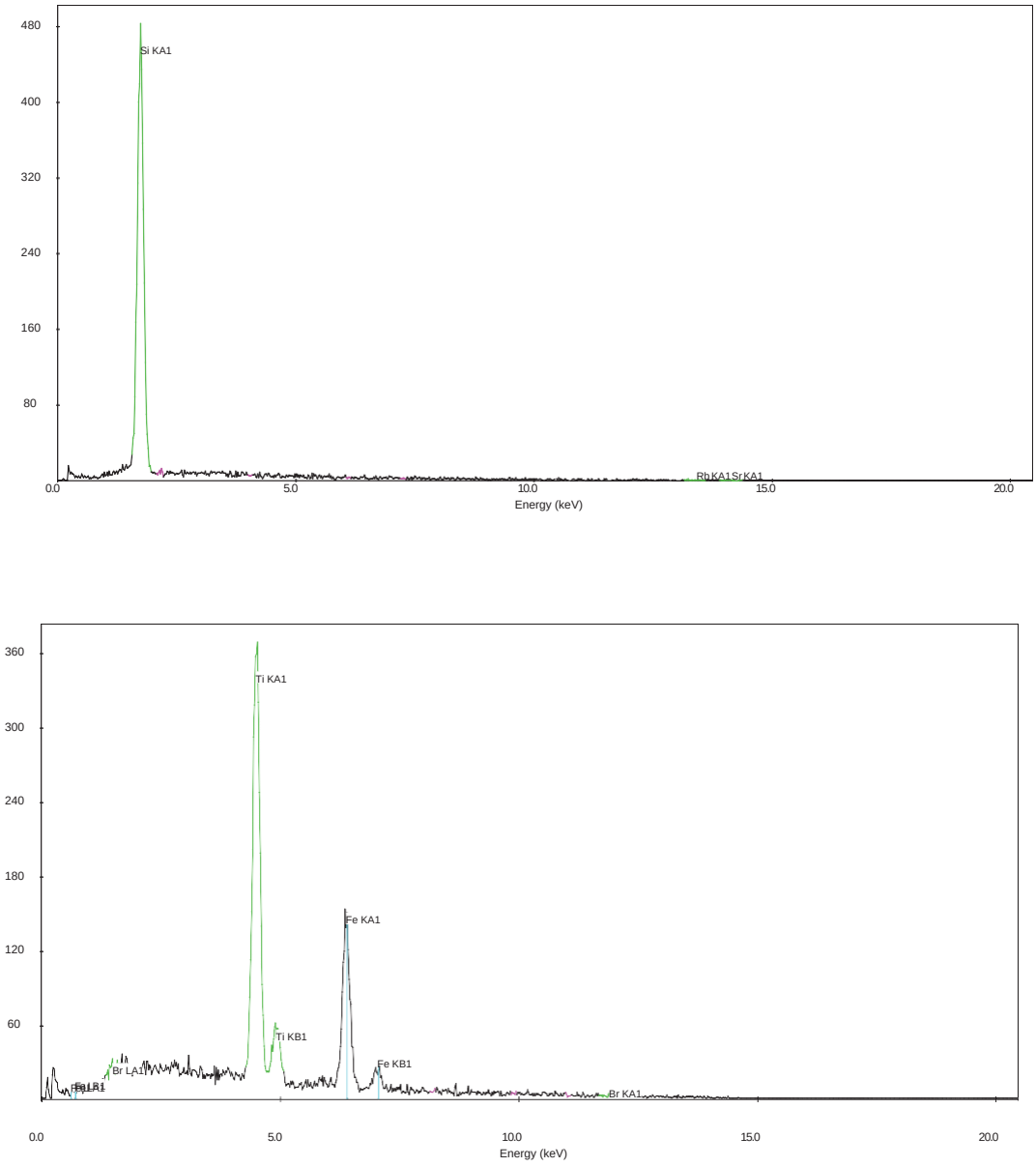

Figure A3 (Top and Bottom): EDS of quartz (top) and ilmenite (bottom) from thin section BRR-OG1.

THIN SECTION BRR-N22

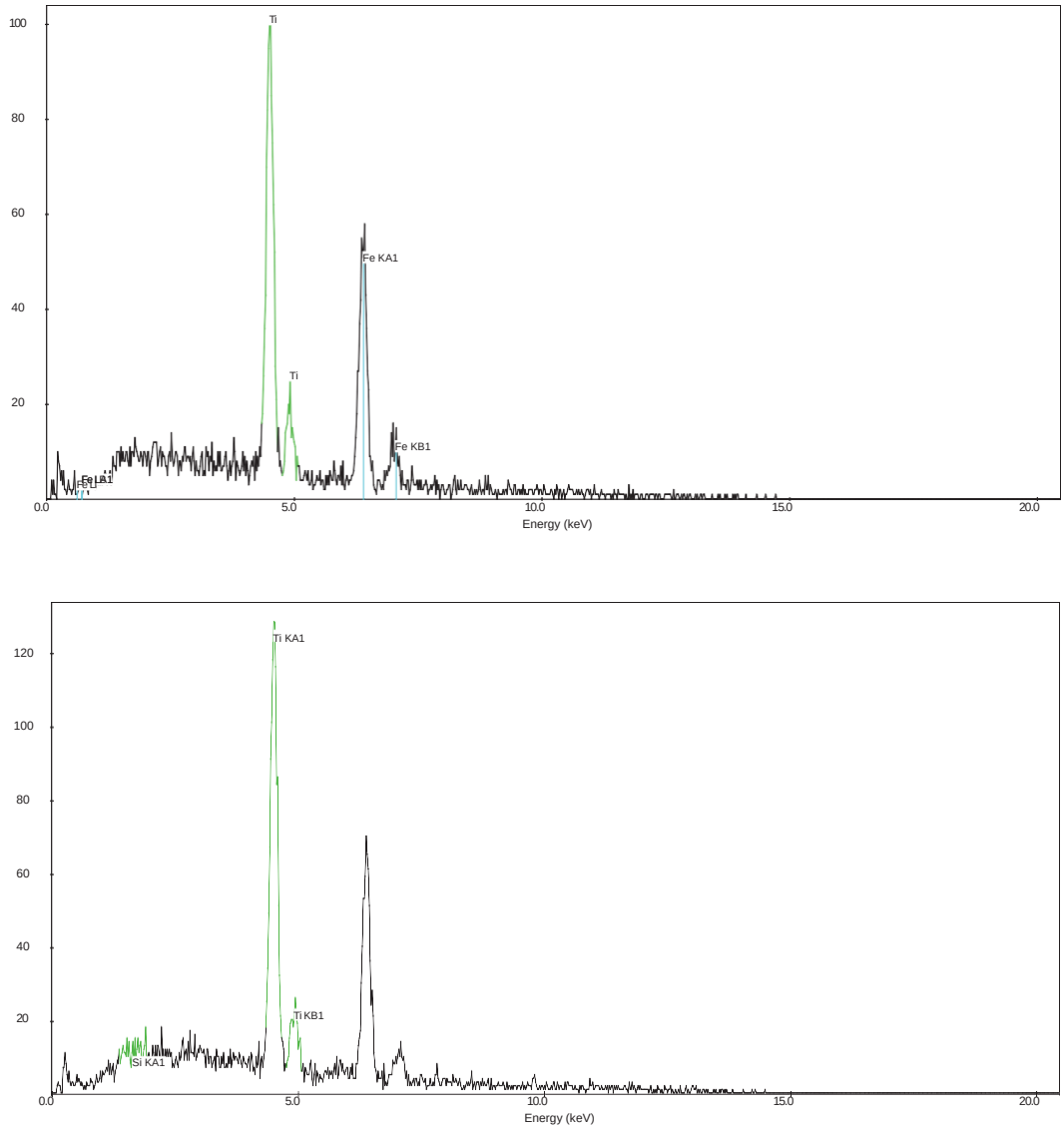

Figure A4 (Top and Bottom): EDS of ilmenite from thin section BRR-N22.

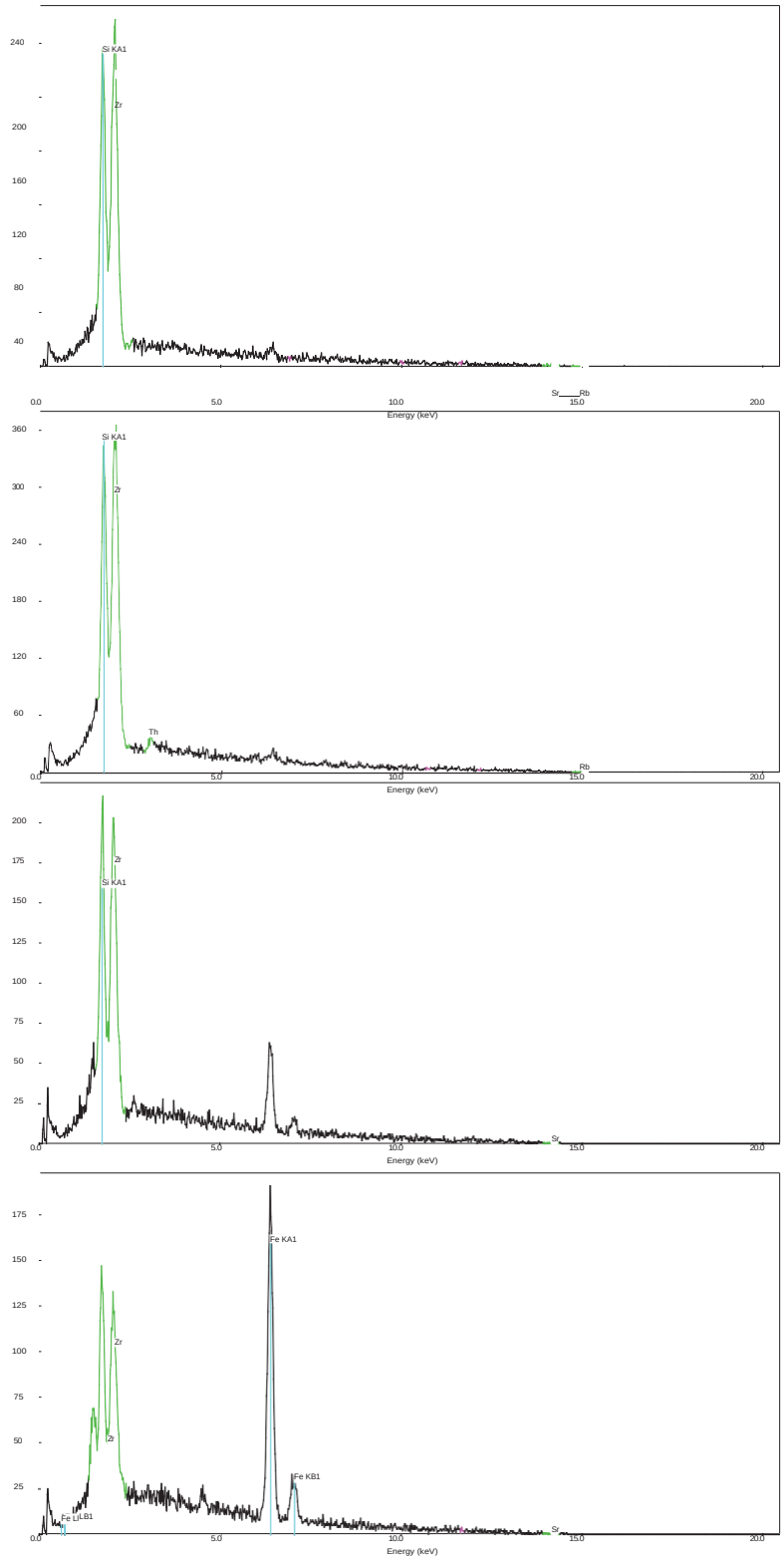

Figure A5: EDS of zircons from thin section BRR-N22

Standard	**Element**	**Spectrometer**			
		1	2	3	4
		Crystal			
		TAP	TAP	PET	LIF
Amelia albite	Na	**X**			
Anorthite	Al3		**X**		
Amelia albite	Si1		**X**		
Anorthite	Ca5			**X**	
Olivine-2566	Mg	**X**			
Microcline	K			**X**	
Fayalite	Fe2				**X**
Barite	Ba3				**X**

Table A4: List of standards used for standardizing microprobe for analysing feldspar composition.

Core-box Photographs

Figure A6: Photograph of AU drill core 09-02, box 1. Depth is 0.3 m to 3.5 m. Top of core is top right of box; bottom is bottom left. Depth markers are in feet.

Figure A7: Photograph of AU drill core 09-02, box 2. Depth is 3.5 m to 6.5 m. Top of core is top right of box; bottom is bottom left.
Depth markers are in feet.

Figure A8: Photograph of AU drill core 09-02, box 3. Depth is 6.5 m to 9.6 m. Top of core is top right of box; bottom is bottom left. Depth markers are in feet.

Figure A9: Photograph of AU drill core 09-02, box 4. Depth is 9.6 m to 12 m. Top of core is top right of box; bottom is bottom left. Depth markers are in feet.

Figure A10: Photograph of AU drill core 09-02, box 5. Depth is 12 m to 15.1 m. Top of core is top right of box; bottom is bottom left. Depth markers are in feet.

Figure A11: Photograph of AU drill core 09-02, box 6. Depth is 15.1 m to 18.7 m. Top of core is top right of box; bottom is bottom left. Depth markers are in feet.

Figure A12: Photograph of AU drill core 09-02, box 7. Depth is 18.7 m to 21.7m. Top of core is top right of box; bottom is bottom left Depth markers are in feet..

Figure A13: Photograph of AU drill core 09-02, box 8. Depth is 21.7 m to 23.3 m. Top of core is top right of box; bottom is bottom left. Depth markers are in feet.

Drill Core Logs

AU-DRILL CORE 09-02

PROJECT NUMBER 09-02
PROJECT NAME Wetumpka Crater breccia
CLIENT Auburn University
ADDRESS Auburn, AL

DRILLING DATE 2009
TOTAL DEPTH 23.3 m
DIAMETER 5 cm

COMMENTS Buck Ridge Road

Box Number	Depth (m)	Graphic Log	Description	Structures	Structure Description	Photo
	0.2		-			
1	0.4		Coarse sand, red to buff colored. Dominant minerals are quartz and muscovite mica.		Muscovite rich white patches with schistose structure	
	0.6					
	0.8					
	1					
	1.2					
	1.4					
	1.6		Broken core, coarse sand			
	1.8		-			
	2		Coarse sand, red to buff colored. Dominant minerals are quartz and muscovite mica.		Schistose structure	
	2.2					
	2.4					
	2.6		Broken core, mixture of coarse red and buff sand			
	2.8		-			
	3					
	3.2					
	3.4					

AU-DRILL CORE 09-02

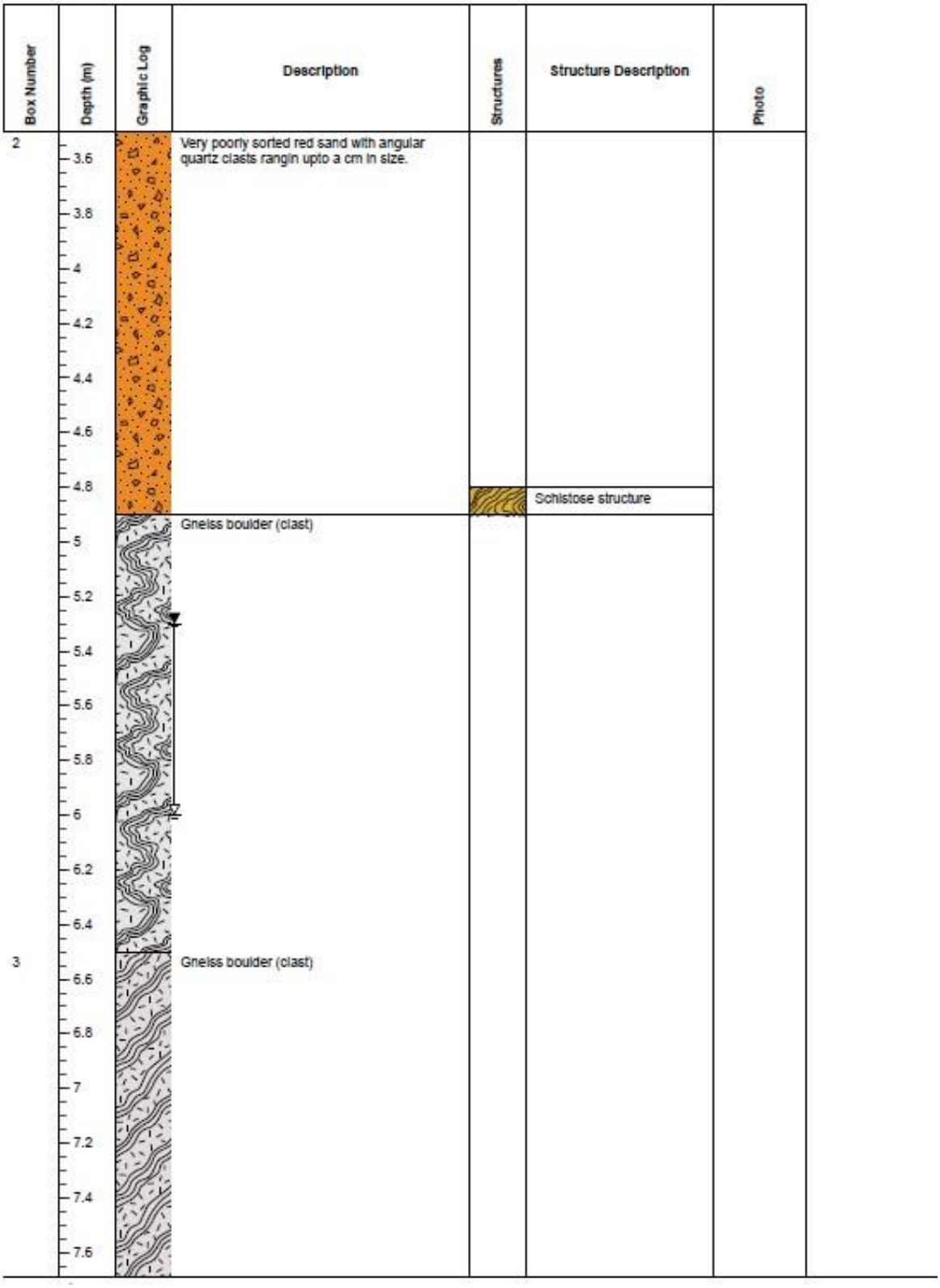

AU-DRILL CORE 09-02

Box Number	Depth (m)	Graphic Log	Description	Structures	Structure Description	Photo
4	7.8 – 9.6					
	9.6 – 9.8		Gneiss boulder (clast)			
	9.8 – 10		Coarse, buff colored sand			
	10 – 10.2		-			
	10.2 – 10.4		Poorly sorted buff colored sand with clay and patches of red sand		Clayey material	
	10.4 – 10.6		-			
	10.6 – 10.8		Buff colored coarse sand			
	10.8 – 11		Grey colored, coarse, poorly sorted sand with angular clasts			
	11 – 11.2		-			
	11.2 – 11.4		Coarse, red sand			
	11.4 – 11.6		Corase grey sand with clay		Clayey material	
	11.6 – 11.8		-			

AU-DRILL CORE 09-02

Box Number	Depth (m)	Graphic Log	Description	Structures	Structure Description	Photo
	12					
5	12.2		Coarse, poorly sorted grey sand with angular quartz clasts			
	12.4					
	12.6					
	12.8					
	13					
	13.2					
	13.4				Red sand with angular quartz clasts	
	13.6					
	13.8					
	14					
	14.2		Red clayey sand with angular quartz			
	14.4		Poorly sorted coarse grey sand with white pulverized lithic fragments. Clay is present in significant amounts.			
	14.6					
	14.8					
	15					
6	15.2		Poorly sorted coarse grey sand with white pulverized lithic fragments. Clay is present in minor amount.			
	15.4					
	15.6					
			-			
	15.8		Poorly sorted coarse grey sand with white pulverized lithic fragments. Clay is present in minor amount.			
	16					

AU-DRILL CORE 09-02

Box Number	Depth (m)	Graphic Log	Description	Structures	Structure Description	Photo
	16.2		-			
	16.4		Poorly sorted coarse grey sand with red and yellow stained patches and significant amount of clay.		Red and yellow staining in sand	
	16.6					
	16.8					
	17					
	17.2					
	17.4					
	17.6					
	17.8					
	18					
	18.2					
	18.4					
	18.6					
7	18.8		Poorly sorted red clayey sand.			
	19					
	19.2					
	19.4					
	19.6					
	19.8					
	20					
	20.2					

AU-DRILL CORE 09-02

Box Number	Depth (m)	Graphic Log	Description	Structures	Structure Description	Photo
	20.4 – 21.6					
8	21.8 – 23.2		Poorly sorted coarse grey sand with red stains and significant amount of clay.		Red staining in sand	
	23.4 – 24.4		Termination Depth at: 23.3 m			

REFERENCES

alabamaview.org (accessed December 2018).

Anderson, R. R, Witzke, B. J., and Roddy, D. J., 1996, The drilling of the 1991–1992 Geological Survey Bureau and U.S. Geological Survey Manson impact structure research cores, in Koeberl, C., and Anderson, R. R., eds., The Manson impact structure, Iowa: Geological Society of America Special Paper 302, p. 45–88.

Anderson, R. R., Hartung, J. B.,Witzke, B. J., Shoemaker, E. M., and Roddy, D. J., 1994, Preliminary results of the U.S. Geological Survey–Iowa Department of Natural Resources Geological Survey Bureau Manson core drilling project, in Dressler, B. O., Grieve, R. A. F., and Sharpton,V. L., eds., Large meteorite impacts and planetary evolution: Geological Society of America Special Paper 293, p. 237–247.

Bell, M. S., Reagan, M. K., Anderson, R. R., and Foster, C. T., Jr., 1996, Petrography of crystalline clast breccias from the Manson M-1 core, in Koeberl, C., and Anderson, R. R., eds., The Manson impact structure, Iowa: Geological Society of America Special Paper 302, p. 433–456.

Chao E. C. T., Huttner R., and Schmidt-Kaler H., 1978, Principal exposures of the Ries meteorite crater in south Germany. Munich: Bayerisches Geologisches Landesamt, 84 p.

Chinchalkar, N.S. and King, D.T. Jr., 2018, Wetumpka Impact Structure, Alabama: large oriented boulders in an interior diamicton: Geological Society of America Abstracts with Programs, v.50, no. 6, 1p.

DeMarchi, L., Agarwal, V., and King D.T. Jr., 2019, Hydrocode Simulations of Wetumpka Impact Crater: Lunar and Planetary Science [Lunar and Planetary Science Conference] abstracts, v. 50, abstract no. 2644, 2p.

Dence, M.R., 1965, The extraterrestrial origin of Canadian craters: Annals of the New York Academy of Sciences v. 123, p. 941–969.

Dence, M.R., 1968, Shock zoning at Canadian craters: petrography and structural implications In: French, B.M., Short, N.M. (Eds.), Shock Metamorphism of Natural Materials. Mono Book Corp, Baltimore, MD, p. 69–184.

Dence, M.R., 1971, Impact melts. Journal of Geophysical Research v. 76, p. 5552–5565.

Dence, M.R., 1972, The nature and significance of terrestrial impact structures: 24th International Geological Congress, Montreal, Canada, Proceedings, Section 15, p. 77–89.

French, B.M. and Koeberl, C., 2010, The convincing identification of terrestrial meteorite impact structures: What works, what doesn't, and why: Earth-Science Reviews v. 98 p. 123–170

French, B.M., 1998, Traces of catastrophe: A handbook of shock metamorphic effects in Terrestrial meteorite impact structures. LPI Contribution No. 954, Houston, Lunar and Planetary Institute. 120 p.

Graup G. 1978. Das Kristallin im N€ordlinger Ries. Petrographische Zusammensetzung und Auswurfsmechanismus der kristallinen Tr€ummermassen, Struktur des kristallinen Untergrundes und Beziehungen zum Moldanubikum. Stuttgart, Germany: Ferdinand Enke Verlag. 190 p.

Hartung, J.B. and Anderson, R.R., 1988, The Manson impact structure; its contribution to impact materials observed at Cretaceous/Tertiary boundary: Proceedings of Lunar and Planetary Science, v.22, p. 101-110.

Heider, E. S. and King, D.T. Jr., 2016, Early modification stage emplacement of shallow crater-filling units, Wetumpka impact structure, Alabama: Gulf Coast Association of Geological Societies Transactions, v. 66, p. 231-249.

Hoppin, R. A., and Dryden, J. E., 1958, An unusual occurrence of Pre-Cambrian crystalline rocks beneath glacial drift near Manson, Iowa: Journal of Geology, v. 66, p. 694–699.

Horz F., Ostertag R., and Rainey D. A., 1983, Bunte Breccia of the Ries: Continuous deposits of large impact craters. Reviews of Geophysics and Space Physics v. 21, p.1667–1725.

Izett, G.A., Cobban, W.A., Dalrymple, G.B., and Obradovich, J.D., 1998, 40Ar/39Ar age of the Manson impact structure, Iowa, and correlative impact ejecta in the Crow Creek Member of the Pierre Shale (Upper Cretaceous), South Dakota and Nebraska: GSA Bulletin, v. 110, no. 3, p. 361–376.

Johnson, R.C., 2007, Wetumpka Impact Structure Modeled as the Exposed Remains of a Large, Shallow-Water, Marine-Target Impact Crater for Analysis and Interpretation of Two Drill Cores Taken from Near the Structure's Geographic Center [Auburn University MS Thesis], 345 p.

King D.T. Jr., Petruny, L.W., Ormö, J., Chinchalkar, N.S. and Heider, E.S., 2019, Crater-Filling Units Of Wetumpka Impact Structure, Alabama: Lunar and Planetary Science [Lunar and Planetary Science Conference] abstracts, v. 50, abstract no. 2662, 2p.

King, D. T., Jr. and Ormö, J., 2011, The marine-target Wetumpka impact structure examined in the field and by shallow core-hole drilling: Geological Society of America, Special Paper 483, p. 287-296.

King, D. T., Jr., Ormö, J., Petruny, L. W., and Neathery, T. L., 2006, Role of water in the formation of the Late Cretaceous Wetumpka impact structure, inner Gulf Coastal Plain of Alabama, USA: Meteoritics and Planetary Science, v. 41, p. 1625-1631.

King, D.T., Jr., 1997, The Wetumpka impact crater and the Late Cretaceous impact record, *in* Neathery, T.L., King, D.T., Jr., and Wolf, L.W., eds., The Wetumpka impact structure and related features, Alabama Geological Society Guidebook 34c: Tuscaloosa, Alabama Geological Society, p. 25-56.

King, D.T., Jr., Morrow, J.R., Petruny, L.W., and Ormö, J., 2015, Surfi cial polymict impact breccia unit, Wetumpka impact structure, Alabama: Shock levels and emplacement mechanism, in Osinski, G.R., and Kring, D.A., eds., Large Meteorite Impacts and Planetary Evolution V: Geological Society of America Special Paper 518, p. 149–164.

King, D.T., Jr., Neathery, T.L., Petruny, L.W., Koeberl, C., and Hames, W.E., 2002, Shallow-marine impact origin of the Wetumpka Structure (Alabama, USA): Earth and Planetary Science Letters, v. 202, p. 541-549.

Koeberl, C., Reimold,W. U., Kracher, A., Träxler, B.,Vormaier, A., and Körner,W., 1996, Mineralogical, petrological, and geochemical studies of drill core samples from the Manson impact structure, Iowa, in Koeberl, C., and Anderson, R. R., eds., The Manson impact structure, Iowa: Anatomy of an impact crater: Geological Society of America Special Paper 302, p. 145–219.

Kring, D. A., 2005, Hypervelocity collisions into continental crust composed of sediments and an underlying crystalline basement: comparing the Ries (~24km) and Chicxulub (~180km) impact craters; Chemie d. Erde – Geochemistry v. 65, p. 1–46.

Lunar and Planetary Institute, 2019, https://www.lpi.usra.edu/exploration/training/illustrations/craterFormation/ (accessed December 2018).

Ling, K.Y., Zhu, X.Q., Tang, H.S., Wang, Z.G., Yan, Han, T., Chen, W.Y., 2015, Mineralogical characteristics of the karstic bauxite deposits in the Xiuwen ore belt, Central Guizhou Province, Southwest China, Ore Geology Reviews, v. 65, p. 84-96.

Markin, J.K., 2015, Lithofacies analysis of AU scientific drill cores 09-03 and 09-04, Wetumpka impact structure, Elmore County, Alabama: [Auburn University MS Thesis], 196 p.

Markin, J.K., and King, D.T., Jr., 2012, Wetumpka impact structure's resurge chalk deposits – Insights from x-ray computed tomography: Gulf Coast Association of Geological Societies Transactions, v. 62, p. 265-271.

Melosh, H.J., 1989, *Impact Cratering: A Geologic Process*: New York, Oxford University Press, 245 p.

Misra, S., Newsom, H.E., Prasad, M.S., Geissman, J.W., Dube, A., and Sengupta, D.,

2009, Geochemical identification of impactor for Lonar Crater, India: Meteoritics and Planetary Science, v. 44, Nr. 7, p. 1001-1018.

Morrow, J. R., and King, D. T., Jr., 2007, Petrography of shocked-quartz sand in slumpback breccia, central Wetumpka impact structure, Alabama: Abstracts from the 70th Annual Meeting of the Meteoritical Society, Tucson, Arizona, v. 42, Abstract #5009.

Neathery, T.L., Bentley, R.D., and Lines, G.C., 1976, Crypto-explosive structure near Wetumpka, Alabama: Geological Society of America Bulletin, v. 87, p. 567-573.

Oberbeck V. R., 1975, The role of ballistic erosion and sedimentation in lunar stratigraphy: Reviews of Geophysics and Space Physics v. 13, p. 337–362.

Ormö, J., and Lindström, M., 2000, When a cosmic impact strikes the sea bed: Geological Magazine, v. 137, p. 67-80.

Ormö, J., Lindström, M., Lepinette, A., Martinez-Frias, J., and Diaz-Martinez, E., 2006, Cratering and modification of wet-target craters: Projectile impact experiments and field observations of the Lockne marine-target crater (Sweden): Meteoritics & Planetary Science v. 41, no. 10, p. 1605–1612.

Osinski G. R., Tornabene L. L., and Grieve R. A. F., 2011, Impact ejecta emplacement on terrestrial planets: Earth and Planetary Science Letters v. 310, p.167–181.

PASSC, 1955, Earth Impact Database: http://www.passc.net/EarthImpactDatabase/New%20website_05-2018/Index.html (accessed October 2018).

Pietrek, A. and Kenkmann, T., 2016, Ries Bunte Breccia revisited: Indications for the presence of water in Itzing and Otting drill cores and implications for the emplacement

process: Meteoritics & Planetary Science v. 51, no. 7, p. 1203–1222.

Pietrek, A., Kenkmann, T., and Jung, D., 2015, Bunte Breccia Revisited: The Distribution and Source of Water In The Ejecta Of Ries Crater; Germany: [Lunar and Planetary Science Conference] abstracts, v. 46, abstract no. 1534, 2 p.

Robbins, E.A., Wolf, L.W., and King, Jr., D.T., 2011, Wetumpka impact structure (Alabama): a gravity model: Lunar and Planetary Science [Lunar and Planetary Science Conference abstracts], v. 42, abstract no. 2732, 2 p.

Rodenas, T.P., 2012, Drill-Core and Geophysical Investigation of the Western Part of the Crystalline Rim of Wetumpka Impact Structure: [Auburn University MS Thesis], 136 p.

Rodesney, S.N., 2014, Provenance and Composition of Impactite Sands; AU Drill Core #09-04, Wetumpka Impact Structure, Alabama: [Auburn University MS Thesis], 94 p.

Schmieder M., Erickson, T.M., and Kring, D.A., 2019, Microstructural characterization of Tio2–II in the Chicxulub Peak Ring: Lunar and Planetary Science [Lunar and Planetary Science Conference] abstracts, v. 50, abstract no. 1658, 2p.

Schmieder, M., Kennedy, T., Jourdan, F., Buchner, E., and Riemold, W.E., 2018, A high- precision $^{40}Ar/^{39}Ar$ age for the Nördlinger Ries impact crater, Germany, and implications for the accurate dating of terrestrial impact events: Geochimica et Cosmochimica Acta v. 220, p.146-157.

Simonson, B.M., 2003, Petrographic Criteria for recognizing certain types of impact spherules in well-preserved Precambrian successions: Astrobiology, Rubey Colloquium Paper, v. 3, Nr. 1, p. 49-65.

Simonson, B.M., and Glass, B.P., 2004, Spherule Layers – Records of Ancient Impacts:

Annual Review Earth Planetary Science v. 32, p. 329-361.

Stoffler D., Artemieva N. A., and Pierazzo E, 2002, Modeling the Ries-Steinheim impact event and the formation of the moldavite strewn field: Meteoritics & Planetary Science v. 37, p.1893–1907.

Stoffler D., Artemieva N. A., W€unnemann K., Reimold W. U., Jacob J., Hansen B. K., and Summerson I. A. T, 2013, Ries crater and suevite revisited - Observations and modeling Part I: Observations: Meteoritics & Planetary Science v. 48, p.515–589.

Von Engelhardt W., 1972, Shock produced rock glasses from the Ries crater: Contributions to Mineralogy and Petrology v. 36, p. 265–292.

Von Engelhardt W., 1997, Suevite breccia of the Ries impact crater, Germany: Petrography, chemistry and shock metamorphism of crystalline rock clasts: Meteoritics & Planetary Science v. 32, p. 545–554.

Vind, J., Malfliet, A., Blanpain, B., Tsakiridis, P.E., Tkaczyk, A.H., Vassiliadou, V., and Panias, D., 2018, Rare Earth Element Phases in Bauxite Residue, Minerals, v. 8, p. 1-32.

Wartho, J.-A., Van Soest, M.C., King, D.T., and Petruny, L.W., 2012, An (U-Th)/He age for the shallow-marine Wetumpka impact structure, Alabama, USA: Meteoritics and Planetary Science, v. 47, no. 8, p. 1243-1255.

Wittmann, A., Kenkmann, T., Schmitt, R.T., Stöffler, D., 2006, Shock-metamorphosed zircon in terrestrial impact craters: Meteoritics and Planetary Science v. 41, p. 433–454.

Wolf, L.W., Plescia, J. and Steltenpohl, M.G., 1997, Geophysical investigation of a "suspect" impact crater in Wetumpka, Alabama, in Neathery, T.L., King, D.T., Jr., and

Wolf, L.W., eds., The Wetumpka impact structure and related features, Alabama Geological Society Guidebook 34c: Tuscaloosa, Alabama Geological Society, p. 57-68.